



Measurement of the associated production of a top-antitop-quark pair and a Higgs boson decaying into a $b\bar{b}$ pair in pp collisions at $\sqrt{s} = 13$ TeV using the ATLAS detector at the LHC

The ATLAS Collaboration

This paper reports the measurement of Higgs boson production in association with a $t\bar{t}$ pair in the $H \rightarrow b\bar{b}$ decay channel. The analysis uses 140 fb^{-1} of 13 TeV proton–proton collision data collected with the ATLAS detector at the Large Hadron Collider. The final states with one or two electrons or muons are employed. An excess of events over the expected background is found with an observed (expected) significance of 4.6 (5.4) standard deviations. The $t\bar{t}H$ cross-section is $\sigma_{t\bar{t}H} = 411^{+101}_{-92} \text{ fb} = 411 \pm 54(\text{stat.})^{+85}_{-75}(\text{syst.}) \text{ fb}$ for a Higgs boson mass of 125.09 GeV, consistent with the prediction of the Standard Model of $507^{+35}_{-50} \text{ fb}$. The cross-section is also measured differentially in bins of the Higgs boson transverse momentum within the simplified template cross-section framework.

Contents

1	Introduction	2
2	ATLAS detector	3
3	Data and Monte Carlo simulation samples	4
4	Objects and event selection	6
5	Background modelling	8
5.1	Modelling of $t\bar{t}$ + jets background	8
5.2	Non-prompt or mis-identified lepton background	9
6	Signal extraction	10
7	Systematic uncertainties	13
8	Results	17
9	Conclusion	28

1 Introduction

After the discovery of the Higgs boson [1–3] in 2012 by the ATLAS [4] and CMS [5] collaborations, attention has turned to detailed measurements of its properties and couplings as a means of testing the predictions of the Standard Model (SM) [6–8]. The Higgs boson coupling to the top quark, the heaviest particle in the SM, is of special interest as it could be very sensitive to effects of physics beyond the SM (BSM) [9]. It is indirectly constrained assuming no BSM contributions to loop-induced processes from measurements of gluon–gluon fusion Higgs boson production and decay into $\gamma\gamma$ [10, 11]. The Higgs boson production in association with a pair of top quarks ($t\bar{t}H$), where the top quark couples to the Higgs boson at tree level, provides a possibility for a direct measurement of the top-quark’s Yukawa coupling without assumptions about the potential presence of BSM physics [12–15]. It was observed by the ATLAS and CMS collaborations using several Higgs boson decay modes [16, 17].

The decay into two b -quarks is predicted to have the largest branching fraction of about 58% [18] and has the advantage of allowing for the reconstruction of the Higgs boson four-momentum from the kinematics of its decay products. Furthermore, the $t\bar{t}H(b\bar{b})$ channel involves only fermionic Higgs boson couplings in the production and decay, leading to an enhanced sensitivity for probing them. However, this final state is affected by a large irreducible background arising from the $t\bar{t}$ production in associations with jets ($t\bar{t}$ + jets), in particular when the jets originate from b - or c -quarks, which is challenging to predict theoretically.

The ATLAS Collaboration has measured the $t\bar{t}H(b\bar{b})$ production at $\sqrt{s} = 13$ TeV in the final state with at least one lepton using the full Run 2 dataset collected in proton–proton (pp) collisions at the Large Hadron Collider (LHC) [19] between 2015 and 2018, corresponding to an integrated luminosity of 139 fb^{-1} [20]. The measured signal strength, defined as the ratio of the measured cross-section to that predicted by the SM, was found to be $0.35^{+0.36}_{-0.34}$, and corresponds to an observed (expected) significance of 1.0 (2.7) standard

deviations. The signal strength was also measured differentially in five intervals of the Higgs boson transverse momentum (p_{T}^H) in the simplified template cross-section framework (STXS) [18], probing potential p_{T}^H -dependent deviations from the SM expectation.

The CMS Collaboration searched for the $t\bar{t}H(b\bar{b})$ production using 35.9 fb^{-1} of data collected at $\sqrt{s} = 13 \text{ TeV}$ in 2016, in events with at least one lepton [21] or no lepton [22], and measured a signal strength of 0.72 ± 0.45 and 0.9 ± 1.5 , respectively. The analysis requiring at least one lepton achieved an observed (expected) significance of 1.6 (2.2) standard deviations.

This paper presents a re-analysis of the full Run 2 dataset collected at $\sqrt{s} = 13 \text{ TeV}$ with the ATLAS detector in final states with one or two leptons, referred to in the following as single-lepton and dilepton channels, and supersedes the result of Ref. [20]. Compared with the previous result, this analysis has an increased acceptance by selecting events with less restrictive requirements on the number of jets identified as originating from b -hadrons (b -jets), resulting in an increased efficiency to select $t\bar{t}H$ signal. It utilises a revised treatment of the different flavour components of the $t\bar{t} + \text{jets}$ background, and in particular, of the $t\bar{t}$ production in association with b -jets, the main background and the dominant source of the systematic uncertainty in the previous $t\bar{t}H(b\bar{b})$ measurement. For the modelling of this background, a new sample of Monte Carlo (MC) simulated events with improved settings was produced, and a corresponding set of systematic uncertainties was developed [23, 24]. This measurement also uses improved analysis techniques: an advanced b -jet identification and an improved event categorisation. In particular, unlike the previous result, where the event categorisation into the background-dominated and signal-rich categories was made based on the number of jets and the number of b -jets, this analysis uses a multiclass neural network to define regions enriched in different components of the main background, the $t\bar{t} + \text{jets}$ production processes, and the signal. A more powerful multivariate discriminant is also employed to separate the signal from background and to reconstruct p_{T}^H . These improvements lead to better overall sensitivity and allow for a measurement of the $t\bar{t}H(b\bar{b})$ production cross-section in six bins of p_{T}^H , $0-60 \text{ GeV}$, $60-120 \text{ GeV}$, $120-200 \text{ GeV}$, $200-300 \text{ GeV}$, $300-450 \text{ GeV}$, and $\geq 450 \text{ GeV}$, as obtained from the MC event record before the Higgs boson decays, in the STXS formalism.

2 ATLAS detector

The ATLAS experiment [25] at the LHC is a multipurpose particle detector with a forward–backward symmetric cylindrical geometry and a near 4π coverage in solid angle.¹ It consists of an inner tracking detector (ID) surrounded by a thin superconducting solenoid providing a 2 T axial magnetic field, electromagnetic and hadronic calorimeters, and a muon spectrometer. The inner tracking detector covers the pseudorapidity range $|\eta| < 2.5$. It consists of silicon pixel, silicon microstrip, and transition radiation tracking detectors. Lead/liquid-argon (LAr) sampling calorimeters provide electromagnetic (EM) energy measurements with high granularity within the region $|\eta| < 3.2$. A steel/scintillator-tile hadronic calorimeter covers the central pseudorapidity range ($|\eta| < 1.7$). The endcap and forward regions are instrumented with LAr calorimeters for EM and hadronic energy measurements up to $|\eta| = 4.9$. The muon spectrometer (MS) surrounds the calorimeters and is based on three large superconducting air-core toroidal

¹ ATLAS uses a right-handed coordinate system with its origin at the nominal interaction point (IP) in the centre of the detector and the z -axis along the beam pipe. The x -axis points from the IP to the centre of the LHC ring, and the y -axis points upwards. Cylindrical coordinates (r, ϕ) are used in the transverse plane, ϕ being the azimuthal angle around the z -axis. The pseudorapidity is defined in terms of the polar angle θ as $\eta = -\ln \tan(\theta/2)$. Angular distance is measured in units of $\Delta R \equiv \sqrt{(\Delta\eta)^2 + (\Delta\phi)^2}$.

magnets with eight coils each. The field integral of the toroids ranges between 2.0 and 6.0 T m across most of the detector. The muon spectrometer includes a system of precision tracking chambers up to $|\eta| = 2.7$ and fast detectors for triggering up to $|\eta| = 2.4$. The luminosity is measured mainly by the LUCID-2 [26] detector, which is located close to the beam pipe. A two-level trigger system is used to select events [27]. The first-level trigger is implemented in hardware and uses a subset of the detector information to accept events at a rate below 100 kHz. This is followed by a software-based trigger that reduces the accepted event rate to 1 kHz on average depending on the data-taking conditions. A software suite [28] is used in data simulation, in the reconstruction and analysis of real and simulated data, in detector operations, and in the trigger and data acquisition systems of the experiment.

3 Data and Monte Carlo simulation samples

This analysis was performed using the pp collision data collected by the ATLAS detector between 2015 and 2018 at $\sqrt{s} = 13$ TeV. After the application of data-quality requirements [29], the dataset corresponds to an integrated luminosity of 140 fb^{-1} . Samples of simulated events were produced to model the different signal and background processes. Additional samples were produced to estimate the modelling uncertainties for each process. The effects of the additional pp collisions in the same or a nearby bunch crossing (pile-up) were modelled by overlaying minimum bias events generated with PYTHIA8 [30] using the A3 set of tunable parameters [31] onto the simulated hard-scatter event. The MC events were weighted to reproduce the distribution of the average number of interactions per bunch crossing observed in the data. The MC samples were processed using the full ATLAS detector simulation [32] based on GEANT4 [33]. Some alternative samples used to evaluate the modelling uncertainties were produced using fast simulation, where the full GEANT4 simulation of the calorimeter response is replaced by a detailed parameterisation of the shower shapes. For the observables used in this analysis, both simulations were found to give similar modelling. All MC samples were reconstructed using the same software as for collider data. Corrections were applied to the simulated events so that the selection efficiencies, energy scales and energy resolutions of the physics objects closely match those determined from data control samples.

All samples generated with POWHEGBOX [34–37] and MADGRAPH5_AMC@NLO [38] were interfaced to PYTHIA8 [39] to simulate the parton shower (PS), fragmentation, and underlying event with the A14 tune [40] and the NNPDF2.3LO [41] parton distribution function (PDF) set. Some alternative samples use the HERWIG7 [42, 43] PS model with the H7UE set of tuned parameters [43] and the MMHT2014LO PDF set [44]. Samples using PYTHIA8 and HERWIG7 have heavy-flavour hadron decays modelled by EvtGen [45]. The masses of the top quark, m_{top} , and of the Higgs boson, m_H , are set to 172.5 GeV and 125 GeV, respectively.

The nominal $t\bar{t}H$ signal sample was generated at next-to-leading order (NLO) in the five flavour scheme (5FS) using the POWHEGBOX [46] generator with the NNPDF3.0NLO [41] PDF set. The h_{damp} parameter² was set to $3/4 \cdot (m_t + m_{\bar{t}} + m_H) = 352.5$ GeV, and the functional form of the renormalisation and factorisation scales was set to $\sqrt[3]{m_T(t) \cdot m_T(\bar{t}) \cdot m_T(H)}$, where $m_T = \sqrt{m^2 + p_T^2}$ is the transverse mass of a generated particle, m is its mass, and p_T is its transverse momentum. It is normalised to the theoretical prediction of Ref. [18]. An alternative $t\bar{t}H$ sample generated with the same POWHEGBOX set-up, but interfaced to HERWIG7 is used to evaluate uncertainties due to the choice of parton shower, hadronisation

² The h_{damp} parameter controls the transverse momentum p_T of the first additional emission beyond the leading-order Feynman diagram in the PS and therefore regulates the high- p_T emission against which the $t\bar{t}$ system recoils.

and underlying event model. The uncertainty related to the matching between the matrix element (ME) generator and the PS is accessed by changing the definition of the hardness of the POWHEG emission calculated by PYTHIA8 via the parameter p_T^{hard} from the value provided by POWHEG to the p_T of the POWHEG emission following Refs. [47, 48].

Several MC samples with different accuracy in ME generator and with different PS models are used in this analysis to model the main $t\bar{t}$ + jets background. This background is categorised according to the flavour of the additional jets in the event, excluding jets from top-quark or W boson decays, using the same procedure as described in Ref. [49]. Generator-level particle jets are reconstructed from stable particles (mean lifetime $\tau > 3 \times 10^{-11}$ seconds, excluding muons and neutrinos) using the anti- k_r algorithm [50] with a radius parameter $R = 0.4$, and are required to have transverse momentum $p_T > 15$ GeV and $|\eta| < 2.5$. The flavour of a jet is determined by counting b - or c -hadrons within $\Delta R < 0.4$ of the jet axis. Jets matched to exactly one b -hadron, with p_T above 5 GeV, are labelled single- b -jets, while those matched to two Jets matched to exactly one b -hadron, with p_T above 5 GeV, are labelled single- b -jets, while those matched to two or more b -hadrons are labelled B -jets (with no p_T requirement on the second b -hadron); single- c - and C -jets are defined analogously, only considering jets not already defined as single- b - or B -jets. Events that have a single- b - or B -jet, are labelled as $t\bar{t} + 1b$ and $t\bar{t} + 1B$ respectively, events with two or more b -jets are labelled as $t\bar{t} + \geq 2b$. These three categories together are collectively referred to as $t\bar{t} + \geq 1b$. Events with no single- b - or B -jet but at least one single- c - or C -jet are labelled as $t\bar{t} + \geq 1c$. Finally, events not containing any heavy-flavour jets aside from those from top-quark or W boson decays are labelled as $t\bar{t} + \text{light}$.

The $t\bar{t} + \text{light}$ and $t\bar{t} + \geq 1c$ contributions are modelled by a MC sample produced with the HVQ programme [35] in the POWHEGBox generator at NLO in QCD in the five flavour scheme (5FS) with the NNPDF3.0NLO PDF set. The h_{damp} parameter was set to $1.5 m_{\text{top}}$ [40, 51]. An additional sample was generated with the h_{damp} parameter increased by a factor of two to evaluate the uncertainty in the modelling of $t\bar{t} + \text{light}$ and $t\bar{t} + \geq 1c$ stemming from the choice of the h_{damp} value.

To predict the $t\bar{t} + \geq 1b$ background with the highest available precision, the $t\bar{t}b\bar{b}$ MC sample is generated at NLO, where the additional b -quarks are included in the ME. The four flavour scheme (4FS) was used for this sample. It was produced with the POWHEGBoxRES [52] generator and OPENLOOPS [53–55], using the implementation of this process in POWHEGBoxRES [56], with the NNPDF3.1NNLOnF4 [41] PDF set interfaced to PYTHIA8. Based on the studies of Ref. [23], the factorisation scale is set to $\frac{1}{2} \sum_{i=t,\bar{t},b,\bar{b},j} m_{T,i}$, the renormalisation scale is set to $\frac{1}{2} \cdot \sqrt[4]{m_T(t) \cdot m_T(\bar{t}) \cdot m_T(b) \cdot m_T(\bar{b})}$, and the h_{damp} parameter is set to $H_T/2$. The POWHEG internal parameter h_{bzd} that regulates the damping function together with the parameter h_{damp} , was set to 5. The choice of model used for the recoil in the initial state parton shower was found to impact significantly the $t\bar{t} + \geq 1b$ background predictions [24]. The corresponding uncertainty is evaluated by changing the PYTHIA8 parameter from a global recoil to a dipole recoil while keeping the rest of the settings identical to the nominal $t\bar{t}b\bar{b}$ sample.

Similar to the $t\bar{t}H$ signal sample, alternative samples were generated to assess the PS and matching uncertainties in the modelling of $t\bar{t} + \text{light}$, $t\bar{t} + \geq 1c$ and $t\bar{t} + \geq 1b$ by replacing in the corresponding nominal set-ups the PYTHIA8 shower model by HERWIG and producing samples with a varied p_T^{hard} parameter.

For an independent pseudo-data test, additional samples of $t\bar{t}$ events were produced to model $t\bar{t} + \text{light}$ and $t\bar{t} + \geq 1c$ events with the SHERPA [57] generator. The NLO-accurate matrix elements for up to one additional parton, and LO-accurate matrix elements for up to four additional partons were calculated with the COMIX [58] and OPENLOOPS libraries. They were matched with the SHERPA PS [59] with the default set of tuned parameters using the MEPS@NLO prescription [60–63] with a matching scale of

30 GeV. Furthermore, $t\bar{t} + \geq 1b$ events were simulated using SHERPA and OPENLOOPS with $t\bar{t}b\bar{b}$ ME calculated at NLO accuracy using COMIX in the 4FS using the same functional form of the factorisation and renormalisation scales as in the nominal $t\bar{t}b\bar{b}$ set-up.

Single-top-quark production processes, i.e. tW associated production, t-channel and s-channel production, were modelled using the POWHEGBOX [64–66] generator at NLO in QCD. The t-channel process was generated in the 4FS with the NNPDF3.0_{NLO}_{NF4} PDF set, while for tW and s-channel processes the 5FS NNPDF3.0_{NLO} PDF was used. The tW MC sample was generated using the factorisation and renormalisation scales set to $H_T/2$ with H_T defined as a sum of the transverse mass of the W boson, the top quark and the transverse momentum of an additional parton. The overlap between tW and $t\bar{t}$ production [66] was removed using the diagram-removal scheme [67]. An alternative tW MC sample implementing the diagram subtraction scheme [66] was produced to evaluate the systematic uncertainty due to the tW and $t\bar{t}$ interference treatment.

The events in the nominal $t\bar{t}W$ sample were simulated using the SHERPA [68] generator with the NNPDF3.0_{NNLO} PDF set. The ME was calculated for up to one additional parton at NLO and up to two partons at LO using COMIX and OPENLOOPS, and merged with the SHERPA PS using the MEPS@NLO prescription with a merging scale of 30 GeV. The alternative sample was generated with MADGRAPH5_AMC@NLO with up to one additional parton in the final state at NLO accuracy in the strong coupling, using the NNPDF3.1_{NNLO} [69] PDF set. The different jet multiplicities were merged using the FxFx NLO ME and PS merging prescription [70] with a merging scale of 30 GeV. Background events from $t\bar{t}Z/\gamma^*$ and the rare processes tZq , tWZ , $tHjb$, tWH and $t\bar{t}t\bar{t}$ were simulated at NLO in QCD using the MADGRAPH5_AMC@NLO generator. The alternative sample used to evaluate the PS uncertainty in the $t\bar{t}Z$ background was generated with the same set-up as the nominal but interfaced to HERWIG7.

The production of $V + \text{jets}$ events (where $V = W$ or Z) was simulated with the SHERPA generator using NLO-accurate matrix elements for up to two partons and LO-accurate matrix elements for up to four partons. Samples of diboson final states (VV) were also simulated with the SHERPA generator.

All MC samples corresponding to small backgrounds were normalised to the most precise available theoretical predictions closely following Ref. [20]. The normalisation of the $t\bar{t}W$ background was updated to the most recent prediction of Ref. [71]. The $t\bar{t} + \text{light}$ and $t\bar{t} + \geq 1c$ components were normalised to the $t\bar{t}$ cross-section computed at next-to-next-to-leading order (NNLO) in QCD including the resummation of next-to-next-to-leading-logarithmic (NNLL) soft-gluon terms [72] while the $t\bar{t} + \geq 1b$ normalisation is taken from the $t\bar{t}b\bar{b}$ MC simulation.

4 Objects and event selection

Events are selected using single-lepton triggers with variable electron and muon transverse momentum thresholds, and various identification and isolation criteria depending on the lepton flavour and the data-taking period [73, 74]. The lowest p_T threshold at trigger level used for muons is 20 GeV (26 GeV), while for electrons the threshold is 24 GeV (26 GeV) in 2015 (2016–2018). Events are required to have at least one vertex with at least two associated ID tracks with $p_T > 0.5$ GeV. In each event, the primary vertex is defined as the reconstructed vertex having the highest scalar sum of squared p_T of associated tracks [75] among the vertices consistent with the average beam-spot position.

Electron candidates are reconstructed from energy deposits in the electromagnetic calorimeter matched to tracks reconstructed in the ID system and are required to satisfy the *MediumLH* identification criterion [76].

They are required to have $p_T > 10$ GeV and $|\eta| < 2.47$, excluding the calorimeter barrel-endcap transition region ($1.37 < |\eta| < 1.52$). Muon candidates are reconstructed from tracks in the MS that are associated with tracks from the ID and are required to satisfy the *Loose* identification criterion [77] and to have $p_T > 10$ GeV, $|\eta| < 2.5$. Electron (muon) candidates must be associated with the primary vertex of the event: the transverse impact parameter divided by its estimated uncertainty, $|d_0|/\sigma(d_0)$, is required to be less than five (three) for electron (muon) candidates. The longitudinal impact parameter must satisfy $|z_0 \sin(\theta)| < 0.5$ mm for both lepton flavours.

Jets are reconstructed from particle flow objects [78] using the anti- k_r jet clustering algorithm in the FASTJET implementation [79] with a radius parameter $R = 0.4$. Jets are required to satisfy the *Tight* criterion of the *jet vertex tagger* (JVT) algorithm [80] to mitigate the contribution from pile-up jets, and to have $p_T > 25$ GeV and $|\eta| < 2.5$. The jet energy scale (JES) and resolution are calibrated using simulations with in situ corrections obtained from data [81]. Events containing jets originating from non-collision sources or detector noise are removed.

Jets containing b -hadrons, referred to as b -jets, are identified using the DL1r b -tagging algorithm [82] that uses a neural network based on the distinctive features of b -hadron decays, primarily the impact parameters of tracks and the displaced vertices reconstructed in the ID. Additional input to this network is provided by discriminating variables constructed by a recurrent neural network, that exploits the spatial and kinematic correlations between tracks originating from the same b -hadron. A multivariate b -tagging discriminant value is calculated for each jet. The b -tagged jets are required to satisfy the working point (WP) corresponding to an efficiency of 70% or 85% for identifying b -quark initiated jets in $t\bar{t}$ simulated events for the single-lepton and dilepton channels, respectively. For the 70% (85%) WP the rejection factors against light-quark/gluon jets and c -quark jets are 625 and 12 (40 and 3), respectively. To fully exploit the b -tagging information of an event, each jet is assigned a b -tagging score that defines if a jet satisfies a given WP but fails to satisfy the adjacent tighter one. Scores from two to five are assigned to jets satisfying WPs from 85% to 60%. If a jet does not pass any WP, a score of one is assigned. In addition to the standard JES calibration, b -tagged jets satisfying the 85% WP receive additional flavour-specific corrections to their four-vectors to improve their energy measurement (scale and resolution) following the *muon-in-jet* procedure described in Ref. [83].

Hadronically decaying τ -leptons (τ_{had}) are distinguished from jets using their track multiplicity and a multivariate discriminant based on their shower shapes in calorimeter and on tracking information [84]. They are required to have $p_T > 25$ GeV and $|\eta| < 2.5$, and to pass the *Medium* τ -lepton identification working point.

The missing transverse momentum vector, with magnitude E_T^{miss} , is defined as the negative sum of the transverse momenta of the reconstructed and calibrated physical objects, plus a ‘soft term’ built from all other tracks associated with the primary vertex [85] and not matched to a reconstructed object.

Targeting event topologies with a Higgs boson decaying into collimated hadronic final states, reclustered (RC) jets [86] are reconstructed from the selected jets, using the anti- k_r jet clustering algorithm with a radius parameter $R = 1.0$. RC jets are required to have an invariant mass $M > 50$ GeV, $p_T > 200$ GeV, $|\eta| < 2.0$, have at least two constituent small- R jets (subjets) and have an angular distance $\Delta R > 1.0$ from all electrons.

An overlap removal procedure is applied to avoid the double counting of detector signatures. Electron candidates sharing a track with a muon candidate are first removed. Jets found within a $\Delta R = 0.2$ cone of an electron are removed and electrons within a $\Delta R = 0.4$ cone of a remaining jet are rejected. Jets with less than three associated tracks and within $\Delta R = 0.2$ of a muon and muons within $\Delta R = 0.4$ of a jet with

more than two associated tracks are rejected. A τ_{had} candidate is rejected if it is separated by $\Delta R < 0.2$ from any selected electron or muon. No overlap removal is performed between jets and τ_{had} candidates.

Events are selected if they contain exactly one lepton candidate in the single-lepton channel and exactly two lepton candidates with opposite electric charges in the dilepton channel. At least one lepton should have $p_{\text{T}} > 27$ GeV and be matched to the corresponding object at the trigger level. In the events with two electrons, the second lepton is required to have $p_{\text{T}} > 15$ GeV while in the other two dilepton channels, $e\mu$ and $\mu\mu$, it must have $p_{\text{T}} > 10$ GeV. In events with two electrons or two muons, the dilepton invariant mass is required to be above 15 GeV, to suppress contribution from the decays of heavy-flavour resonances and low-mass Drell–Yan processes, and be outside a window of ± 8 GeV centered at the Z boson mass. To maintain orthogonality with other $t\bar{t}H$ decay channels, events are vetoed if they contain one or more (two or more) τ_{had} candidates in the dilepton (single-lepton) channel.

To reduce the non-prompt and mis-identified lepton background contribution, additional lepton identification and isolation requirements are applied. Electrons (muons) are required to satisfy the *TightLH* [76] (*Medium* [77]) identification criteria and the *FCTight* (*TightTrackOnly_VarRad*) isolation criteria [76, 77]. Events for which the leptons fail to meet these requirements are removed.

In the single-lepton channel two event categories are defined, referred in the following as resolved and boosted categories. The latter is designed to select events in which the Higgs boson is produced with high transverse momentum as a collimated large- R jet. Events that do not satisfy the boosted category selection are assigned to the resolved one. In the single-lepton resolved channel, events are selected if they contain at least five jets, at least three of which satisfy the 70% b -tagging WP. In the single-lepton boosted channel, events are required to have at least one large- R jet and at least four small- R jets, including those contained within the large- R jet, at least three of which must satisfy the 85% b -tagging WP. In the dilepton channel, events are selected if they contain at least three jets satisfying the 85% b -tagging WP, and among these at least two jets that satisfy the 70% b -tagging WP. These requirements are henceforth referred to as “preselection” and have an acceptance of 6.3% for selecting $t\bar{t}H$ events with $H \rightarrow b\bar{b}$ decay, an acceptance that is more than a factor of three larger than in the previous analysis [20]. The corresponding acceptance in the signal regions is 2.1%.

5 Background modelling

The largest background from $t\bar{t}$ + jets production is modelled by MC simulation with the data-driven corrections described in Section 5.1. Small backgrounds include single top production, $t\bar{t}W$, $t\bar{t}Z$, $t\bar{t}t\bar{t}$, rare top-quark processes and non-top-quark processes such as V + jets and diboson production. All of them are estimated from simulations. The contribution from the background arising from non-prompt or mis-identified leptons is determined from data in the single-lepton channel (see Section 5.2), and from MC simulation in the dilepton channel, where this background arises primarily from $t\bar{t}$ events with one prompt lepton and is very small.

5.1 Modelling of $t\bar{t}$ + jets background

The $t\bar{t}$ sample used to model the $t\bar{t}$ + light and $t\bar{t}$ + $\geq 1c$ contributions is generated at NLO as described in Section 3, with up to one additional parton from the ME calculation. All jets not originating from the decay chain of one of the top quarks, i.e. additional jets, are produced by the parton shower. The dedicated

measurement [87] demonstrated deficiencies in modelling the number of additional jets in the $t\bar{t}$ events and the scalar sum of the transverse momenta of the top quarks. Moreover, the rate of $t\bar{t}$ production in association with c - and b -jets was observed to be underestimated in the previous analysis [20]. The new $t\bar{t}b\bar{b}$ MC sample produced for this analysis with lower value of the renormalisation scale than the one used in Ref. [20] predicts larger inclusive $t\bar{t} + \geq 1b$ cross-section, which is expected to match data well. Nevertheless, the rate of the components of the $t\bar{t} + \geq 1b$ background defined in Section 3, $t\bar{t} + 1B$, $t\bar{t} + 1b$ and $t\bar{t} + \geq 2b$, could still be mismodelled. Thus, to obtain a reliable estimate of the $t\bar{t} + \text{jets}$ background, the $t\bar{t}$ MC events are reweighted using data. The corrections applied include a rescaling of the $t\bar{t} + \text{jets}$ flavour components followed by a kinematic reweighting and are described in the next paragraph. Any possible residual mismodelling is accounted for by the systematic uncertainties in the profile likelihood fit used for the extraction of the signal strength which is described in Section 6.

Initial scaling factors for the five $t\bar{t} + \text{jets}$ flavour components, $t\bar{t} + \text{light}$, $t\bar{t} + \geq 1c$, $t\bar{t} + 1B$, $t\bar{t} + 1b$ and $t\bar{t} + \geq 2b$, are obtained separately for the single-lepton and dilepton channels from the profile-likelihood fit to data. The fit is performed in background-dominated control regions including all systematic uncertainties (see Section 7). These scaling factors have similar values to those shown in Table 5. Following the flavour components rescaling, a reweighting is used to mitigate the kinematic mismodelling of the scalar sum of the p_T 's of the reconstructed leptons and jets, H_T , observed for the $t\bar{t} + \text{light}$ and $t\bar{t} + \geq 1c$ components of the inclusive $t\bar{t} + \text{jets}$ POWHEG + PYTHIA8 sample. The $t\bar{t} + \geq 1b$ component is excluded from the reweighting since it is simulated by a dedicated $t\bar{t}b\bar{b}$ MC sample. Thus the reweighting derived in the regions dominated by $t\bar{t} + \text{light}$ and $t\bar{t} + \geq 1c$ might not be applicable to $t\bar{t} + \geq 1b$. A dedicated reweighting was investigated for the $t\bar{t} + \geq 1b$ component but found to have a negligible effect and is not used in the analysis.

The reweighting corrects the distributions of H_T in exclusive jet multiplicity bins from $N_{\text{jets}} = 5$ to $N_{\text{jets}} \geq 8$ in the single-lepton channel and from $N_{\text{jets}} = 3$ to $N_{\text{jets}} \geq 6$ in the dilepton channel. It is derived in $t\bar{t}$ enriched regions selected by using looser b -tagging requirements after subtracting from data all contributions except for $t\bar{t} + \text{light}$ and $t\bar{t} + \geq 1c$ and taking the ratio of data to the sum of $t\bar{t} + \text{light}$ and $t\bar{t} + \geq 1c$ yields predicted by MC in each H_T bin. These regions are orthogonal to the signal and control regions of the analysis and contain less than 0.2% of signal.

The reweighting factors are also derived in the same way for each systematic variation affecting the $t\bar{t} + \text{light}$ and $t\bar{t} + \geq 1c$ predictions, such that all systematic variations match the H_T distribution in data.

5.2 Non-prompt or mis-identified lepton background

A data-driven method, referred to as ‘‘fake factor’’ method [88], based on the measurement of lepton selection efficiencies using different identification and isolation criteria, is used to estimate the non-prompt or mis-identified (fake) lepton background in the single-lepton channel.

The fake rate is measured in a fake-dominated region selected by requiring exactly one lepton with loose identification and isolation criteria, at least two jets, at least two b -tagged jets satisfying the 70% WP, and a scalar sum of missing transverse energy and the leptonically-decaying W boson mass below 60 GeV. It is parameterised as a function of the leading jet p_T and the lepton $|\eta|$. The expected number of events arising from the fake lepton background is determined by applying the measured lepton fake rate to data events satisfying the selection requirements of each analysis region except that the lepton is required to pass loose identification and isolation criteria and to fail the tighter requirements.

6 Signal extraction

After the preselection, events are classified into non-overlapping background-dominated or control regions (CR) and signal-enriched regions (SR) with higher signal-to-background ratios. The CRs provide stringent constraints on the normalisation of the backgrounds and the systematic uncertainties in a combined fit with the signal regions.

To define the regions in the single-lepton and dilepton channels, a multiclass classification neural network based on the permutation-invariant transformer architecture with attention mechanism [89] is trained to predict the probability of an event to be from the $t\bar{t}H$ signal or from one of the five $t\bar{t} + \text{jets}$ background categories introduced in Section 3: $t\bar{t} + 1b$, $t\bar{t} + 1B$, $t\bar{t} + \geq 2b$, $t\bar{t} + \geq 1c$, $t\bar{t} + \text{light jets}$. The probability p_i of a network class i is converted into a discriminant d_i in order to maximise the separation between the class and all the other classes ($i \neq j$), to yield a similar number of events in the $t\bar{t} + 1b$, $t\bar{t} + 1B$, and inclusive $t\bar{t} + \geq 2b$ control regions, and to maximise sensitivity. They are defined as

$$d_i = \frac{p_i}{\sum_{j \neq i} p_j \cdot \hat{N}_{ij}}. \quad (1)$$

Here, the denominator of each discriminant is a weighted average of all the remaining class probabilities $p_{j \neq i}$. The weights $\hat{N}_{ij} = N_j / \sum_{k \neq i} N_k$ are the respective fractions of event yields N_j relative to the total yield of all the remaining classes $k \neq i$. These yields are determined from MC simulation after the preselection and incorporate the $t\bar{t} + \text{jets}$ scaling factors described in Section 5.1.

In the single-lepton (dilepton) channel, events fulfilling $d_{t\bar{t}H} > 4.072$ ($d_{t\bar{t}H} > 9.031$) are assigned to the signal region. The thresholds are defined to maximize the ratio of signal to the square root of the background in the inclusive signal regions. All other events are assigned to the $t\bar{t} + \text{jets}$ background category with the highest value of the discriminant. By far the dominant Higgs boson decay mode in the signal region is $H \rightarrow b\bar{b}$ with a fraction of more than 97% (94%) of the $t\bar{t}H$ events in the single-lepton (dilepton) channel followed by the $H \rightarrow WW$ decay. This motivates the training of a second neural network, based on the same architecture to identify the two jets most likely originating from the Higgs boson decay, to reconstruct p_T^H that is used to further classify the signal region events into the six reconstructed STXS regions. The boundaries of the regions are optimised to maximise fraction of the events with the corresponding truth p_T^H , listed in Figure 1, separately per $t\bar{t}$ decay channel to capture potential differences due to the final states and separate neural networks. This optimisation leads, in particular, to improved purity in the highest truth p_T^H bins, the region of the phase space where this analysis provides a particularly valuable contribution to the global Higgs boson combination. The optimal reconstructed p_T^H boundaries are found to be [0, 60, 114, 186, 270, 402, ∞] GeV in the dilepton channel and [0, 60, 114, 192, 282, 408, ∞] GeV in the single-lepton resolved channel. They are referred to in the following as STXS 1–6 regions.

The inclusive control region dominated by the $t\bar{t} + \geq 2b$ background in the single-lepton channel is further split into three categories encompassing STXS regions 1–2, 3–4, and 5–6, to ensure a good control of the $t\bar{t} + \geq 2b$ background modelling over the bins of reconstructed Higgs boson p_T . These regions are henceforth referred to as $t\bar{t} + \geq 2b$ CR 1, CR 2, and CR 3. The split is not applied in the dilepton channel due to limited statistics.

Events fulfilling the boosted selection criteria are assigned to dedicated boosted signal and control regions.

RC jets are used as input to a multiclass deep neural network (DNN), trained to distinguish high- p_T Higgs boson candidates decaying into collimated final states from top quarks and multijet backgrounds following the same strategy as in the previous analysis [20]. An event is flagged as containing a boosted Higgs boson

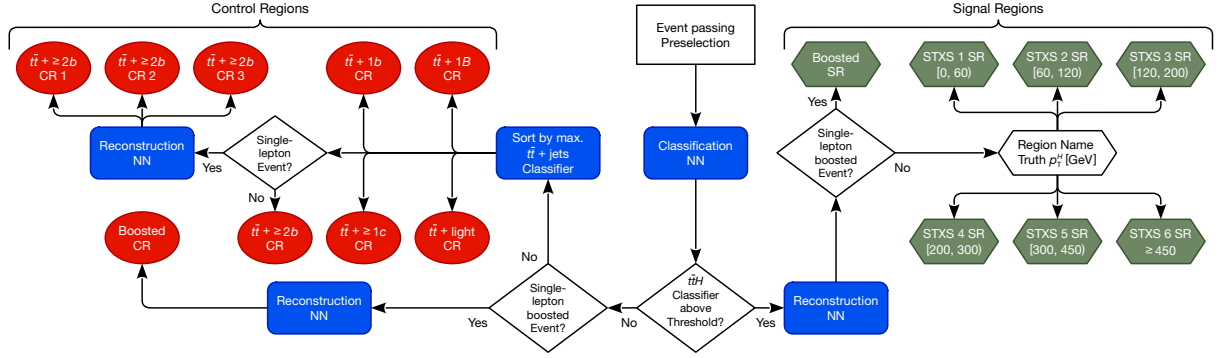


Figure 1: Flowchart depicting the event classification and Higgs boson p_T reconstruction strategy used in the analysis.

candidate if one of the RC jets has a high probability of originating from a Higgs boson, as estimated by the DNN. Boosted Higgs boson candidates are required to have $p_T \geq 300$ GeV, a mass consistent with the Higgs boson mass window of 100 GeV to 140 GeV, contain at least two subjects, of which exactly two are required to satisfy the b -tagging 85% WP, and have a DNN score above 0.4. At least two small- R jets that do not form the Higgs boson candidate are required to satisfy the b -tagging 77% WP.

The flowchart in Figure 1 summarises the event classification strategy.

The transformer networks are trained using low-level features of the reconstructed jets, electrons, muons, and the missing transverse momentum of the event. For each reconstructed object, the kinematic features used are the x -, y - and z -component of the momentum (p_x , p_y , p_z), the energy, the p_T , the mass, the pseudorapidity, the azimuthal angle and its sine and cosine. Supplying redundant four-vector information is observed to improve network performance. Additionally, the DL1r pseudo-continuous b -tagging score is included for jets, and the electric charge and a variable indicating if it is an electron or a muon is included for leptons.

The multiclass event-classification network is trained using events sampled from the nominal and alternative $t\bar{t}H$ and $t\bar{t} + \text{jets}$ background samples to profit from an increased number of events in training. The classification network yields an area under the receiver-operator characteristic curve (AUC) of 0.753 (0.774) for discriminating between $t\bar{t}H$ and the $t\bar{t} + \geq 1b$ background for events satisfying the preselection in the single-lepton resolved (dilepton) channel. The Higgs boson p_T reconstruction network is trained using only the $t\bar{t}H$ samples. Figure 2 shows for each bin of truth p_T^H the fraction of $t\bar{t}H$ events assigned to each of the STXS signal regions.

In the single-lepton channel, a total of 15 analysis regions are defined, including six STXS signal regions, two boosted regions (signal and control) and seven control regions targeting the different components of the $t\bar{t} + \text{jets}$ background. In the dilepton channel, a total of 11 analysis regions are defined, including the six STXS signal regions and five $t\bar{t} + \text{jets}$ control regions. The expected yields in the single-lepton (dilepton) signal and control regions are summarised in Tables 1 and 2 (3 and 4) after applying the data-driven corrections to the $t\bar{t} + \text{jets}$ background discussed in Section 5.1.

The $t\bar{t}H$ inclusive signal strength, $\mu_{t\bar{t}H}$, defined as the ratio of the measured $t\bar{t}H$ cross-section including all Higgs boson decay modes to the corresponding SM prediction, or the signal strengths in each of the six STXS bins, μ_i , and the normalisation factors of the components of the $t\bar{t} + \text{jets}$ background are determined via a binned likelihood fit to the distributions in all signal and control regions defined above. The $t\bar{t}H$ signal sample is split up according to the true p_T^H in each event, and the μ_i act on the respective component. In the

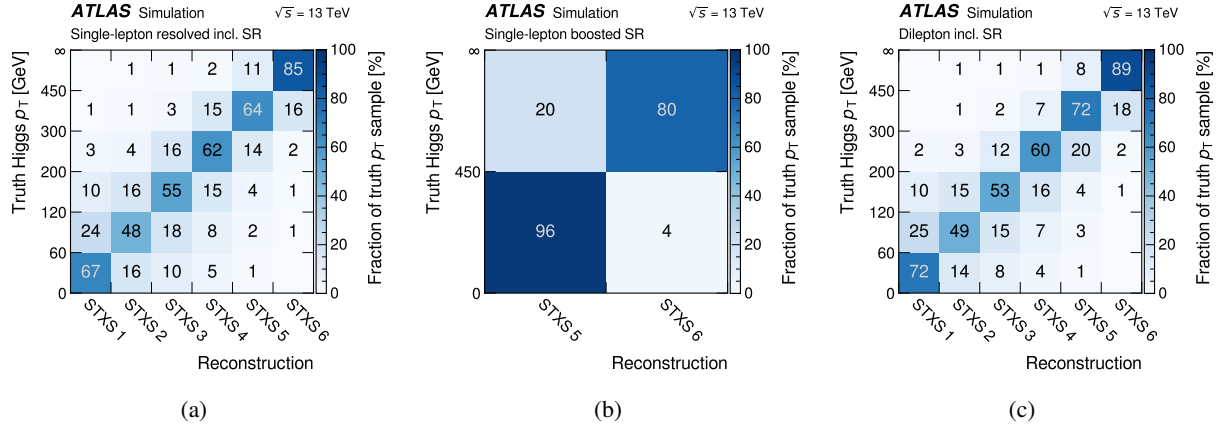


Figure 2: STXS migration matrices for the $t\bar{t}H$ signal regions in (a) the single-lepton resolved, (b) the single-lepton boosted, and (c) the dilepton channel. The yield fractions of the predicted STXS bins are normalised per truth STXS sample.

resolved signal and control regions, the corresponding discriminant distribution is used in the likelihood fit, while in the boosted regions, event yields in two bins of the reconstructed p_T^H distribution, 300–450 GeV and ≥ 450 GeV, are used in the fit.

The $t\bar{t} + 1b$, $t\bar{t} + \geq 1c$ and $t\bar{t} + \text{light}$ normalisation factors are chosen to float independently in the single-lepton and dilepton channels, while the normalisations of the $t\bar{t} + \geq 2b$ and $t\bar{t} + 1B$ backgrounds are scaled in a correlated way between the two channels. This choice is made based on studies of the different correlation assumptions between the normalisation factors in the combined fit. The chosen configuration provides enough freedom for the fit model and minimises pulls and constraints of the nuisance parameters in the fit to data.

The inclusive measurement of the signal strength and cross-section is performed in the full phase space. The measurement of these parameters in STXS bins is carried out for $t\bar{t}H$ events with a Higgs boson produced centrally within $|y| \leq 2.5$ at truth level, while the remaining forward events are considered as background.

The statistical model is based on a likelihood function built with HistFactory [90] as the product over every bin of the Poisson probability for the observed data, given the SM prediction. The value of each nuisance parameter, describing the systematic uncertainties for both signal and background processes (see Section 7), is constrained by a Gaussian penalty term present in the likelihood function, while all normalisation factors are unconstrained. The statistical uncertainty arising from the limited number of simulated events is included in the likelihood in the form of additional nuisance parameters with Poisson constraint terms. The maximum-likelihood fit is performed with the RooFit package [91]. A test statistic based on the profile likelihood ratio is used to assess the compatibility of the observed data with the background-only hypothesis ($\mu = 0$) [92].

Tests of the statistical model fitted to pseudodata constructed with the SHERPA $t\bar{t} + \text{jets}$ samples were performed to help inform the choice of fit variables and uncertainty model, with the goal of minimising bias, maximising robustness and optimising sensitivity.

Table 1: Expected yields in the single-lepton signal regions before the fit to data. The data-driven corrections to the $t\bar{t}$ + jets background are applied and all uncertainties are included, except the ones associated with the $t\bar{t}$ + jets background normalisation factors, which are not defined pre-fit. The “Other” category includes the s - and t -channel single-top, tZq and tWZ processes. The $t\bar{t}H$ signal is normalised to the SM $t\bar{t}H$ cross-section. For presentation purposes, uncertainties are symmetrised.

	STXS 1 SR	STXS 2 SR	STXS 3 SR	STXS 4 SR	STXS 5 SR	STXS 6 SR	Boosted SR
$t\bar{t}H$ truth p_T^H 0–60 GeV	77 ± 12	18.7 ± 3.2	11.1 ± 2.3	5.7 ± 1.0	1.66 ± 0.2	0.42 ± 0.09	0.58 ± 0.13
$t\bar{t}H$ truth p_T^H 60–120 GeV	49 ± 5	99 ± 13	37 ± 6	15.5 ± 2.2	4.4 ± 0.5	1.25 ± 0.19	1.54 ± 0.25
$t\bar{t}H$ truth p_T^H 120–200 GeV	22.7 ± 2.2	37 ± 4	125 ± 16	34 ± 5	8.1 ± 1.3	2.0 ± 0.4	2.31 ± 0.28
$t\bar{t}H$ truth p_T^H 200–300 GeV	4.0 ± 0.5	5.5 ± 0.7	22.5 ± 2.9	88 ± 12	19.4 ± 3.0	2.7 ± 0.4	3.3 ± 0.6
$t\bar{t}H$ truth p_T^H 300–450 GeV	0.39 ± 0.11	0.64 ± 0.16	1.4 ± 0.4	7.6 ± 1.3	32 ± 5	8.0 ± 1.3	20 ± 3
$t\bar{t}H$ truth p_T^H ≥ 450 GeV	<0.1	<0.1	0.14 ± 0.06	0.21 ± 0.09	1.30 ± 0.31	9.8 ± 1.8	6.9 ± 1.3
$t\bar{t}H$ $ y > 2.5$	0.16 ± 0.06	0.10 ± 0.04	<0.1	<0.1	<0.1	<0.1	<0.1
$t\bar{t}$ + $\geq 2b$	870 ± 80	870 ± 90	980 ± 100	640 ± 60	270 ± 40	92 ± 21	103 ± 8
$t\bar{t}$ + $1b$	210 ± 60	210 ± 50	250 ± 80	180 ± 60	78 ± 28	25 ± 9	17 ± 5
$t\bar{t}$ + $1B$	64 ± 19	73 ± 24	100 ± 40	87 ± 30	46 ± 19	22 ± 11	11 ± 4
$t\bar{t}$ + $\geq 1c$	210 ± 50	210 ± 50	250 ± 50	190 ± 50	88 ± 24	27 ± 13	22 ± 8
$t\bar{t}$ + light	42 ± 16	45 ± 12	68 ± 22	64 ± 19	31 ± 11	12 ± 11	3.2 ± 3
$t\bar{t}Z$	36 ± 6	38 ± 6	53 ± 8	43 ± 8	24 ± 5	7.2 ± 1.1	5.8 ± 1.2
tW	20 ± 8	35 ± 12	60 ± 33	55 ± 32	33 ± 25	17 ± 15	5 ± 4
W + jets	10 ± 6	12 ± 8	30 ± 15	29 ± 14	23 ± 12	12 ± 6	3.7 ± 1.9
$t\bar{t}W$	4.2 ± 0.5	5.9 ± 0.8	9.8 ± 1.6	8.9 ± 1.9	5.6 ± 0.7	3.2 ± 0.5	1.06 ± 0.26
Z + jets	2.5 ± 1.1	5.1 ± 2	6.5 ± 2.6	7.4 ± 2.7	3.1 ± 1.1	1.7 ± 0.6	0.5 ± 0.2
Diboson	1.3 ± 0.8	2.5 ± 1.40	4.4 ± 2.3	4.7 ± 2.7	3.1 ± 1.6	1.4 ± 0.7	0.7 ± 0.4
$t\bar{t}t\bar{t}$	5.1 ± 2.2	6.7 ± 3	11 ± 5	9 ± 4	4.8 ± 2.1	2.5 ± 1.1	1.1 ± 0.5
$tHj\bar{b}$	0.77 ± 0.22	1.06 ± 0.21	1.61 ± 0.32	1.58 ± 0.28	1.11 ± 0.30	0.26 ± 0.12	0.72 ± 0.14
tWH	1.68 ± 0.23	2.16 ± 0.27	3.8 ± 0.4	4.1 ± 0.5	2.22 ± 0.25	1.03 ± 0.12	1.01 ± 0.11
Other	11.3 ± 1.2	11 ± 1.5	14.4 ± 2	11.9 ± 1.5	7.3 ± 1.1	2.43 ± 0.35	2.2 ± 0.6
Fakes	29 ± 12	29 ± 15	27 ± 12	31 ± 19	22 ± 13	3.8 ± 2.5	8 ± 5
Total	1670 ± 160	1710 ± 170	2060 ± 210	1520 ± 150	710 ± 80	250 ± 40	221 ± 19
Data	1672	1657	2016	1441	676	241	216

7 Systematic uncertainties

Multiple sources of systematic uncertainty, arising from detector effects, theoretical assumptions and the limited number of events in the MC simulations, are considered in the analysis. They affect the categorisation of events as well as the normalisation and shape of the distributions used in the signal extraction fit.

All the sources of experimental uncertainty, except the uncertainty in the integrated luminosity, affect both the normalisations and the shapes of the distributions in all simulated samples. The uncertainty in the integrated luminosity is 0.83% [93], obtained using the LUCID-2 detector [26] for the primary luminosity measurements, complemented by measurements using the inner detector and calorimeters. The uncertainty in the pile-up modelling is obtained by varying the pile-up reweighting in the simulation within its uncertainties.

The correction factors applied to the simulated samples to improve the description of the lepton reconstruction, identification and isolation efficiencies, momentum scale and resolution, and lepton trigger efficiencies are varied within their uncertainties [76, 77] to estimate the corresponding systematic uncertainty.

The JES uncertainty [81] accounts for contributions from jet-flavour composition, η -intercalibration, punch-through, single-particle response, calorimeter response to different jet flavours, and pile-up, resulting in 31 uncorrelated JES uncertainty components. The jet energy resolution was measured separately for data

Table 2: Expected yields in the single-lepton control regions before the fit to data. The data-driven corrections to the $t\bar{t}$ + jets background are applied and all uncertainties are included, except the ones associated with the $t\bar{t}$ + jets background normalisation factors, which are not defined pre-fit. The ‘‘Other’’ category includes the s - and t -channel single-top, tZq and tWZ processes. The $t\bar{t}H$ signal is normalised to the SM $t\bar{t}H$ cross-section. For presentation purposes, uncertainties are symmetrised.

	$t\bar{t}$ + light CR	$t\bar{t}$ + $\geq 1c$ CR	$t\bar{t}$ + $1b$ CR	$t\bar{t}$ + $1B$ CR	$t\bar{t}$ + $\geq 2b$ CR 1	$t\bar{t}$ + $\geq 2b$ CR 2	$t\bar{t}$ + $\geq 2b$ CR 3	Boosted CR
$t\bar{t}H$ truth p_T^H 0–60 GeV	56 ± 6	59 ± 7	89 ± 11	46 ± 6	80 ± 10	12.5 ± 1.7	2.09 ± 0.26	0.54 ± 0.14
$t\bar{t}H$ truth p_T^H 60–120 GeV	86 ± 5	98 ± 8	133 ± 12	92 ± 13	112 ± 11	33 ± 5	4.5 ± 0.9	1.15 ± 0.23
$t\bar{t}H$ truth p_T^H 120–200 GeV	59 ± 4	76 ± 7	76 ± 8	88 ± 11	41 ± 4	68 ± 8	5.4 ± 1.1	1.36 ± 0.28
$t\bar{t}H$ truth p_T^H 200–300 GeV	23 ± 2.5	31.9 ± 3.5	21.2 ± 3.1	41 ± 5	7.3 ± 1.1	34 ± 4	6.7 ± 1.1	1.42 ± 0.32
$t\bar{t}H$ truth p_T^H 300–450 GeV	7.7 ± 1.0	10 ± 1.5	4.7 ± 0.8	14.3 ± 2	1.12 ± 0.27	4.4 ± 0.8	9.8 ± 1.5	4.8 ± 0.7
$t\bar{t}H$ truth $p_T^H \geq 450$ GeV	1.67 ± 0.27	2.4 ± 0.5	0.78 ± 0.19	4.1 ± 0.7	0.18 ± 0.05	0.35 ± 0.12	3 ± 0.7	1.75 ± 0.32
$t\bar{t}H$ $ \eta > 2.5$	0.98 ± 0.08	0.72 ± 0.17	1.38 ± 0.22	0.57 ± 0.15	0.37 ± 0.05	0.188 ± 0.029	<0.1	<0.1
$t\bar{t}$ + $\geq 2b$	2320 ± 280	3800 ± 400	5400 ± 600	3500 ± 400	7200 ± 600	4900 ± 500	1140 ± 170	141 ± 10
$t\bar{t}$ + $1b$	3900 ± 400	4600 ± 700	10600 ± 1700	5100 ± 600	2100 ± 500	1120 ± 320	230 ± 100	54 ± 19
$t\bar{t}$ + $1B$	890 ± 80	1390 ± 270	1780 ± 270	5100 ± 400	530 ± 190	380 ± 140	100 ± 50	32 ± 7
$t\bar{t}$ + $\geq 1c$	17000 ± 3300	17900 ± 2600	7800 ± 1000	5400 ± 1300	2500 ± 500	1220 ± 270	240 ± 70	133 ± 35
$t\bar{t}$ + light	31800 ± 3500	5900 ± 1100	4000 ± 600	2000 ± 500	700 ± 180	320 ± 110	49 ± 26	34 ± 8
$t\bar{t}Z$	152 ± 20	171 ± 25	151 ± 21	146 ± 22	122 ± 18	117 ± 15	36 ± 5	5.7 ± 0.9
tW	1040 ± 200	750 ± 220	820 ± 240	560 ± 190	350 ± 140	360 ± 150	130 ± 90	10 ± 6
W + jets	370 ± 180	370 ± 180	230 ± 120	170 ± 80	370 ± 190	250 ± 130	90 ± 40	5.6 ± 2.9
$t\bar{t}W$	100 ± 12	114 ± 17	43 ± 7	44 ± 5	25.6 ± 3.5	26 ± 5	10.5 ± 1.6	1.97 ± 0.33
Z + jets	110 ± 40	110 ± 40	110 ± 40	64 ± 23	100 ± 40	55 ± 20	16 ± 6	0.9 ± 0.4
Diboson	37 ± 19	39 ± 20	23 ± 12	21 ± 11	24 ± 13	23 ± 12	10 ± 5	1.1 ± 0.7
$t\bar{t}t\bar{t}$	2.9 ± 1.2	24 ± 10	7.1 ± 3	19 ± 8	21 ± 9	33 ± 14	17 ± 7	1.4 ± 0.6
$tHjb$	8.2 ± 1.4	5.4 ± 0.9	8.1 ± 1.6	3.5 ± 0.6	5.4 ± 1.1	3.6 ± 0.7	0.53 ± 0.15	0.65 ± 0.20
tWH	7.1 ± 0.7	6.7 ± 0.7	9.6 ± 1	5.7 ± 0.6	5.4 ± 0.6	5.8 ± 0.7	1.78 ± 0.2	0.44 ± 0.07
Other	370 ± 40	370 ± 40	303 ± 35	228 ± 22	179 ± 22	111 ± 12	27.4 ± 2.8	3.9 ± 0.9
Fakes	810 ± 300	800 ± 400	880 ± 350	340 ± 140	660 ± 300	280 ± 130	57 ± 32	6.3 ± 3.3
Total	59000 ± 6000	37000 ± 4000	32500 ± 2900	22900 ± 2200	15200 ± 1700	9400 ± 1000	2190 ± 270	440 ± 50
Data	61954	36528	32887	23245	15595	9397	2097	426

and MC using two in situ techniques [81]. The systematic uncertainty is defined as the quadratic difference between the jet energy resolutions for data and simulation and split into 13 uncorrelated uncertainty components. The uncertainty associated with the JVT discriminant is obtained by varying the efficiency correction factors [80].

The uncertainties associated with the b -tagging algorithm calibration are derived separately for b -jets, c -jets and light-flavour jets, as a function of the jet p_T , and decomposed into several uncorrelated components for each category, corresponding to the number of p_T bins multiplied by the number of DL1r pseudo-continuous scores [94–96]. This yields a total of 45 components for b -jets and 20 each for c - and light jets. For jets with a p_T above the p_T threshold where the b -tagging algorithm is calibrated, high- p_T extrapolation uncertainties derived using MC simulation are included.

The uncertainty in E_T^{miss} results from the propagation of the uncertainties in the energy scales and resolutions of photons, leptons and jets, and from the modelling of its soft term [85].

For the $t\bar{t}H$ signal, two cross-section uncertainties are applied accounting for the effect of varying the PDF and α_S and for missing higher order terms in the fixed order perturbative QCD calculations. They amount to $\pm 3.6\%$ and $\pm 9.2\%$, respectively [18]. The systematic uncertainty in the $t\bar{t}H$ cross-section includes theory uncertainties due to migrations of events between the truth Higgs boson p_T bins [97]. An uncertainty of 2.2% is assigned to the $H \rightarrow b\bar{b}$ branching fraction [18]. Two uncertainties due to missing higher order terms in the MC simulation are estimated by varying independently the renormalisation and factorisation scales in the ME of the nominal MC sample by a factor of two up and down. The uncertainties in the amount of initial- and final-state QCD radiation (ISR and FSR) predicted by the PS are estimated by varying

Table 3: Expected yields in the dilepton signal regions before the fit to data. The data-driven corrections to the $t\bar{t}$ +jets background are applied and all uncertainties are included, except the ones associated with the $t\bar{t}$ +jets background normalisation factors, which are not defined pre-fit. The “Other” category includes the tZq , tWZ and diboson processes. The $t\bar{t}H$ signal is normalised to the SM $t\bar{t}H$ cross-section. For presentation purposes, uncertainties are symmetrised.

	STXS 1 SR	STXS 2 SR	STXS 3 SR	STXS 4 SR	STXS 5 SR	STXS 6 SR
$t\bar{t}H$ truth p_T^H 0–60 GeV	10.6 ± 1.5	2.03 ± 0.31	1.14 ± 0.17	0.63 ± 0.11	0.19 ± 0.07	0.046 ± 0.023
$t\bar{t}H$ truth p_T^H 60–120 GeV	6.5 ± 0.7	13.0 ± 1.8	4.1 ± 0.7	1.9 ± 0.4	0.7 ± 0.11	0.13 ± 0.07
$t\bar{t}H$ truth p_T^H 120–200 GeV	3.06 ± 0.34	4.7 ± 0.5	16.3 ± 2.0	5.0 ± 0.7	1.36 ± 0.19	0.24 ± 0.07
$t\bar{t}H$ truth p_T^H 200–300 GeV	0.5 ± 0.07	0.72 ± 0.08	2.5 ± 0.29	13.0 ± 1.7	4.4 ± 0.6	0.41 ± 0.06
$t\bar{t}H$ truth p_T^H 300–450 GeV	<0.1	<0.1	0.197 ± 0.033	0.82 ± 0.18	8.0 ± 1.1	1.98 ± 0.32
$t\bar{t}H$ truth $p_T^H \geq 450$ GeV	<0.1	<0.1	<0.1	<0.1	0.26 ± 0.08	2.8 ± 0.5
$t\bar{t}H$ $ y > 2.5$	<0.1	<0.1	<0.1	<0.1	<0.1	<0.1
$t\bar{t} + \geq 2b$	81 ± 8	76 ± 7	81 ± 13	59 ± 4	36.2 ± 3.0	11.7 ± 2.1
$t\bar{t} + 1b$	14 ± 5	15 ± 6	20 ± 9	17 ± 5	11 ± 6	2.9 ± 1.9
$t\bar{t} + 1B$	4.4 ± 2.6	4.8 ± 3.2	5.7 ± 2.3	6.2 ± 1.9	6.6 ± 2.9	3.5 ± 2.3
$t\bar{t} + \geq 1c$	11.3 ± 2.4	11.7 ± 2.6	15.4 ± 3.4	12.5 ± 2.6	7.1 ± 2.6	3.0 ± 1.7
$t\bar{t}$ + light	1.1 ± 0.7	0.9 ± 0.5	1.4 ± 0.8	1.0 ± 0.5	1.0 ± 0.4	0.37 ± 0.30
$t\bar{t}Z$	4.6 ± 0.7	4.6 ± 1.1	7.2 ± 1.1	6.2 ± 1.3	5.3 ± 1.1	2 ± 0.6
$t\bar{t}W$	1.7 ± 0.8	3 ± 1.8	6 ± 4	8 ± 5	7 ± 5	3.1 ± 2.9
$t\bar{t}W$	0.65 ± 0.11	1.18 ± 0.15	2.1 ± 0.23	2.64 ± 0.3	2.7 ± 0.4	1.2 ± 0.5
Z + jets	1.8 ± 0.9	1.9 ± 0.9	3.4 ± 1.3	3.8 ± 1.4	3.3 ± 1.2	1.8 ± 0.7
$t\bar{t}t\bar{t}$	0.9 ± 0.4	1.1 ± 0.5	1.8 ± 0.7	1.7 ± 0.7	1.3 ± 0.6	0.65 ± 0.28
$t\bar{t}WH$	0.23 ± 0.04	0.31 ± 0.04	0.57 ± 0.07	0.7 ± 0.08	0.66 ± 0.07	0.24 ± 0.03
Other	<0.1	<0.1	0.28 ± 0.14	0.42 ± 0.19	0.23 ± 0.08	0.29 ± 0.13
Fakes	1.7 ± 0.9	2.2 ± 1.1	3.2 ± 1.6	2.9 ± 1.5	2.6 ± 1.3	1.1 ± 0.6
Total	144 ± 13	144 ± 13	173 ± 20	143 ± 12	100 ± 11	38 ± 6
Data	150	149	161	149	76	35

the scale in α_S^{ISR} according to the values given by *var3c* in the PYTHIA8 A14 tune and by varying the scale in α_S^{FSR} by a factor two up and down. To assess the uncertainties associated with the PS, hadronisation and underlying event, the nominal $t\bar{t}H$ sample is compared with the alternative POWHEG+HERWIG7 sample, while the uncertainty due to the NLO matching procedure is estimated with POWHEG+PYTHIA8 with a varied p_T^{hard} parameter value.

All the modelling uncertainties in the $t\bar{t}$ +jets background have independent nuisance parameters for the $t\bar{t} + 1b$, $t\bar{t} + 1B$, $t\bar{t} + \geq 2b$, $t\bar{t} + \geq 1c$ and $t\bar{t}$ +light processes. These systematic variations are normalised to conserve the total nominal event count after the preselection for each process. Uncertainties due to missing higher order terms in the perturbative QCD calculations, in the amount of ISR and FSR as well as the uncertainties associated with the PS and hadronisation, and with the NLO matching procedure are estimated in the same way as for the $t\bar{t}H$ signal.

For $t\bar{t} + \geq 1b$, the choice of recoil scheme in the ISR PS has a sizeable effect in the normalisations and shapes of the distributions used in the analysis within the detector acceptance [23]. The uncertainty associated with the choice of the global recoil scheme is assessed by comparing the nominal sample with an alternative sample produced with the dipole recoil scheme. For $t\bar{t}$ +light and $t\bar{t} + \geq 1c$, the uncertainty in the choice of the h_{damp} parameter is estimated by using the alternative POWHEGBOX+PYTHIA8 sample with $h_{\text{damp}} = 3 m_{\text{top}}$.

Uncertainties related to the H_T reweighting procedure described in Section 5.1 are assigned independently in the single-lepton and dilepton channels. The $t\bar{t}$ +light and $t\bar{t} + \geq 1c$ normalisation factors are varied within their uncertainties to estimate the corresponding systematic uncertainty. An additional uncertainty

Table 4: Expected yields in the dilepton control regions before the fit to data. The data-driven corrections to the $t\bar{t}$ + jets background are applied and all uncertainties are included, except the ones associated with the $t\bar{t}$ + jets background normalisation factors, which are not defined pre-fit. The “Other” category includes the tZq , tWZ and diboson processes. The $t\bar{t}H$ signal is normalised to the SM $t\bar{t}H$ cross-section. For presentation purposes, uncertainties are symmetrised.

	$t\bar{t}$ + light CR	$t\bar{t}$ + $\geq 1c$ CR	$t\bar{t}$ + $1b$ CR	$t\bar{t}$ + $1B$ CR	$t\bar{t}$ + $\geq 2b$ CR
$t\bar{t}H$ truth p_T^H 0–60 GeV	11.9 ± 1.4	19.7 ± 2.3	19.8 ± 2.3	9.9 ± 1.4	26.0 ± 3.0
$t\bar{t}H$ truth p_T^H 60–120 GeV	17.0 ± 1.3	34.5 ± 2.9	29.5 ± 3.0	20.4 ± 2.5	42.0 ± 4.0
$t\bar{t}H$ truth p_T^H 120–200 GeV	10.0 ± 0.9	27.1 ± 2.7	17.0 ± 2.1	19.2 ± 2.4	34.0 ± 3.5
$t\bar{t}H$ truth p_T^H 200–300 GeV	3.1 ± 0.35	11.1 ± 1.3	4.6 ± 0.7	9.2 ± 1.2	14.9 ± 1.9
$t\bar{t}H$ truth p_T^H 300–450 GeV	0.94 ± 0.15	3.5 ± 0.5	0.94 ± 0.19	3.3 ± 0.5	5.4 ± 0.8
$t\bar{t}H$ truth $p_T^H \geq 450$ GeV	0.33 ± 0.07	0.65 ± 0.12	0.116 ± 0.033	0.97 ± 0.15	1.33 ± 0.26
$t\bar{t}H$ $ \eta > 2.5$	0.31 ± 0.05	0.25 ± 0.04	0.4 ± 0.05	0.127 ± 0.028	0.166 ± 0.018
$t\bar{t}$ + $\geq 2b$	495 ± 35	860 ± 60	1080 ± 200	650 ± 100	2700 ± 200
$t\bar{t}$ + $1b$	1410 ± 130	1790 ± 230	3600 ± 700	1540 ± 180	1200 ± 400
$t\bar{t}$ + $1B$	310 ± 40	460 ± 40	540 ± 210	1560 ± 230	310 ± 110
$t\bar{t}$ + $\geq 1c$	5600 ± 500	7700 ± 600	2210 ± 280	1590 ± 330	1070 ± 170
$t\bar{t}$ + light	9200 ± 1500	2800 ± 400	590 ± 130	410 ± 90	190 ± 70
$t\bar{t}Z$	43 ± 6	81 ± 12	35 ± 6	36 ± 5	92 ± 12
tW	300 ± 60	210 ± 50	220 ± 70	150 ± 50	300 ± 140
$t\bar{t}W$	37 ± 5	72 ± 7	12.1 ± 1.3	14.3 ± 3.3	29.8 ± 3.5
Z + jets	340 ± 130	260 ± 100	250 ± 90	93 ± 34	320 ± 120
$t\bar{t}t\bar{t}$	1.6 ± 0.7	10 ± 4	1 ± 0.4	4.8 ± 2	28 ± 12
tWH	0.98 ± 0.11	2.24 ± 0.22	2.69 ± 0.29	1.42 ± 0.14	4.0 ± 0.4
Other	5.6 ± 2.4	8.1 ± 3.1	4.4 ± 2.0	2.1 ± 0.7	12 ± 5
Fakes	110 ± 50	120 ± 60	40 ± 20	40 ± 20	80 ± 40
Total	18000 ± 2000	14400 ± 1100	8700 ± 900	6200 ± 500	6400 ± 700
Data	18557	14361	8624	5830	6448

is estimated by comparing the distributions with and without the weights derived in the H_T reweighting procedure, in bins of jet multiplicity.

A $\pm 5\%$ normalisation uncertainty is considered for the cross-sections of the t - and s - single-top production modes [98, 99]. The normalisation uncertainty of the tW background is 3.7% [100]. Modelling uncertainties in the tW production due to the choice of the PS and hadronisation model, the NLO matching and the h_{damp} parameter choice are evaluated in the same way as for the $t\bar{t}$ + light and $t\bar{t}$ + $\geq 1c$ backgrounds. The uncertainty associated with the interference between tW and $t\bar{t}$ production at NLO is assessed by comparing the nominal POWHEGBOX+PYTHIA8 sample produced using the diagram removal scheme to an alternative sample produced with the same generator but using the diagram subtraction scheme.

The total uncertainty in the theoretical $t\bar{t}W$ cross-section computed at NNLO in the QCD and at NLO in the electro-weak interactions is 7.4% [71]. The modelling uncertainty in the $t\bar{t}W$ background is evaluated by comparing the nominal SHERPA simulation with the sample produced using MADGRAPH5_AMC@NLO. For the $t\bar{t}Z$ production, the uncertainty in the predicted cross-section at NLO in QCD is 12% [18]. The modelling uncertainty in the $t\bar{t}Z$ background is evaluated by comparing the nominal MADGRAPH5_AMC@NLO+PYTHIA8 sample with the sample where PYTHIA8 is replaced by HERWIG7 to simulate the PS and hadronisation.

A normalisation uncertainty of $^{+70\%}_{-15\%}$ is assigned for the $t\bar{t}t\bar{t}$ background. The down variation corresponds to the theory uncertainty covering effects from varying the factorisation and renormalisation scales, the PDFs and α_S [101] while the up variation covers the measured $t\bar{t}t\bar{t}$ cross-section [102]. For tZq , the total normalisation uncertainty is 7.9% [38]. A normalisation uncertainty of 15.4% (9.2%) calculated using

MADGRAPH5_AMC@NLO at NLO is applied to the $tHjb$ (tWH) background normalisation [103]. For tWZ , an uncertainty of $\pm 50\%$ is used [38].

The treatment of V + jets uncertainties follows the previous analysis [104]. An uncertainty of 40% is assumed for the W + jets cross-section, with an additional 30% normalisation uncertainty used for W boson production in association with heavy-flavour jets, taken as uncorrelated between events with two and events with more than two truth-level heavy-flavour jets. These uncertainties are based on variations of the factorisation and renormalisation scales and of the matching parameters in the SHERPA samples. An uncertainty of 35% is applied to the Z + jets normalisation to account for both the variations of the scales and matching parameters in the SHERPA samples and the uncertainty in the correction factor for the Z boson production accompanied by two b -jets extracted from data. A 50% normalisation uncertainty is used for the diboson background, which includes uncertainties in the inclusive cross-section and additional jet production [105–107].

A 50% normalisation uncertainty is assigned to the fake-lepton background estimate in the single-lepton and dilepton channels separately. An additional uncertainty obtained by using an alternative parameterisation of the fake rate (Section 5.2) is considered in the single-lepton channel.

8 Results

An excess of events over the expected background is found with an observed (expected) significance of 4.6 (5.4) standard deviations, in a combined profile-likelihood fit to data in all signal and control regions. The measured $t\bar{t}H$ signal strength for $m_H = 125.09$ GeV [108] is

$$\mu_{t\bar{t}H} = 0.81^{+0.22}_{-0.19} = 0.81 \pm 0.11(\text{stat.})^{+0.20}_{-0.16}(\text{syst.}). \quad (2)$$

The total statistical uncertainty is defined as the uncertainty in $\mu_{t\bar{t}H}$ when all nuisance parameters associated with the systematic uncertainties are fixed to their best-fit values. The total systematic uncertainty is then defined as the difference in quadrature between the total and statistical uncertainties. The systematic uncertainty in the signal strength $\mu_{t\bar{t}H}$ includes the theoretical uncertainties in the SM $t\bar{t}H$ cross-section described in Section 7. The measured $t\bar{t}H$ signal strength in the single-lepton channel is

$$\mu_{t\bar{t}H} = 0.72 \pm 0.12(\text{stat.})^{+0.21}_{-0.17}(\text{syst.}) \quad (3)$$

and in the dilepton channel is

$$\mu_{t\bar{t}H} = 1.03 \pm 0.26(\text{stat.})^{+0.28}_{-0.22}(\text{syst.}). \quad (4)$$

The combined $\mu_{t\bar{t}H}$ is converted into an inclusive cross-section using the SM theoretical cross-section of 507^{+35}_{-50} fb for $m_H = 125.09$ GeV and excluding its uncertainty [18]. The resulting cross-section is

$$\sigma_{t\bar{t}H} = 411^{+101}_{-92} \text{ fb} = 411 \pm 54(\text{stat.})^{+85}_{-75}(\text{syst.}) \text{ fb}, \quad (5)$$

with a relative uncertainty of $^{+25\%}_{-22\%}$, consistent with the SM prediction. The sensitivity is driven by the single-lepton channel, where the systematic component of the uncertainty dominates. The sensitivity of the dilepton channel is limited by the size of the dataset.

The measured values of the $t\bar{t}$ + jets background normalisation factors, that are free parameters of the fit, are listed in Table 5. They are compatible between the single-lepton and the dilepton channels within two

standard deviations. For $t\bar{t} + 1b$, the measured value of the normalisation factor is slightly larger in the dilepton channel than in the single-lepton channel.

Compared with the previous analysis using the same dataset, the current analysis selects 64% (29%) new events in the single-lepton (dilepton) SR that did not enter the selection of the previous analysis. This is consistent with the increase of the overall acceptance by a factor of three. The statistical correlation between the two analyses is estimated using a bootstrap method to be 19%, assuming that the systematic uncertainties are independent. This assumption is justified by the fact that the systematic model of the most important $t\bar{t} + \geq 1b$ background is different between the two analyses and the experimental uncertainties are updated. Based on this, the probability that the current result is compatible with the result of Ref. [20] is estimated as 21%.

Figure 3 shows the measured values of $\sigma_{t\bar{t}H}/\sigma^{\text{SM}}$ in bins of the Higgs boson p_{T} , obtained from a combined profile-likelihood fit to data with a free $t\bar{t}H$ signal strength parameter for each bin. The result of this measurement is compatible with the SM prediction with a p-value of 89%, taking into account theoretical uncertainties in the SM $t\bar{t}H$ cross-section. The measured value of the inclusive signal strength is also shown. The measurement of $\sigma_{t\bar{t}H}/\sigma^{\text{SM}}$ in the [300, 450) GeV and [450, ∞) GeV p_{T}^H bins is limited by statistical uncertainties. In the remaining bins, there is a similar contribution from statistical and systematic uncertainties. Defining boosted regions improves sensitivity in the [450, ∞) GeV p_{T}^H bin by about 15%, compared with the scenario where only the resolved event selection is applied to these events. The correlations between the parameters of interest are shown in Figure 4. They do not exceed 30% and are larger in the lower Higgs boson transverse momentum region.

The fitted values of $t\bar{t} + \text{jets}$ background normalisation factors are consistent with those obtained in the fit with a single $\mu_{t\bar{t}H}$ parameter shown in Table 5.

The absolute and relative systematic uncertainties in the measurement of $\sigma_{t\bar{t}H}$, grouped in categories, are shown in Table 6, and the effect of individual nuisance parameters ranked according to their impact on the inclusive $\sigma_{t\bar{t}H}/\sigma^{\text{SM}}$ is shown in Figure 5. The largest impact originates from the signal modelling, followed by the $t\bar{t} + \geq 2b$ background modelling. In both cases, the dominant effects arise from the modelling of the FSR and the choice of the PS model. Among the experimental uncertainties, the largest effects come from the b -jet tagging and the jet energy scale.

Among the eight highest ranked nuisance parameters in Figure 5, the largest constraints are observed for the $t\bar{t} + \geq 2b$ uncertainties arising from the dipole shower model and the choice of matching algorithm. These constraints predominantly originate from the single-lepton channel, and more specifically the SRs

Table 5: Best-fit values of the $t\bar{t} + \text{jets}$ normalisation factors obtained from the fit to data with a single inclusive $t\bar{t}H$ signal strength parameter. Independent normalisation factors for $t\bar{t} + 1b$, $t\bar{t} + \geq 1c$ and $t\bar{t} + \text{light}$ components are used in the dilepton and single-lepton channels. Before the fit, the $t\bar{t} + \text{light}$ and $t\bar{t} + \geq 1c$ components are normalised to the $t\bar{t}$ cross-section computed at NNLO in QCD including the resummation of NNLL soft-gluon terms [72] while the $t\bar{t} + \geq 1b$ normalisation is taken from the $t\bar{t}b\bar{b}$ MC simulation.

Normalisation factor	$t\bar{t} + \text{light}$	$t\bar{t} + \geq 1c$	$t\bar{t} + 1b$	$t\bar{t} + 1B$	$t\bar{t} + \geq 2b$
Single-lepton	$0.78^{+0.08}_{-0.08}$	$1.51^{+0.19}_{-0.18}$	$1.06^{+0.10}_{-0.10}$	$1.15^{+0.15}_{-0.14}$	$0.94^{+0.08}_{-0.08}$
Dilepton	$0.88^{+0.11}_{-0.10}$	$1.36^{+0.10}_{-0.10}$	$1.24^{+0.09}_{-0.09}$		

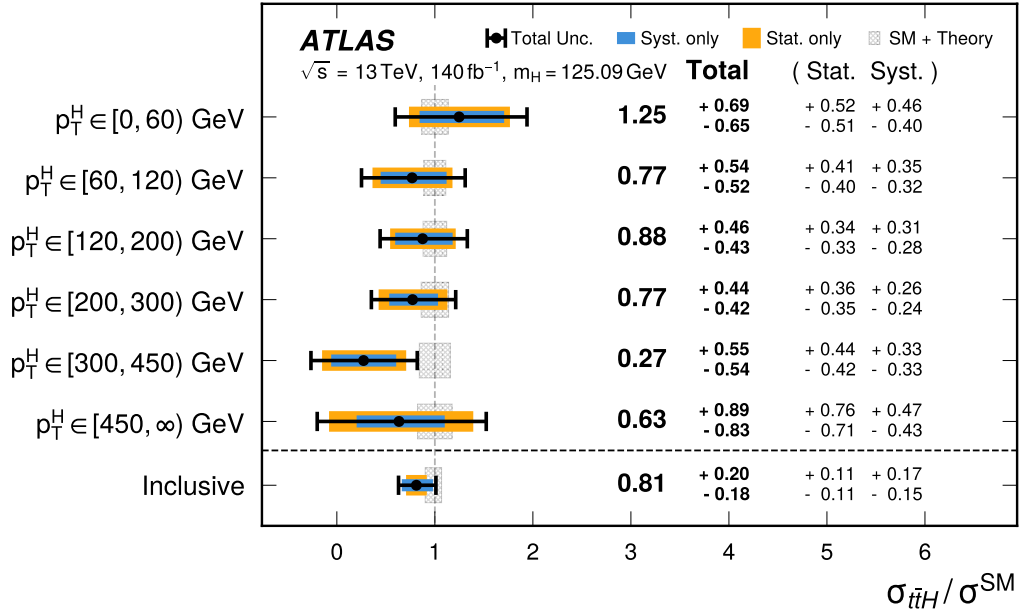


Figure 3: The $t\bar{t}H$ cross-sections measured in bins of truth Higgs boson p_T for a Higgs boson rapidity $|y| \leq 2.5$, and measured inclusively in the full phase space, normalised to their SM predictions, as obtained from a combined profile-likelihood fit to data in all signal and control regions. The uncertainties are shown separately for the measurement and the prediction.

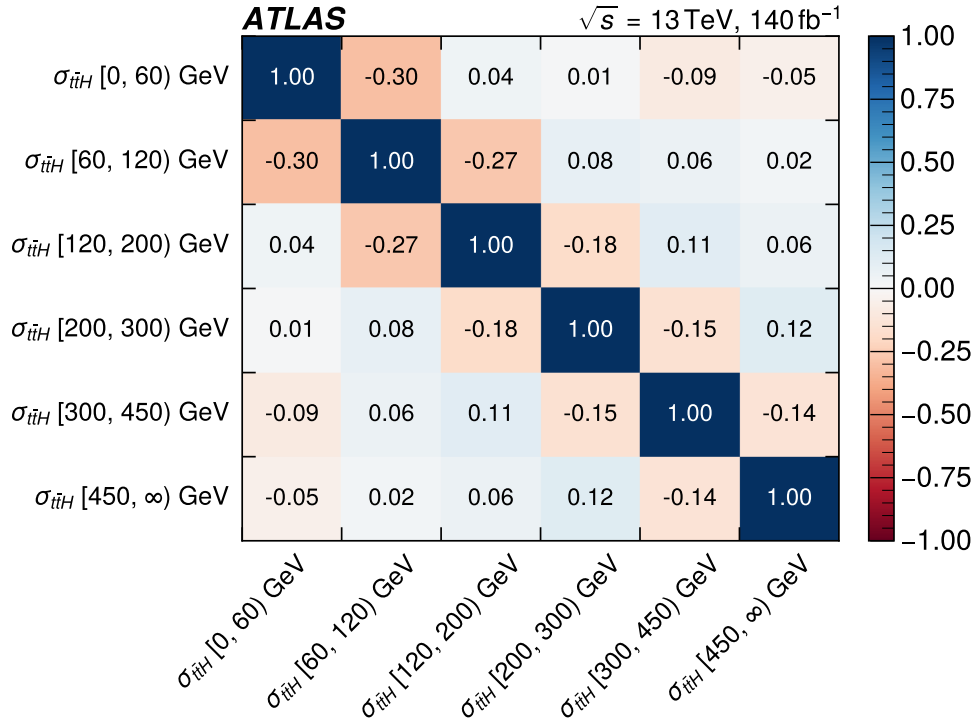


Figure 4: Post-fit correlations between the measured values of the $t\bar{t}H$ cross-section, $\sigma_{t\bar{t}H}$, in bins of truth p_T^H .

and the $t\bar{t} + \geq 2b$ CR where the $t\bar{t} + \geq 2b$ background contribution is large. The constraints are more pronounced when the $t\bar{t} + \geq 2b$ CR is split into three in the single-lepton channel to better control the $t\bar{t} + \geq 2b$ background modelling in bins of the reconstructed Higgs boson p_T .

Table 6: A list of the absolute and relative uncertainties in the measured $\sigma_{t\bar{t}H}$ grouped in categories. The contributions from different sources of uncertainty are evaluated after the fit. The quoted values are obtained by repeating the fit, while fixing the set of nuisance parameters of the sources corresponding to each category to their best-fit values, and subtracting in quadrature the resulting uncertainty from the total uncertainty of the nominal fit presented in the last row. The total uncertainty is different from the sum in quadrature of the different components due to correlations between nuisance parameters in the fit. The $t\bar{t}H$ and $t\bar{t} + \geq 1b$ radiation uncertainty categories include the renormalisation and factorisation scales, ISR and FSR uncertainties. The “ $t\bar{t}H$ theory” category includes STXS-related theoretical uncertainties and uncertainty in the $H \rightarrow b\bar{b}$ branching fraction. The “Minor background modelling” category includes uncertainties in the fake-lepton background and in minor backgrounds as defined in the text. The total statistical uncertainty includes uncertainties in the normalisation factors.

Uncertainty source	$\Delta\sigma_{t\bar{t}H}$ (fb)		$\Delta\sigma_{t\bar{t}H}/\sigma_{t\bar{t}H}$ (%)	
Process modelling				
<i>t\bar{t}H</i> modelling				
<i>t\bar{t}H</i> radiation	+35	-21	+9	-5
<i>t\bar{t}H</i> parton shower	+32	-19	+8	-5
<i>t\bar{t}H</i> matching	<0.1	-0.3	<0.1	-0.1
<i>t\bar{t}H</i> theory	+25	-17	+6	-4
$t\bar{t} + \geq 1b$ modelling				
$t\bar{t} + \geq 1b$ radiation	± 31		± 8	
$t\bar{t} + \geq 1b$ parton shower	± 29		± 7	
$t\bar{t} + \geq 1b$ matching	± 19		± 5	
$t\bar{t} + \geq 1c$ modelling	± 18		± 4	
$t\bar{t} + \text{light}$ modelling	± 5		± 1	
tW modelling	± 16		± 4	
Minor background modelling	± 19		± 5	
Flavour tagging	± 36		± 9	
Jet modelling	± 22		± 5	
Monte-Carlo statistics	± 17		± 4	
Other instrumental	± 10		± 2	
Total systematic uncertainty	+85	-75	+21	-18
Normalisation factors	± 21		± 5	
Total statistical uncertainty	± 54		± 13	
Total uncertainty	+101	-92	+25	-22

The observed yields in all signal and control regions are compared to the post-fit predictions in Figures 6 and 7. In each region, all bins are aggregated into a single bin. Figures 8 (9) and 10 (11) show a more detailed comparison in the single-lepton (dilepton) signal and control regions. The signal and background predictions in all post-fit distributions are obtained by setting the free parameters and the nuisance parameters to their best-fit values. In all post-fit plots, the uncertainty band includes all uncertainties and

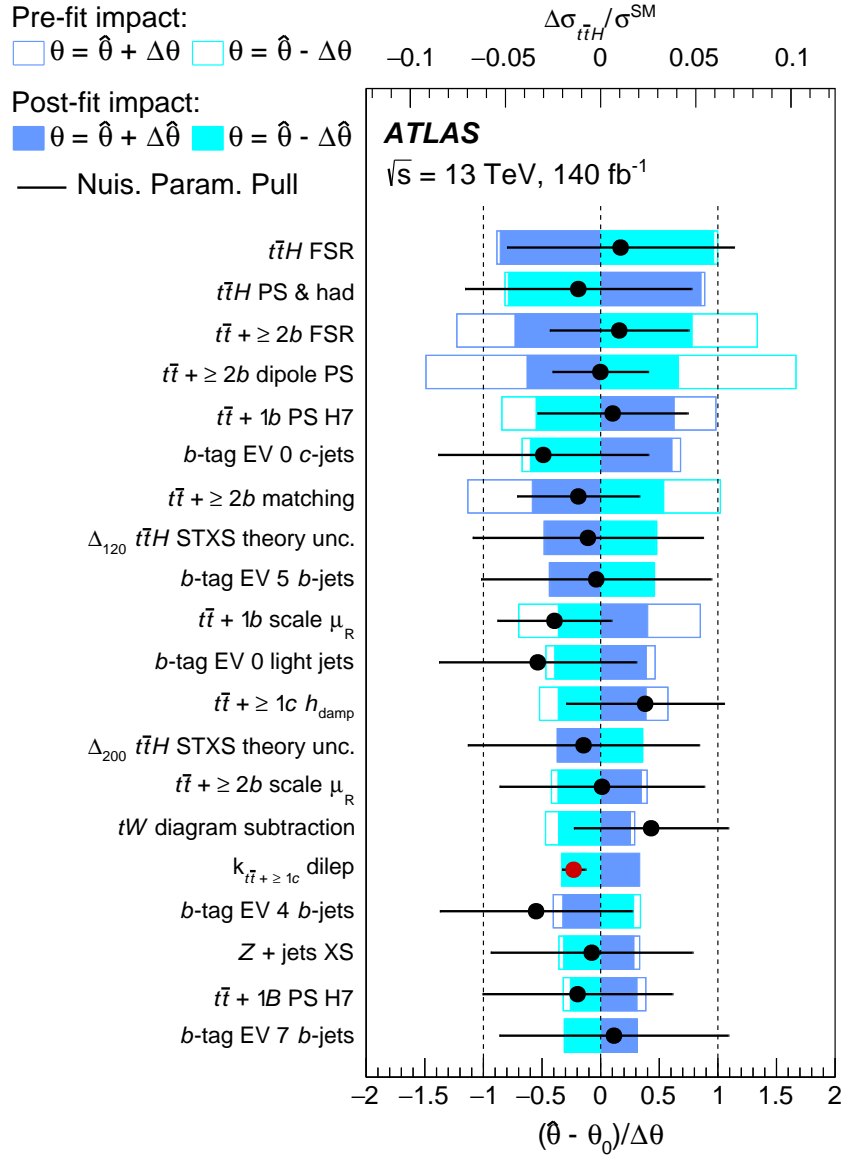


Figure 5: Ranking of the 20 modelling and experimental systematic uncertainties with the largest post-fit impact on the inclusive cross-section. The empty (filled) blue rectangles correspond to the pre-(post-)fit impact on $\sigma_{t\bar{t}H}/\sigma^{\text{SM}}$ and refer to the upper scale of the plot. The impact of each nuisance parameter, $\Delta\sigma_{t\bar{t}H}/\sigma^{\text{SM}}$, is computed by comparing the nominal best-fit value of $\sigma_{t\bar{t}H}/\sigma^{\text{SM}}$ with the result of the fit when fixing the considered nuisance parameter to its best-fit value, $\hat{\theta}$, shifted by its pre-fit (post-fit) uncertainties $\pm\Delta\theta$ ($\pm\Delta\hat{\theta}$). The black markers show the pulls of the nuisance parameters relative to their nominal values, $\theta_0 = 0$. The red marker shows the pull of the $t\bar{t} + \text{jets}$ normalisation factors relative to its nominal value, $\theta_0 = 1$. The pulls and their relative post-fit errors, $\Delta\hat{\theta}/\Delta\theta$, refer to the lower scale of the plot.

their correlations. The discriminant output in the plots is rescaled to be between zero and one using a logistic function.

The global goodness of fit [109, 110] is 87% for the $\sigma_{t\bar{t}H}/\sigma^{\text{SM}}$ measurement in p_{T}^H bins, highlighting that good post-fit modelling is achieved.

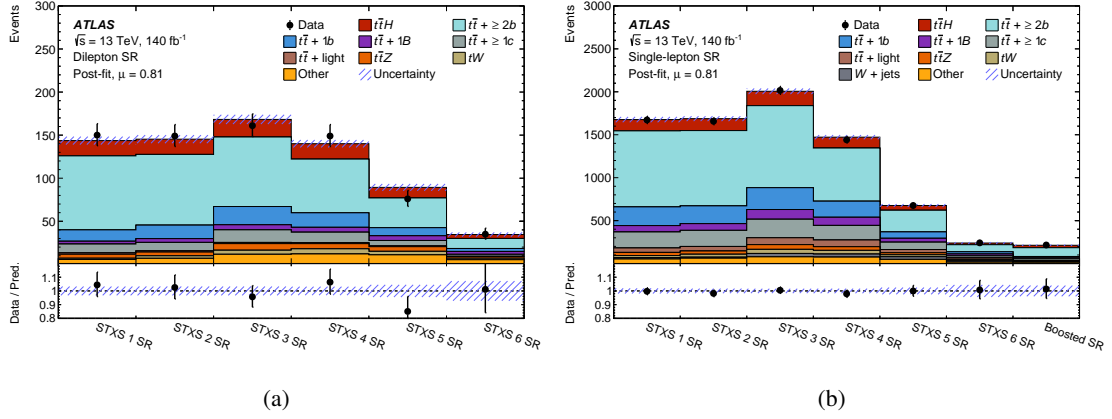


Figure 6: Post-fit summary of the yields in the (a) dilepton and (b) single-lepton signal regions, with all regions aggregated into a single bin each. The uncertainty band includes all uncertainties and their correlations.

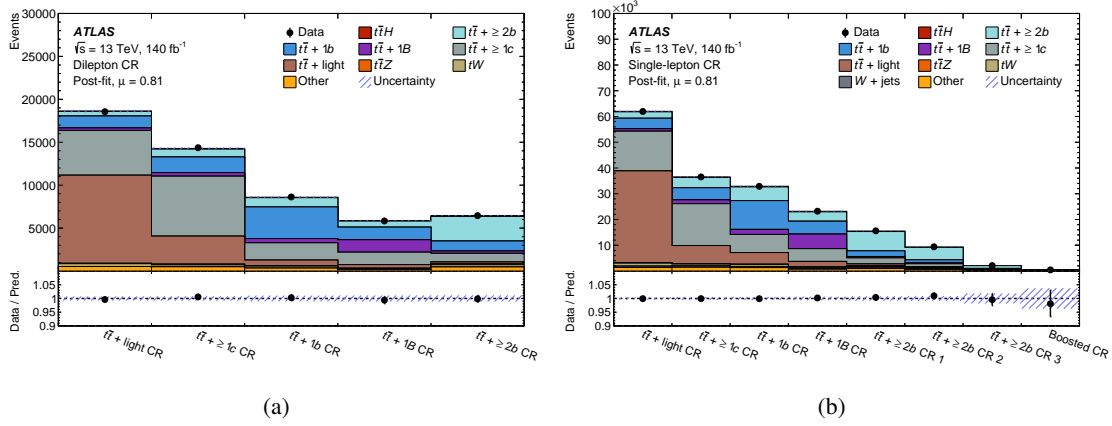


Figure 7: Post-fit summary of the yields in the (a) dilepton and (b) single-lepton control regions, with all regions aggregated into a single bin each. The uncertainty band includes all uncertainties and their correlations.

Figure 12 shows the event yield in data compared with the post-fit signal (S) and total background (B) predictions. It is ordered by the signal-to-background ratio of the bins from all the fitted regions. The predictions are shown for the best-fit signal strength and for the SM prediction. The observed data shows an excess over the background compatible with the best-fit signal strength $\mu_{\tilde{t}\tilde{t}H} = 0.81$ in the high $\log_{10}(S/B)$ region.

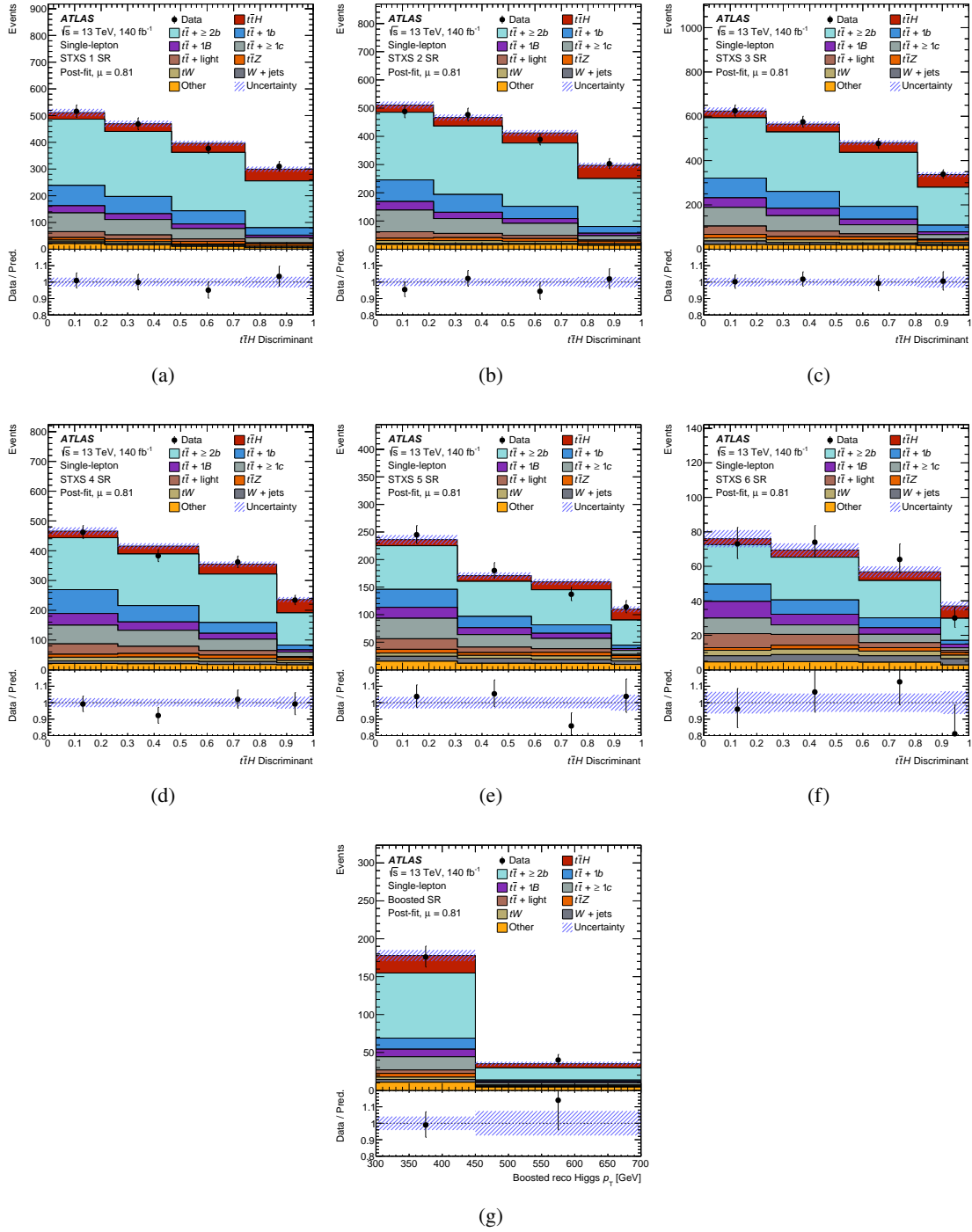


Figure 8: Post-fit data/prediction comparisons of the signal region distributions entering the fit in the single-lepton channel. The discriminants are rescaled to lie between zero and one using a logistic function. The signal and background normalisation parameters and nuisance parameters are set to their best-fit value. The uncertainty band includes all uncertainties and their correlations. For the reconstructed Higgs boson p_T in the boosted signal region, the first (last) bin includes the underflow (overflow) contributions.

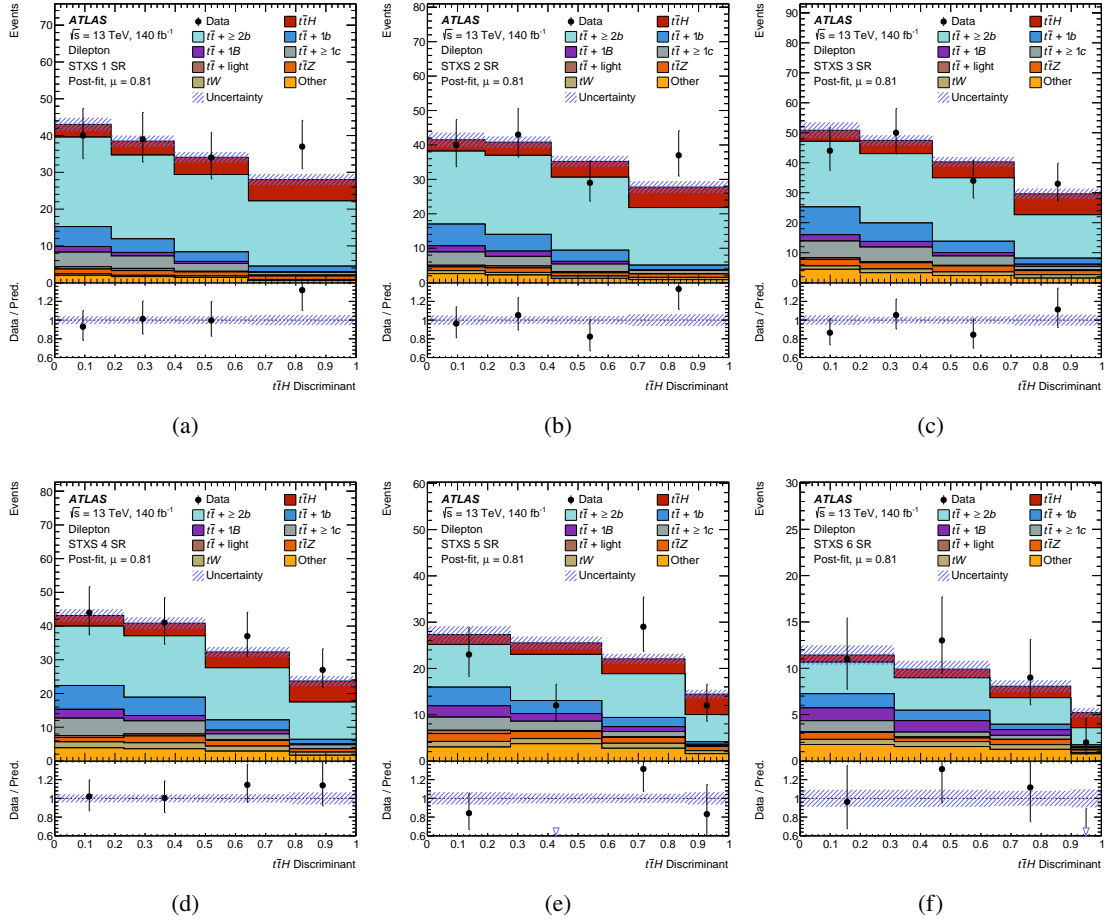


Figure 9: Post-fit data/prediction comparisons of the signal region distributions entering the fit in the dilepton channel. The discriminants are rescaled to lie between zero and one using a logistic function. The signal and background normalisation parameters and nuisance parameters are set to their best-fit value. The uncertainty band includes all uncertainties and their correlations.

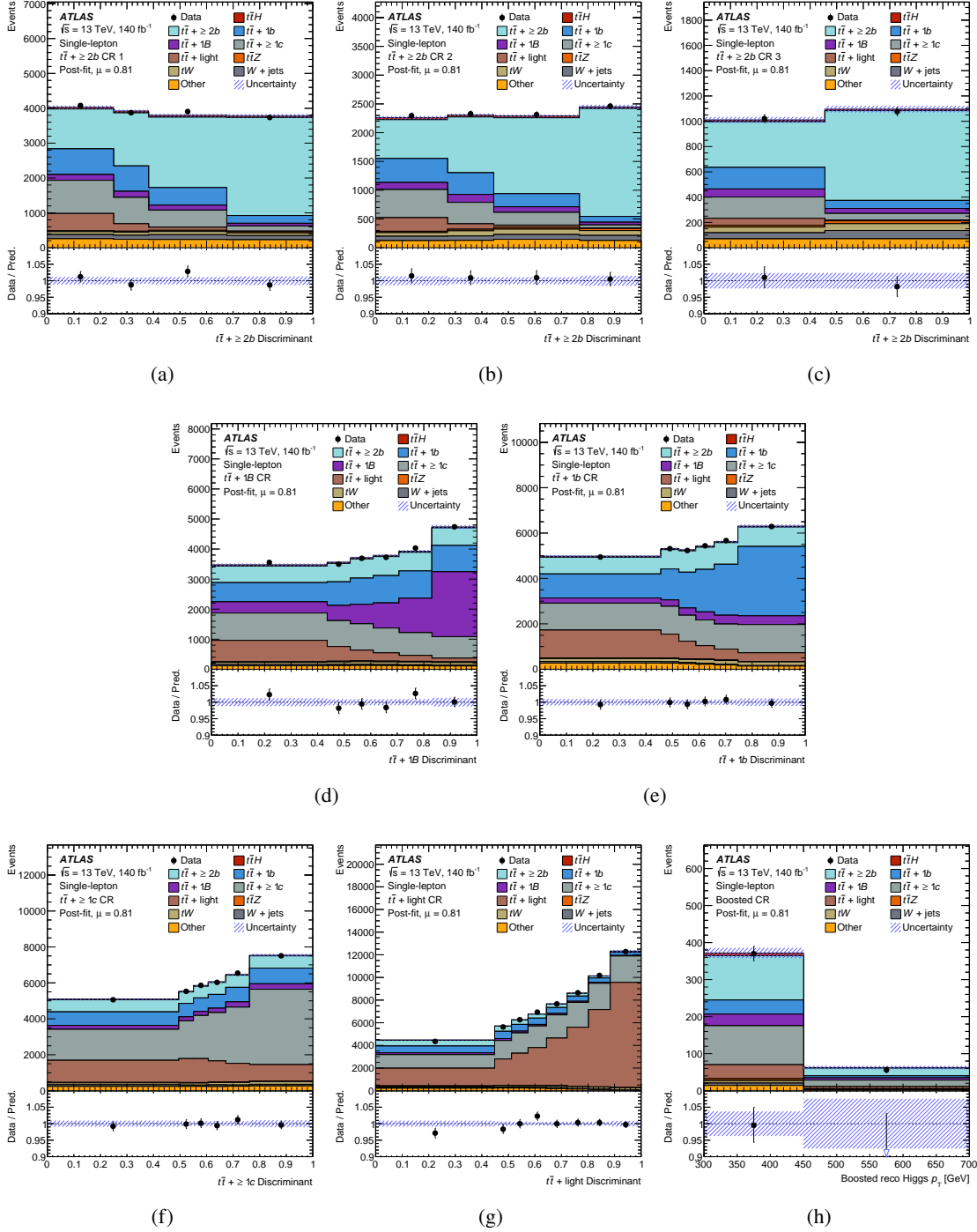


Figure 10: Post-fit data/prediction comparisons of the control region distributions entering the fit in the single-lepton channel. The discriminants are rescaled to lie between zero and one using a logistic function. The signal and background normalisation parameters and nuisance parameters are set to their best-fit value. The uncertainty band includes all uncertainties and their correlations. For the reconstructed Higgs boson p_T in the boosted control region, the first (last) bin includes the underflow (overflow) contributions.

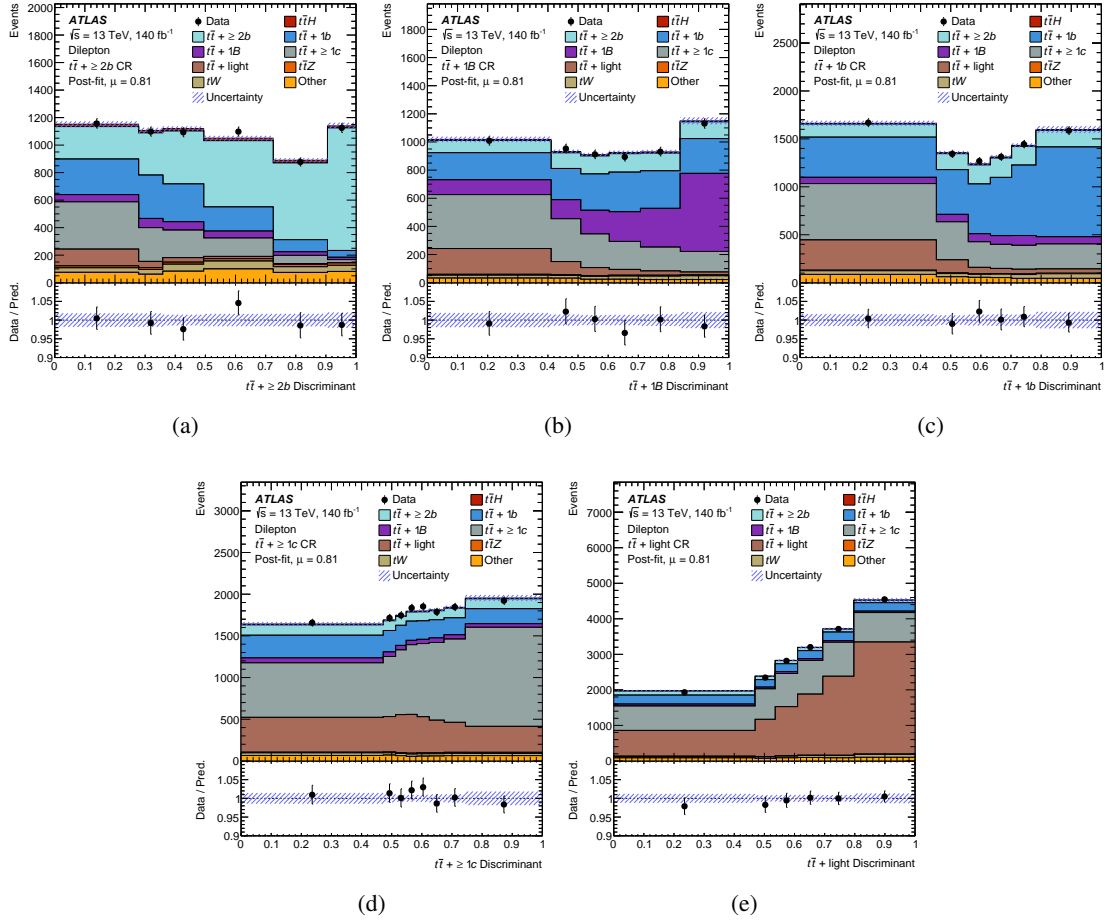


Figure 11: Post-fit data/prediction of the control region distributions entering the fit in the dilepton channel. The discriminants are rescaled to lie between zero and one using a logistic function. The signal and background normalisation parameters and nuisance parameters are set to their best-fit value. The uncertainty band includes all uncertainties and their correlations.

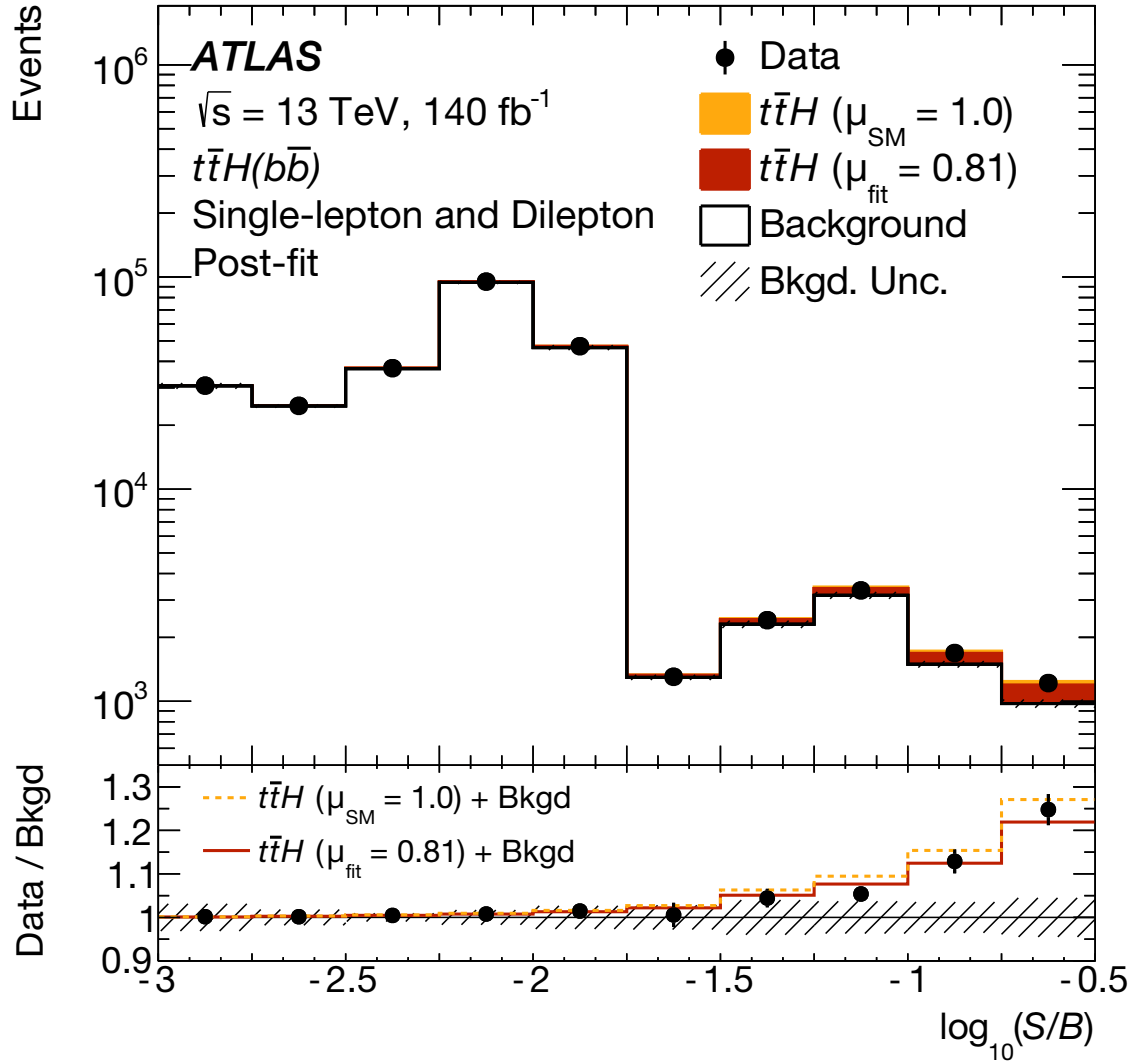


Figure 12: Observed and expected event yields as a function of $\log_{10}(S/B)$, where S and B are the post-fit signal and total background yields, respectively. The bins in all fitted regions are ordered and grouped in bins of $\log_{10}(S/B)$. The signal is shown for the best-fit signal strength, $\mu = 0.81$, or the SM prediction, $\mu = 1.0$. The lower panel shows the ratio of the data to the post-fit background prediction, compared with the signal-plus-background prediction with the best-fit signal strength and the SM prediction. The shaded band represents the total uncertainty in the background prediction. The first (last) bin includes the underflow (overflow) contributions.

9 Conclusion

The associated production of a Higgs boson with a pair of top quarks was measured in the $H \rightarrow b\bar{b}$ decay channel, using the full Run 2 proton–proton collision dataset collected at $\sqrt{s} = 13$ TeV by the ATLAS detector at the LHC, corresponding to 140 fb^{-1} . The measurement uses final states containing one or two leptons. The measured inclusive cross section assuming a Higgs boson mass of 125.09 GeV is $411 \pm 54(\text{stat.})_{-75}^{+85}(\text{syst.}) \text{ fb}$ with a relative uncertainty of 24%, consistent with the SM prediction. The measurement is dominated by the systematic uncertainties arising from the $t\bar{t}H$ signal modelling followed by the $t\bar{t} + \text{jets}$ background modelling. The observed (expected) significance of the $t\bar{t}H$ signal relative to the SM background-only hypothesis is 4.6 (5.4) standard deviations. The cross-section measurement is also performed in six bins of p_{T}^H in the STXS framework with the highest bin probing Higgs bosons with p_{T}^H above 450 GeV. The uncertainty in the measurement for p_{T}^H above 300 GeV is dominated by the limited number of data events.

With respect to the previous iteration of the analysis, this measurement profits from looser selection requirements and improved b -jet identification that increase the $t\bar{t}H$ signal acceptance. Control regions enriched in each of the $t\bar{t} + \text{jets}$ components are defined based on a more powerful multiclass neural network. Together with data-driven modelling corrections for the $t\bar{t} + \geq 1c$ and $t\bar{t} + \text{light}$ components, and a dedicated MC simulation and systematic model for the $t\bar{t} + \geq 1b$ component, they provide improved signal sensitivity and better control over the background, such that the modelling uncertainty in $t\bar{t} + \geq 1b$ is no longer the dominant contribution to the total systematic uncertainty.

This analysis is the most precise $t\bar{t}H$ cross-section measurement in a single decay channel, inclusively and in each p_{T}^H bin.

Acknowledgements

We thank CERN for the very successful operation of the LHC and its injectors, as well as the support staff at CERN and at our institutions worldwide without whom ATLAS could not be operated efficiently.

The crucial computing support from all WLCG partners is acknowledged gratefully, in particular from CERN, the ATLAS Tier-1 facilities at TRIUMF/SFU (Canada), NDGF (Denmark, Norway, Sweden), CC-IN2P3 (France), KIT/GridKA (Germany), INFN-CNAF (Italy), NL-T1 (Netherlands), PIC (Spain), RAL (UK) and BNL (USA), the Tier-2 facilities worldwide and large non-WLCG resource providers. Major contributors of computing resources are listed in Ref. [111].

We gratefully acknowledge the support of ANPCyT, Argentina; YerPhI, Armenia; ARC, Australia; BMWFW and FWF, Austria; ANAS, Azerbaijan; CNPq and FAPESP, Brazil; NSERC, NRC and CFI, Canada; CERN; ANID, Chile; CAS, MOST and NSFC, China; Minciencias, Colombia; MEYS CR, Czech Republic; DNRF and DNSRC, Denmark; IN2P3-CNRS and CEA-DRF/IRFU, France; SRNSFG, Georgia; BMBF, HGF and MPG, Germany; GSRI, Greece; RGC and Hong Kong SAR, China; ISF and Benoziy Center, Israel; INFN, Italy; MEXT and JSPS, Japan; CNRST, Morocco; NWO, Netherlands; RCN, Norway; MNiSW, Poland; FCT, Portugal; MNE/IFA, Romania; MESTD, Serbia; MSSR, Slovakia; ARRS and MIZŠ, Slovenia; DSI/NRF, South Africa; MICINN, Spain; SRC and Wallenberg Foundation, Sweden; SERI, SNSF and Cantons of Bern and Geneva, Switzerland; MOST, Taipei; TENMAK, Türkiye; STFC, United Kingdom; DOE and NSF, United States of America.

Individual groups and members have received support from BCKDF, CANARIE, CRC and DRAC, Canada; CERN-CZ, FORTE and PRIMUS, Czech Republic; COST, ERC, ERDF, Horizon 2020, ICSC-NextGenerationEU and Marie Skłodowska-Curie Actions, European Union; Investissements d’Avenir Labex, Investissements d’Avenir Idex and ANR, France; DFG and AvH Foundation, Germany; Herakleitos, Thales and Aristeia programmes co-financed by EU-ESF and the Greek NSRF, Greece; BSF-NSF and MINERVA, Israel; NCN and NAWA, Poland; La Caixa Banking Foundation, CERCA Programme Generalitat de Catalunya and PROMETEO and GenT Programmes Generalitat Valenciana, Spain; Göran Gustafssons Stiftelse, Sweden; The Royal Society and Leverhulme Trust, United Kingdom.

In addition, individual members wish to acknowledge support from Armenia: Yerevan Physics Institute (FAPERJ); CERN: European Organization for Nuclear Research (CERN PJAS); Chile: Agencia Nacional de Investigación y Desarrollo (FONDECYT 1230812, FONDECYT 1230987, FONDECYT 1240864); China: Chinese Ministry of Science and Technology (MOST-2023YFA1605700), National Natural Science Foundation of China (NSFC - 12175119, NSFC 12275265, NSFC-12075060); Czech Republic: Czech Science Foundation (GACR - 24-11373S), Ministry of Education Youth and Sports (FORTE CZ.02.01.01/00/22_008/0004632), PRIMUS Research Programme (PRIMUS/21/SCI/017); EU: H2020 European Research Council (ERC - 101002463); European Union: European Research Council (ERC - 948254, ERC 101089007), Horizon 2020 Framework Programme (MUCCA - CHIST-ERA-19-XAI-00), European Union, Future Artificial Intelligence Research (FAIR-NextGenerationEU PE00000013), Italian Center for High Performance Computing, Big Data and Quantum Computing (ICSC, NextGenerationEU); France: Agence Nationale de la Recherche (ANR-20-CE31-0013, ANR-21-CE31-0013, ANR-21-CE31-0022), Investissements d’Avenir Labex (ANR-11-LABX-0012); Germany: Baden-Württemberg Stiftung (BW Stiftung-Postdoc Eliteprogramme), Deutsche Forschungsgemeinschaft (DFG - 469666862, DFG - CR 312/5-2); Italy: Istituto Nazionale di Fisica Nucleare (ICSC, NextGenerationEU); Japan: Japan Society for the Promotion of Science (JSPS KAKENHI JP22H01227, JSPS KAKENHI JP22H04944, JSPS KAKENHI JP22KK0227, JSPS KAKENHI JP23KK0245); Netherlands: Netherlands Organisation for Scientific Research (NWO Veni 2020 - VI.Veni.202.179); Norway: Research Council of Norway (RCN-314472); Poland: Polish National Agency for Academic Exchange (PPN/PPO/2020/1/00002/U/00001), Polish National Science Centre (NCN 2021/42/E/ST2/00350, NCN OPUS nr 2022/47/B/ST2/03059, NCN UMO-2019/34/E/ST2/00393, UMO-2020/37/B/ST2/01043, UMO-2021/40/C/ST2/00187, UMO-2022/47/O/ST2/00148, UMO-2023/49/B/ST2/04085, UMO-2023/51/B/ST2/00920); Slovenia: Slovenian Research Agency (ARIS grant J1-3010); Spain: Generalitat Valenciana (Artemisa, FEDER, IDIFEDER/2018/048), Ministry of Science and Innovation (MCIN & NextGenEU PCI2022-135018-2, MICIN & FEDER PID2021-125273NB, RYC2019-028510-I, RYC2020-030254-I, RYC2021-031273-I, RYC2022-038164-I), PROMETEO and GenT Programmes Generalitat Valenciana (CIDEAGENT/2019/027); Sweden: Swedish Research Council (Swedish Research Council 2023-04654, VR 2018-00482, VR 2022-03845, VR 2022-04683, VR 2023-03403, VR grant 2021-03651), Knut and Alice Wallenberg Foundation (KAW 2018.0157, KAW 2018.0458, KAW 2019.0447, KAW 2022.0358); Switzerland: Swiss National Science Foundation (SNSF - PCEFP2_194658); United Kingdom: Leverhulme Trust (Leverhulme Trust RPG-2020-004), Royal Society (NIF-R1-231091); United States of America: U.S. Department of Energy (ECA DE-AC02-76SF00515), Neubauer Family Foundation.

References

- [1] F. Englert and R. Brout, *Broken Symmetry and the Mass of Gauge Vector Mesons*, [*Phys. Rev. Lett.* **13** \(1964\) 321](#).
- [2] P. W. Higgs, *Broken Symmetries and the Masses of Gauge Bosons*, [*Phys. Rev. Lett.* **13** \(1964\) 508](#).
- [3] G. S. Guralnik, C. R. Hagen and T. W. B. Kibble, *Global Conservation Laws and Massless Particles*, [*Phys. Rev. Lett.* **13** \(1964\) 585](#).
- [4] ATLAS Collaboration, *Observation of a new particle in the search for the Standard Model Higgs boson with the ATLAS detector at the LHC*, [*Phys. Lett. B* **716** \(2012\) 1](#), arXiv: [1207.7214 \[hep-ex\]](#).
- [5] CMS Collaboration, *Observation of a new boson at a mass of 125 GeV with the CMS experiment at the LHC*, [*Phys. Lett. B* **716** \(2012\) 30](#), arXiv: [1207.7235 \[hep-ex\]](#).
- [6] S. L. Glashow, *Partial-symmetries of Weak Interactions*, [*Nucl. Phys.* **22** \(1961\) 579](#).
- [7] S. Weinberg, *A Model of Leptons*, [*Phys. Rev. Lett.* **19** \(1967\) 1264](#).
- [8] A. Salam, *Weak and Electromagnetic Interactions*, [*Conf. Proc.* **C680519** \(1968\) 367](#).
- [9] C. Englert et al., *Precision measurements of Higgs couplings: implications for new physics scales*, [*J. Phys. G* **41** \(2014\) 113001](#), arXiv: [1403.7191 \[hep-ph\]](#).
- [10] ATLAS Collaboration, *A detailed map of Higgs boson interactions by the ATLAS experiment ten years after the discovery*, [*Nature* **607** \(2022\) 52](#), arXiv: [2207.00092 \[hep-ex\]](#), Erratum: [*Nature* **612** \(2022\) E24](#).
- [11] CMS Collaboration, *A portrait of the Higgs boson by the CMS experiment ten years after the discovery*, [*Nature* **607** \(2022\) 60](#), arXiv: [2207.00043 \[hep-ex\]](#), Erratum: [*Nature* **623** \(2023\) E4](#).
- [12] J. N. Ng and P. Zakarauskas, *QCD-parton calculation of conjoined production of Higgs bosons and heavy flavors in $p\bar{p}$ collision*, [*Phys. Rev. D* **29** \(1984\) 876](#).
- [13] Z. Kunszt, *Associated production of heavy Higgs boson with top quarks*, [*Nucl. Phys. B* **247** \(1984\) 339](#).
- [14] S. Dawson, L. H. Orr, L. Reina and D. Wackerroth, *Next-to-leading order QCD corrections to $pp \rightarrow t\bar{t}h$ at the CERN Large Hadron Collider*, [*Phys. Rev. D* **67** \(2003\) 071503](#), arXiv: [hep-ph/0211438](#).
- [15] W. Beenakker et al., *Higgs Radiation Off Top Quarks at the Tevatron and the LHC*, [*Phys. Rev. Lett.* **87** \(2001\) 201805](#), arXiv: [hep-ph/0107081](#).
- [16] ATLAS Collaboration, *Observation of Higgs boson production in association with a top quark pair at the LHC with the ATLAS detector*, [*Phys. Lett. B* **784** \(2018\) 173](#), arXiv: [1806.00425 \[hep-ex\]](#).
- [17] CMS Collaboration, *Observation of $t\bar{t}H$ Production*, [*Phys. Rev. Lett.* **120** \(2018\) 231801](#), arXiv: [1804.02610 \[hep-ex\]](#).
- [18] D. de Florian et al., *Handbook of LHC Higgs Cross Sections: 4. Deciphering the Nature of the Higgs Sector*, (2017), arXiv: [1610.07922 \[hep-ph\]](#).

- [19] L. Evans and P. Bryant, *LHC Machine*, *JINST* **3** (2008) S08001.
- [20] ATLAS Collaboration, *Measurement of Higgs boson decay into b -quarks in associated production with a top-quark pair in pp collisions at $\sqrt{s} = 13$ TeV with the ATLAS detector*, *JHEP* **06** (2022) 097, arXiv: 2111.06712 [hep-ex].
- [21] CMS Collaboration, *Search for $t\bar{t}H$ production in the $H \rightarrow b\bar{b}$ decay channel with leptonic $t\bar{t}$ decays in proton–proton collisions at $\sqrt{s} = 13$ TeV*, *JHEP* **03** (2019) 026, arXiv: 1804.03682 [hep-ex].
- [22] CMS Collaboration, *Search for $t\bar{t}H$ production in the all-jet final state in proton–proton collisions at $\sqrt{s} = 13$ TeV*, *JHEP* **06** (2018) 101, arXiv: 1803.06986 [hep-ex].
- [23] ATLAS Collaboration, *Studies of Monte Carlo predictions for the $t\bar{t}b\bar{b}$ process*, ATL-PHYS-PUB-2022-006, 2022, URL: <https://cds.cern.ch/record/2802806>.
- [24] ATLAS Collaboration, *Study of $t\bar{t}b\bar{b}$ and $t\bar{t}W$ background modelling for $t\bar{t}H$ analyses*, ATL-PHYS-PUB-2022-026, 2022, URL: <https://cds.cern.ch/record/2810864>.
- [25] ATLAS Collaboration, *The ATLAS Experiment at the CERN Large Hadron Collider*, *JINST* **3** (2008) S08003.
- [26] G. Avoni et al., *The new LUCID-2 detector for luminosity measurement and monitoring in ATLAS*, *JINST* **13** (2018) P07017.
- [27] ATLAS Collaboration, *Performance of the ATLAS trigger system in 2015*, *Eur. Phys. J. C* **77** (2017) 317, arXiv: 1611.09661 [hep-ex].
- [28] ATLAS Collaboration, *Software and computing for Run 3 of the ATLAS experiment at the LHC*, (2024), arXiv: 2404.06335 [hep-ex].
- [29] ATLAS Collaboration, *ATLAS data quality operations and performance for 2015–2018 data-taking*, *JINST* **15** (2020) P04003, arXiv: 1911.04632 [physics.ins-det].
- [30] T. Sjöstrand, S. Mrenna and P. Skands, *A brief introduction to PYTHIA 8.1*, *Comput. Phys. Commun.* **178** (2008) 852, arXiv: 0710.3820 [hep-ph].
- [31] ATLAS Collaboration, *The Pythia 8 A3 tune description of ATLAS minimum bias and inelastic measurements incorporating the Donnachie–Landshoff diffractive model*, ATL-PHYS-PUB-2016-017, 2016, URL: <https://cds.cern.ch/record/2206965>.
- [32] ATLAS Collaboration, *The ATLAS Simulation Infrastructure*, *Eur. Phys. J. C* **70** (2010) 823, arXiv: 1005.4568 [physics.ins-det].
- [33] S. Agostinelli et al., *GEANT4 – a simulation toolkit*, *Nucl. Instrum. Meth. A* **506** (2003) 250.
- [34] P. Nason, *A new method for combining NLO QCD with shower Monte Carlo algorithms*, *JHEP* **11** (2004) 040, arXiv: hep-ph/0409146.
- [35] S. Frixione, G. Ridolfi and P. Nason, *A positive-weight next-to-leading-order Monte Carlo for heavy flavour hadroproduction*, *JHEP* **09** (2007) 126, arXiv: 0707.3088 [hep-ph].
- [36] S. Frixione, P. Nason and C. Oleari, *Matching NLO QCD computations with parton shower simulations: the POWHEG method*, *JHEP* **11** (2007) 070, arXiv: 0709.2092 [hep-ph].

- [37] S. Alioli, P. Nason, C. Oleari and E. Re, *A general framework for implementing NLO calculations in shower Monte Carlo programs: the POWHEG BOX*, *JHEP* **06** (2010) 043, arXiv: [1002.2581 \[hep-ph\]](#).
- [38] J. Alwall et al., *The automated computation of tree-level and next-to-leading order differential cross sections, and their matching to parton shower simulations*, *JHEP* **07** (2014) 079, arXiv: [1405.0301 \[hep-ph\]](#).
- [39] T. Sjöstrand et al., *An introduction to PYTHIA 8.2*, *Comput. Phys. Commun.* **191** (2015) 159, arXiv: [1410.3012 \[hep-ph\]](#).
- [40] ATLAS Collaboration, *ATLAS Pythia 8 tunes to 7 TeV data*, ATL-PHYS-PUB-2014-021, 2014, URL: <https://cds.cern.ch/record/1966419>.
- [41] NNPDF Collaboration, R. D. Ball et al., *Parton distributions for the LHC run II*, *JHEP* **04** (2015) 040, arXiv: [1410.8849 \[hep-ph\]](#).
- [42] M. Bähr et al., *Herwig++ physics and manual*, *Eur. Phys. J. C* **58** (2008) 639, arXiv: [0803.0883 \[hep-ph\]](#).
- [43] J. Bellm et al., *Herwig 7.0/Herwig++ 3.0 release note*, *Eur. Phys. J. C* **76** (2016) 196, arXiv: [1512.01178 \[hep-ph\]](#).
- [44] L. A. Harland-Lang, A. D. Martin, P. Motylinski and R. S. Thorne, *Parton distributions in the LHC era: MMHT 2014 PDFs*, *Eur. Phys. J. C* **75** (2015) 204, arXiv: [1412.3989 \[hep-ph\]](#).
- [45] D. J. Lange, *The EvtGen particle decay simulation package*, *Nucl. Instrum. Meth. A* **462** (2001) 152.
- [46] H. B. Hartanto, B. Jäger, L. Reina and D. Wackerth, *Higgs boson production in association with top quarks in the POWHEG BOX*, *Phys. Rev. D* **91** (2015) 094003, arXiv: [1501.04498 \[hep-ph\]](#).
- [47] ATLAS Collaboration, *Studies on the improvement of the matching uncertainty definition in top-quark processes simulated with POWHEG+PYTHIA8*, ATL-PHYS-PUB-2023-029, 2013, URL: <https://cds.cern.ch/record/2872787>.
- [48] S. Höche, S. Mrenna, S. Payne, C. T. Preuss and P. Skands, *A Study of QCD Radiation in VBF Higgs Production with Vincia and Pythia*, *SciPost Phys.* **12** (2022) 010, arXiv: [2106.10987 \[hep-ph\]](#).
- [49] ATLAS Collaboration, *Search for the Standard Model Higgs boson produced in association with top quarks and decaying into $b\bar{b}$ in pp collisions at $\sqrt{s} = 8$ TeV with the ATLAS detector*, *Eur. Phys. J. C* **75** (2015) 349, arXiv: [1503.05066 \[hep-ex\]](#).
- [50] M. Cacciari, G. P. Salam and G. Soyez, *The anti- k_t jet clustering algorithm*, *JHEP* **04** (2008) 063, arXiv: [0802.1189 \[hep-ph\]](#).
- [51] ATLAS Collaboration, *Studies on top-quark Monte Carlo modelling for Top2016*, ATL-PHYS-PUB-2016-020, 2016, URL: <https://cds.cern.ch/record/2216168>.
- [52] T. Ježo, J. M. Lindert, N. Moretti and S. Pozzorini, *New NLOPS predictions for $t\bar{t} + b$ -jet production at the LHC*, *Eur. Phys. J. C* **78** (2018) 502, arXiv: [1802.00426 \[hep-ph\]](#).
- [53] F. Buccioni et al., *OpenLoops 2*, *Eur. Phys. J. C* **79** (2019) 866, arXiv: [1907.13071 \[hep-ph\]](#).

- [54] F. Cascioli, P. Maierhöfer and S. Pozzorini, *Scattering Amplitudes with Open Loops*, *Phys. Rev. Lett.* **108** (2012) 111601, arXiv: [1111.5206 \[hep-ph\]](#).
- [55] A. Denner, S. Dittmaier and L. Hofer, *COLLIER: A fortran-based complex one-loop library in extended regularizations*, *Comput. Phys. Commun.* **212** (2017) 220, arXiv: [1604.06792 \[hep-ph\]](#).
- [56] T. Ježo, *Powheg-Box-Res ttbb source code*, 2019, URL: https://gitlab.cern.ch/tjezo/powheg-box-res_ttbb/.
- [57] E. Bothmann et al., *Event generation with Sherpa 2.2*, *SciPost Phys.* **7** (2019) 034, arXiv: [1905.09127 \[hep-ph\]](#).
- [58] T. Gleisberg and S. Höche, *Comix, a new matrix element generator*, *JHEP* **12** (2008) 039, arXiv: [0808.3674 \[hep-ph\]](#).
- [59] S. Schumann and F. Krauss, *A parton shower algorithm based on Catani–Seymour dipole factorisation*, *JHEP* **03** (2008) 038, arXiv: [0709.1027 \[hep-ph\]](#).
- [60] S. Höche, F. Krauss, M. Schönherr and F. Siegert, *A critical appraisal of NLO+PS matching methods*, *JHEP* **09** (2012) 049, arXiv: [1111.1220 \[hep-ph\]](#).
- [61] S. Höche, F. Krauss, M. Schönherr and F. Siegert, *QCD matrix elements + parton showers. The NLO case*, *JHEP* **04** (2013) 027, arXiv: [1207.5030 \[hep-ph\]](#).
- [62] S. Catani, F. Krauss, B. R. Webber and R. Kuhn, *QCD Matrix Elements + Parton Showers*, *JHEP* **11** (2001) 063, arXiv: [hep-ph/0109231](#).
- [63] S. Höche, F. Krauss, S. Schumann and F. Siegert, *QCD matrix elements and truncated showers*, *JHEP* **05** (2009) 053, arXiv: [0903.1219 \[hep-ph\]](#).
- [64] E. Re, *Single-top Wt-channel production matched with parton showers using the POWHEG method*, *Eur. Phys. J. C* **71** (2011) 1547, arXiv: [1009.2450 \[hep-ph\]](#).
- [65] S. Alioli, P. Nason, C. Oleari and E. Re, *NLO single-top production matched with shower in POWHEG: s- and t-channel contributions*, *JHEP* **09** (2009) 111, arXiv: [0907.4076 \[hep-ph\]](#), Erratum: *JHEP* **02** (2010) 011.
- [66] S. Frixione, E. Laenen, P. Motylinski, C. White and B. R. Webber, *Single-top hadroproduction in association with a W boson*, *JHEP* **07** (2008) 029, arXiv: [0805.3067 \[hep-ph\]](#).
- [67] ATLAS Collaboration, *Studies of $t\bar{t}/tW$ interference effects in $b\bar{b}\ell^+\ell'^-\nu\bar{\nu}'$ final states with POWHEG and MADGRAPH5_AMC@NLO setups*, ATL-PHYS-PUB-2021-042, 2021, URL: <https://cds.cern.ch/record/2792254>.
- [68] T. Gleisberg et al., *Event generation with SHERPA 1.1*, *JHEP* **02** (2009) 007, arXiv: [0811.4622 \[hep-ph\]](#).
- [69] NNPDF Collaboration, R. D. Ball et al., *Parton distributions from high-precision collider data*, *Eur. Phys. J. C* **77** (2017), arXiv: [1706.00428 \[hep-ph\]](#).
- [70] R. Frederix and S. Frixione, *Merging meets matching in MC@NLO*, *JHEP* **12** (2012) 061, arXiv: [1209.6215 \[hep-ph\]](#).

- [71] L. Buonocore et al., *Precise Predictions for the Associated Production of a W Boson with a Top-Antitop Quark Pair at the LHC*, *Phys. Rev. Lett.* **131** (2023), arXiv: 2306.16311 [hep-ph].
- [72] M. Czakon and A. Mitov, *Top++: A program for the calculation of the top-pair cross-section at hadron colliders*, *Comput. Phys. Commun.* **185** (2014) 2930, arXiv: 1112.5675 [hep-ph].
- [73] ATLAS Collaboration, *Performance of the ATLAS muon triggers in Run 2*, *JINST* **15** (2020) P09015, arXiv: 2004.13447 [physics.ins-det].
- [74] ATLAS Collaboration, *Performance of electron and photon triggers in ATLAS during LHC Run 2*, *Eur. Phys. J. C* **80** (2020) 47, arXiv: 1909.00761 [hep-ex].
- [75] ATLAS Collaboration, *Vertex Reconstruction Performance of the ATLAS Detector at $\sqrt{s} = 13$ TeV*, ATL-PHYS-PUB-2015-026, 2015, URL: <https://cds.cern.ch/record/2037717>.
- [76] ATLAS Collaboration, *Electron and photon performance measurements with the ATLAS detector using the 2015–2017 LHC proton–proton collision data*, *JINST* **14** (2019) P12006, arXiv: 1908.00005 [hep-ex].
- [77] ATLAS Collaboration, *Muon reconstruction and identification efficiency in ATLAS using the full Run 2 pp collision data set at $\sqrt{s} = 13$ TeV*, *Eur. Phys. J. C* **81** (2021) 578, arXiv: 2012.00578 [hep-ex].
- [78] ATLAS Collaboration, *Jet reconstruction and performance using particle flow with the ATLAS Detector*, *Eur. Phys. J. C* **77** (2017) 466, arXiv: 1703.10485 [hep-ex].
- [79] M. Cacciari, G. P. Salam and G. Soyez, *FastJet user manual*, *Eur. Phys. J. C* **72** (2012) 1896, arXiv: 1111.6097 [hep-ph].
- [80] ATLAS Collaboration, *Performance of pile-up mitigation techniques for jets in pp collisions at $\sqrt{s} = 8$ TeV using the ATLAS detector*, *Eur. Phys. J. C* **76** (2016) 581, arXiv: 1510.03823 [hep-ex].
- [81] ATLAS Collaboration, *Jet energy scale and resolution measured in proton–proton collisions at $\sqrt{s} = 13$ TeV with the ATLAS detector*, *Eur. Phys. J. C* **81** (2021) 689, arXiv: 2007.02645 [hep-ex].
- [82] ATLAS Collaboration, *ATLAS flavour-tagging algorithms for the LHC Run 2 pp collision dataset*, *Eur. Phys. J. C* **83** (2023) 681, arXiv: 2211.16345 [physics.data-an].
- [83] ATLAS Collaboration, *Evidence for the $H \rightarrow b\bar{b}$ decay with the ATLAS detector*, *JHEP* **12** (2017) 024, arXiv: 1708.03299 [hep-ex].
- [84] ATLAS Collaboration, *Identification of hadronic tau lepton decays using neural networks in the ATLAS experiment*, ATL-PHYS-PUB-2019-033, 2019, URL: <https://cds.cern.ch/record/2688062>.
- [85] ATLAS Collaboration, *The performance of missing transverse momentum reconstruction and its significance with the ATLAS detector using 140fb^{-1} of $\sqrt{s} = 13$ TeV pp collisions*, (2024), arXiv: 2402.05858 [hep-ex].
- [86] B. Nachman, P. Nef, A. Schwartzman, M. Swiatlowski and C. Wanotayaroj, *Jets from jets: re-clustering as a tool for large radius jet reconstruction and grooming at the LHC*, *JHEP* **02** (2015) 075, arXiv: 1407.2922 [hep-ph].

- [87] ATLAS Collaboration, *Measurements of top-quark pair differential and double-differential cross-sections in the ℓ +jets channel with pp collisions at $\sqrt{s} = 13$ TeV using the ATLAS detector*, *Eur. Phys. J. C* **79** (2019) 1028, arXiv: [1908.07305 \[hep-ex\]](#),
Erratum: *Eur. Phys. J. C* **80** (2020) 1092.
- [88] ATLAS Collaboration, *Tools for estimating fake/non-prompt lepton backgrounds with the ATLAS detector at the LHC*, *JINST* **18** (2023) T11004, arXiv: [2211.16178 \[hep-ex\]](#).
- [89] A. Vaswani et al., *Attention Is All You Need*, 2023, arXiv: [1706.03762 \[cs.CL\]](#).
- [90] K. Cranmer, G. Lewis, L. Moneta, A. Shibata and W. Verkerke, *HistFactory: A tool for creating statistical models for use with RooFit and RooStats*, CERN-OPEN-2012-016, 2012, URL: <https://cds.cern.ch/record/1456844>.
- [91] W. Verkerke and D. Kirkby, *The RooFit toolkit for data modeling*, 2003, arXiv: [physics/0306116 \[physics.data-an\]](#).
- [92] G. Cowan, K. Cranmer, E. Gross and O. Vitells, *Asymptotic formulae for likelihood-based tests of new physics*, *Eur. Phys. J. C* **71** (2011) 1554, arXiv: [1007.1727 \[physics.data-an\]](#), Erratum: *Eur. Phys. J. C* **73** (2013) 2501.
- [93] ATLAS Collaboration, *Luminosity determination in pp collisions at $\sqrt{s} = 13$ TeV using the ATLAS detector at the LHC*, *Eur. Phys. J. C* **83** (2023) 982, arXiv: [2212.09379 \[hep-ex\]](#).
- [94] ATLAS Collaboration, *ATLAS b -jet identification performance and efficiency measurement with $t\bar{t}$ events in pp collisions at $\sqrt{s} = 13$ TeV*, *Eur. Phys. J. C* **79** (2019) 970, arXiv: [1907.05120 \[hep-ex\]](#).
- [95] ATLAS Collaboration, *Measurement of the c -jet mistagging efficiency in $t\bar{t}$ events using pp collision data at $\sqrt{s} = 13$ TeV collected with the ATLAS detector*, *Eur. Phys. J. C* **82** (2022) 95, arXiv: [2109.10627 \[hep-ex\]](#).
- [96] ATLAS Collaboration, *Calibration of the light-flavour jet mistagging efficiency of the b -tagging algorithms with Z +jets events using 139fb^{-1} of ATLAS proton–proton collision data at $\sqrt{s} = 13$ TeV*, *Eur. Phys. J. C* **83** (2023) 728, arXiv: [2301.06319 \[hep-ex\]](#).
- [97] ATLAS Collaboration, *Evaluation of QCD uncertainties for Higgs boson production through gluon fusion and in association with two top quarks for simplified template cross-section measurements*, ATL-PHYS-PUB-2023-031, 2023, URL: <https://cds.cern.ch/record/2878797>.
- [98] N. Kidonakis, *Next-to-next-to-leading-order collinear and soft gluon corrections for t -channel single top quark production*, *Phys. Rev. D* **83** (2011) 091503, arXiv: [1103.2792 \[hep-ph\]](#).
- [99] N. Kidonakis, *Next-to-next-to-leading logarithm resummation for s -channel single top quark production*, *Phys. Rev. D* **81** (2010) 054028, arXiv: [1001.5034 \[hep-ph\]](#).
- [100] N. Kidonakis and N. Yamanaka, *Higher-order corrections for tW production at high-energy hadron colliders*, *JHEP* **05** (2021) 278, arXiv: [2102.11300 \[hep-ph\]](#).

- [101] M. van Beekveld, A. Kulesza and L. M. Valero, *Threshold resummation for the production of four top quarks at the LHC*, 2022, arXiv: [2212.03259 \[hep-ph\]](#).
- [102] ATLAS Collaboration, *Observation of four-top-quark production in the multilepton final state with the ATLAS detector*, [Eur. Phys. J. C **83** \(2023\) 496](#), arXiv: [2303.15061 \[hep-ex\]](#).
- [103] ATLAS Collaboration, *Probing the CP nature of the top-Higgs Yukawa coupling in $t\bar{t}H$ and tH events with $H \rightarrow b\bar{b}$ decays using the ATLAS detector at the LHC*, [Phys. Lett. B **849** \(2023\) 138469](#), arXiv: [2303.05974 \[hep-ex\]](#).
- [104] ATLAS Collaboration, *Probing the CP nature of the top-Higgs Yukawa coupling in $t\bar{t}H$ and tH events with $H \rightarrow b\bar{b}$ decays using the ATLAS detector at the LHC*, [Phys. Lett. B **849** \(2024\) 138469](#), arXiv: [2303.05974 \[hep-ex\]](#).
- [105] M. Grazzini, S. Kallweit, D. Rathlev and M. Wiesemann, *$W^\pm Z$ production at hadron colliders in NNLO QCD*, [Phys. Lett. B **761** \(2016\) 179](#), arXiv: [1604.08576 \[hep-ph\]](#).
- [106] ATLAS Collaboration, *Multi-boson simulation for 13 TeV ATLAS analyses*, ATL-PHYS-PUB-2016-002, 2016, URL: <https://cds.cern.ch/record/2119986>.
- [107] ATLAS Collaboration, *Measurement of $W^\pm Z$ production cross sections and gauge boson polarisation in pp collisions at $\sqrt{s} = 13$ TeV with the ATLAS detector*, [Eur. Phys. J. C **79** \(2019\) 535](#), arXiv: [1902.05759 \[hep-ex\]](#).
- [108] ATLAS and CMS Collaborations, *Combined Measurement of the Higgs Boson Mass in pp Collisions at $\sqrt{s} = 7$ and 8 TeV with the ATLAS and CMS Experiments*, [Phys. Rev. Lett. **114** \(2015\) 191803](#), arXiv: [1503.07589 \[hep-ex\]](#).
- [109] S. Baker and R. D. Cousins, *Clarification of the Use of CHI-square and Likelihood Functions in Fits to Histograms*, [Nucl. Instrum. Meth. **221** \(1984\) 437](#).
- [110] R. D. Cousins, *Lectures on Statistics in Theory: Prelude to Statistics in Practice*, 2024, arXiv: [1807.05996 \[physics.data-an\]](#).
- [111] ATLAS Collaboration, *ATLAS Computing Acknowledgements*, ATL-SOFT-PUB-2023-001, 2023, URL: <https://cds.cern.ch/record/2869272>.

The ATLAS Collaboration

G. Aad ¹⁰⁴, E. Aakvaag ¹⁷, B. Abbott ¹²³, S. Abdelhameed ^{119a}, K. Abeling ⁵⁶, N.J. Abicht ⁵⁰, S.H. Abidi ³⁰, M. Aboeela ⁴⁵, A. Aboulhorma ^{36e}, H. Abramowicz ¹⁵⁴, H. Abreu ¹⁵³, Y. Abulaiti ¹²⁰, B.S. Acharya ^{70a,70b,k}, A. Ackermann ^{64a}, C. Adam Bourdarios ⁴, L. Adamczyk ^{87a}, S.V. Addepalli ²⁷, M.J. Addison ¹⁰³, J. Adelman ¹¹⁸, A. Adiguzel ^{22c}, T. Adye ¹³⁷, A.A. Affolder ¹³⁹, Y. Afik ⁴⁰, M.N. Agaras ¹³, J. Agarwala ^{74a,74b}, A. Aggarwal ¹⁰², C. Agheorghiesei ^{28c}, F. Ahmadov ^{39,x}, W.S. Ahmed ¹⁰⁶, S. Ahuja ⁹⁷, X. Ai ^{63e}, G. Aielli ^{77a,77b}, A. Aikot ¹⁶⁶, M. Ait Tamliah ^{36e}, B. Aitbenkikh ^{36a}, M. Akbiyik ¹⁰², T.P.A. Åkesson ¹⁰⁰, A.V. Akimov ³⁸, D. Akiyama ¹⁷¹, N.N. Akolkar ²⁵, S. Aktas ^{22a}, K. Al Houry ⁴², G.L. Alberghi ^{24b}, J. Albert ¹⁶⁸, P. Albicocco ⁵⁴, G.L. Albouy ⁶¹, S. Alderweireldt ⁵³, Z.L. Alegria ¹²⁴, M. Aleksa ³⁷, I.N. Aleksandrov ³⁹, C. Alexa ^{28b}, T. Alexopoulos ¹⁰, F. Alfonsi ^{24b}, M. Algren ⁵⁷, M. Alhroob ¹⁷⁰, B. Ali ¹³⁵, H.M.J. Ali ^{93,r}, S. Ali ³², S.W. Alibocus ⁹⁴, M. Aliev ^{34c}, G. Alimonti ^{72a}, W. Alkahi ⁵⁶, C. Allaire ⁶⁷, B.M.M. Allbrooke ¹⁴⁹, J.S. Allen ¹⁰³, J.F. Allen ⁵³, C.A. Allendes Flores ^{140f}, P.P. Allport ²¹, A. Aloisio ^{73a,73b}, F. Alonso ⁹², C. Alpighiani ¹⁴¹, Z.M.K. Alsolami ⁹³, M. Alvarez Estevez ¹⁰¹, A. Alvarez Fernandez ¹⁰², M. Alves Cardoso ⁵⁷, M.G. Alvigi ^{73a,73b}, M. Aly ¹⁰³, Y. Amaral Coutinho ^{84b}, A. Ambler ¹⁰⁶, C. Amelung ³⁷, M. Amerl ¹⁰³, C.G. Ames ¹¹¹, D. Amidei ¹⁰⁸, B. Amini ⁵⁵, K.J. Amirie ¹⁵⁸, S.P. Amor Dos Santos ^{133a}, K.R. Amos ¹⁶⁶, D. Amperiadou ¹⁵⁵, S. An ⁸⁵, V. Ananiev ¹²⁸, C. Anastopoulos ¹⁴², T. Andeen ¹¹, J.K. Anders ³⁷, A.C. Anderson ⁶⁰, S.Y. Andreato ^{48a,48b}, A. Andreazza ^{72a,72b}, S. Angelidakis ⁹, A. Angerami ⁴², A.V. Anisenkov ³⁸, A. Annovi ^{75a}, C. Antel ⁵⁷, E. Antipov ¹⁴⁸, M. Antonelli ⁵⁴, F. Anulli ^{76a}, M. Aoki ⁸⁵, T. Aoki ¹⁵⁶, M.A. Aparo ¹⁴⁹, L. Aperio Bella ⁴⁹, C. Appelt ¹⁹, A. Apyan ²⁷, S.J. Arbiol Val ⁸⁸, C. Arcangeletti ⁵⁴, A.T.H. Arce ⁵², J-F. Arguin ¹¹⁰, S. Argyropoulos ¹⁵⁵, J.-H. Arling ⁴⁹, O. Arnaez ⁴, H. Arnold ¹⁴⁸, G. Artoni ^{76a,76b}, H. Asada ¹¹³, K. Asai ¹²¹, S. Asai ¹⁵⁶, N.A. Asbah ³⁷, R.A. Ashby Pickering ¹⁷⁰, K. Assamagan ³⁰, R. Astalos ^{29a}, K.S.V. Astrand ¹⁰⁰, S. Atashi ¹⁶², R.J. Atkin ^{34a}, M. Atkinson ¹⁶⁵, H. Atmani ^{36f}, P.A. Atmasiddha ¹³¹, K. Augsten ¹³⁵, S. Auricchio ^{73a,73b}, A.D. Auriol ²¹, V.A. Austrup ¹⁰³, G. Avolio ³⁷, K. Axiotis ⁵⁷, G. Azuelos ^{110,ac}, D. Babal ^{29b}, H. Bachacou ¹³⁸, K. Bachas ^{155,o}, A. Bachiou ³⁵, F. Backman ^{48a,48b}, A. Badea ⁴⁰, T.M. Baer ¹⁰⁸, P. Bagnaia ^{76a,76b}, M. Bahmani ¹⁹, D. Bahner ⁵⁵, K. Bai ¹²⁶, J.T. Baines ¹³⁷, L. Baines ⁹⁶, O.K. Baker ¹⁷⁵, E. Bakos ¹⁶, D. Bakshi Gupta ⁸, L.E. Balabram Filho ^{84b}, V. Balakrishnan ¹²³, R. Balasubramanian ⁴, E.M. Baldin ³⁸, P. Balek ^{87a}, E. Ballabene ^{24b,24a}, F. Balli ¹³⁸, L.M. Baltes ^{64a}, W.K. Balunas ³³, J. Balz ¹⁰², I. Bamwidhi ^{119b}, E. Banas ⁸⁸, M. Bandieramonte ¹³², A. Bandyopadhyay ²⁵, S. Bansal ²⁵, L. Barak ¹⁵⁴, M. Barakat ⁴⁹, E.L. Barberio ¹⁰⁷, D. Barberis ^{58b,58a}, M. Barbero ¹⁰⁴, M.Z. Barel ¹¹⁷, T. Barillari ¹¹², M-S. Barisits ³⁷, T. Barklow ¹⁴⁶, P. Baron ¹²⁵, D.A. Baron Moreno ¹⁰³, A. Baroncelli ^{63a}, A.J. Barr ¹²⁹, J.D. Barr ⁹⁸, F. Barreiro ¹⁰¹, J. Barreiro Guimarães da Costa ¹⁴, U. Barron ¹⁵⁴, M.G. Barros Teixeira ^{133a}, S. Barsov ³⁸, F. Bartels ^{64a}, R. Bartoldus ¹⁴⁶, A.E. Barton ⁹³, P. Bartos ^{29a}, A. Basan ¹⁰², M. Baselga ⁵⁰, A. Bassalat ^{67,b}, M.J. Basso ^{159a}, S. Bataju ⁴⁵, R. Bate ¹⁶⁷, R.L. Bates ⁶⁰, S. Batlamous ¹⁰¹, B. Batool ¹⁴⁴, M. Battaglia ¹³⁹, D. Battulga ¹⁹, M. Baucé ^{76a,76b}, M. Bauer ⁸⁰, P. Bauer ²⁵, L.T. Bazzano Hurrell ³¹, J.B. Beacham ⁵², T. Beau ¹³⁰, J.Y. Beaucamp ⁹², P.H. Beauchemin ¹⁶¹, P. Bechtel ²⁵, H.P. Beck ^{20,n}, K. Becker ¹⁷⁰, A.J. Beddall ⁸³, V.A. Bednyakov ³⁹, C.P. Bee ¹⁴⁸, L.J. Beemster ¹⁶, T.A. Beermann ³⁷, M. Begalli ^{84d}, M. Beger ³⁰, A. Behera ¹⁴⁸, J.K. Behr ⁴⁹, J.F. Beirer ³⁷, F. Beisiegel ²⁵, M. Belfkir ^{119b}, G. Bella ¹⁵⁴, L. Bellagamba ^{24b}, A. Bellerive ³⁵, P. Bellos ²¹, K. Beloborodov ³⁸, D. Benčekroun ^{36a}, F. Bendebba ^{36a}, Y. Benhammou ¹⁵⁴,

K.C. Benkendorfer ⁶², L. Beresford ⁴⁹, M. Beretta ⁵⁴, E. Bergeaas Kuutmann ¹⁶⁴, N. Berger ⁴,
 B. Bergmann ¹³⁵, J. Beringer ^{18a}, G. Bernardi ⁵, C. Bernius ¹⁴⁶, F.U. Bernlochner ²⁵,
 F. Bernon ³⁷, A. Berrocal Guardia ¹³, T. Berry ⁹⁷, P. Berta ¹³⁶, A. Berthold ⁵¹, S. Bethke ¹¹²,
 A. Betti ^{76a,76b}, A.J. Bevan ⁹⁶, N.K. Bhalla ⁵⁵, S. Bhatta ¹⁴⁸, D.S. Bhattacharya ¹⁶⁹,
 P. Bhattarai ¹⁴⁶, K.D. Bhide ⁵⁵, V.S. Bhopatkar ¹²⁴, R.M. Bianchi ¹³², G. Bianco ^{24b,24a},
 O. Biebel ¹¹¹, R. Bielski ¹²⁶, M. Biglietti ^{78a}, C.S. Billingsley ⁴⁵, Y. Bimgdi ^{36f}, M. Bindi ⁵⁶,
 A. Bingul ^{22b}, C. Bini ^{76a,76b}, G.A. Bird ³³, M. Birman ¹⁷², M. Biros ¹³⁶, S. Biryukov ¹⁴⁹,
 T. Bisanz ⁵⁰, E. Bisceglie ^{44b,44a}, J.P. Biswal ¹³⁷, D. Biswas ¹⁴⁴, I. Bloch ⁴⁹, A. Blue ⁶⁰,
 U. Blumenschein ⁹⁶, J. Blumenthal ¹⁰², V.S. Bobrovnikov ³⁸, M. Boehler ⁵⁵, B. Boehm ¹⁶⁹,
 D. Bogavac ³⁷, A.G. Bogdanchikov ³⁸, L.S. Boggia ¹³⁰, C. Bohm ^{48a}, V. Boisvert ⁹⁷,
 P. Bokan ³⁷, T. Bold ^{87a}, M. Bomben ⁵, M. Bona ⁹⁶, M. Boonekamp ¹³⁸, C.D. Booth ⁹⁷,
 A.G. Borbély ⁶⁰, I.S. Bordulev ³⁸, G. Borissov ⁹³, D. Bortoletto ¹²⁹, D. Boscherini ^{24b},
 M. Bosman ¹³, J.D. Bossio Sola ³⁷, K. Bouaouda ^{36a}, N. Bouchhar ¹⁶⁶, L. Boudet ⁴,
 J. Boudreau ¹³², E.V. Bouhova-Thacker ⁹³, D. Boumediene ⁴¹, R. Bouquet ^{58b,58a}, A. Boveia ¹²²,
 J. Boyd ³⁷, D. Boye ³⁰, I.R. Boyko ³⁹, L. Bozianu ⁵⁷, J. Bracinek ²¹, N. Brahimi ⁴,
 G. Brandt ¹⁷⁴, O. Brandt ³³, F. Braren ⁴⁹, B. Brau ¹⁰⁵, J.E. Brau ¹²⁶, R. Brenner ¹⁷²,
 L. Brenner ¹¹⁷, R. Brenner ¹⁶⁴, S. Bressler ¹⁷², G. Brianti ^{79a,79b}, D. Britton ⁶⁰, D. Britzger ¹¹²,
 I. Brock ²⁵, G. Brooijmans ⁴², E.M. Brooks ^{159b}, E. Brost ³⁰, L.M. Brown ¹⁶⁸, L.E. Bruce ⁶²,
 T.L. Bruckler ¹²⁹, P.A. Bruckman de Renstrom ⁸⁸, B. Brüers ⁴⁹, A. Bruni ^{24b}, G. Bruni ^{24b},
 M. Bruschi ^{24b}, N. Bruscinò ^{76a,76b}, T. Buanes ¹⁷, Q. Buat ¹⁴¹, D. Buchin ¹¹², A.G. Buckley ⁶⁰,
 O. Bulekov ³⁸, B.A. Bullard ¹⁴⁶, S. Burdin ⁹⁴, C.D. Burgard ⁵⁰, A.M. Burger ³⁷,
 B. Burghgrave ⁸, O. Burlayenko ⁵⁵, J. Burleson ¹⁶⁵, J.T.P. Burr ³³, J.C. Burzynski ¹⁴⁵,
 E.L. Busch ⁴², V. Büscher ¹⁰², P.J. Bussey ⁶⁰, J.M. Butler ²⁶, C.M. Buttar ⁶⁰,
 J.M. Butterworth ⁹⁸, W. Buttinger ¹³⁷, C.J. Buxo Vazquez ¹⁰⁹, A.R. Buzykaev ³⁸,
 S. Cabrera Urbán ¹⁶⁶, L. Cadamuro ⁶⁷, D. Caforio ⁵⁹, H. Cai ¹³², Y. Cai ^{14,114c}, Y. Cai ^{114a},
 V.M.M. Cairo ³⁷, O. Cakir ^{3a}, N. Calace ³⁷, P. Calafiura ^{18a}, G. Calderini ¹³⁰, P. Calfayan ⁶⁹,
 G. Callea ⁶⁰, L.P. Caloba ^{84b}, D. Calvet ⁴¹, S. Calvet ⁴¹, M. Calvetti ^{75a,75b}, R. Camacho Toro ¹³⁰,
 S. Camarda ³⁷, D. Camarero Munoz ²⁷, P. Camarri ^{77a,77b}, M.T. Camerlingo ^{73a,73b},
 D. Cameron ³⁷, C. Camincher ¹⁶⁸, M. Campanelli ⁹⁸, A. Camplani ⁴³, V. Canale ^{73a,73b},
 A.C. Canbay ^{3a}, E. Canonero ⁹⁷, J. Cantero ¹⁶⁶, Y. Cao ¹⁶⁵, F. Capocasa ²⁷, M. Capua ^{44b,44a},
 A. Carbone ^{72a,72b}, R. Cardarelli ^{77a}, J.C.J. Cardenas ⁸, G. Carducci ^{44b,44a}, T. Carli ³⁷,
 G. Carlino ^{73a}, J.I. Carlotto ¹³, B.T. Carlson ^{132,p}, E.M. Carlson ^{168,159a}, J. Carmignani ⁹⁴,
 L. Carminati ^{72a,72b}, A. Carnelli ¹³⁸, M. Carnesale ^{76a,76b}, S. Caron ¹¹⁶, E. Carquin ^{140f},
 I.B. Carr ¹⁰⁷, S. Carrá ^{72a}, G. Carratta ^{24b,24a}, A.M. Carroll ¹²⁶, M.P. Casado ^{13,h}, M. Caspar ⁴⁹,
 F.L. Castillo ⁴, L. Castillo Garcia ¹³, V. Castillo Gimenez ¹⁶⁶, N.F. Castro ^{133a,133e},
 A. Catinaccio ³⁷, J.R. Catmore ¹²⁸, T. Cavaliere ⁴, V. Cavaliere ³⁰, N. Cavalli ^{24b,24a},
 L.J. Caviedes Betancourt ^{23b}, Y.C. Cekmecelioglu ⁴⁹, E. Celebi ⁸³, S. Cella ³⁷,
 M.S. Centonze ^{71a,71b}, V. Cepaitis ⁵⁷, K. Cerny ¹²⁵, A.S. Cerqueira ^{84a}, A. Cerri ¹⁴⁹,
 L. Cerrito ^{77a,77b}, F. Cerutti ^{18a}, B. Cervato ¹⁴⁴, A. Cervelli ^{24b}, G. Cesarini ⁵⁴, S.A. Cetin ⁸³,
 D. Chakraborty ¹¹⁸, J. Chan ^{18a}, W.Y. Chan ¹⁵⁶, J.D. Chapman ³³, E. Chapon ¹³⁸,
 B. Chargeishvili ^{152b}, D.G. Charlton ²¹, M. Chatterjee ²⁰, C. Chauhan ¹³⁶, Y. Che ^{114a},
 S. Chekanov ⁶, S.V. Chekulaev ^{159a}, G.A. Chelkov ^{39,a}, A. Chen ¹⁰⁸, B. Chen ¹⁵⁴, B. Chen ¹⁶⁸,
 H. Chen ^{114a}, H. Chen ³⁰, J. Chen ^{63c}, J. Chen ¹⁴⁵, M. Chen ¹²⁹, S. Chen ⁸⁹, S.J. Chen ^{114a},
 X. Chen ^{63c}, X. Chen ^{15,ab}, Y. Chen ^{63a}, C.L. Cheng ¹⁷³, H.C. Cheng ^{65a}, S. Cheong ¹⁴⁶,
 A. Cheplakov ³⁹, E. Cheremushkina ⁴⁹, E. Cherepanova ¹¹⁷, R. Cherkaoui El Moursli ^{36e},
 E. Cheu ⁷, K. Cheung ⁶⁶, L. Chevalier ¹³⁸, V. Chiarella ⁵⁴, G. Chiarelli ^{75a}, N. Chiedde ¹⁰⁴,
 G. Chiodini ^{71a}, A.S. Chisholm ²¹, A. Chitan ^{28b}, M. Chitishvili ¹⁶⁶, M.V. Chizhov ³⁹,

K. Choi ¹¹, Y. Chou ¹⁴¹, E.Y.S. Chow ¹¹⁶, K.L. Chu ¹⁷², M.C. Chu ^{65a}, X. Chu ^{14,114c},
 Z. Chubinidze ⁵⁴, J. Chudoba ¹³⁴, J.J. Chwastowski ⁸⁸, D. Cieri ¹¹², K.M. Ciesla ^{87a},
 V. Cindro ⁹⁵, A. Ciocio ^{18a}, F. Cirotto ^{73a,73b}, Z.H. Citron ¹⁷², M. Citterio ^{72a}, D.A. Ciubotaru ^{28b},
 A. Clark ⁵⁷, P.J. Clark ⁵³, N. Clarke Hall ⁹⁸, C. Clarry ¹⁵⁸, J.M. Clavijo Columbie ⁴⁹,
 S.E. Clawson ⁴⁹, C. Clement ^{48a,48b}, Y. Coadou ¹⁰⁴, M. Cobal ^{70a,70c}, A. Coccaro ^{58b},
 R.F. Coelho Barrue ^{133a}, R. Coelho Lopes De Sa ¹⁰⁵, S. Coelli ^{72a}, L.S. Colangeli ¹⁵⁸, B. Cole ⁴²,
 J. Collot ⁶¹, P. Conde Muiño ^{133a,133g}, M.P. Connell ^{34c}, S.H. Connell ^{34c}, E.I. Conroy ¹²⁹,
 F. Conventi ^{73a,ad}, H.G. Cooke ²¹, A.M. Cooper-Sarkar ¹²⁹, F.A. Corchia ^{24b,24a},
 A. Cordeiro Oudot Choi ¹³⁰, L.D. Corpe ⁴¹, M. Corradi ^{76a,76b}, F. Corriveau ^{106,w},
 A. Cortes-Gonzalez ¹⁹, M.J. Costa ¹⁶⁶, F. Costanza ⁴, D. Costanzo ¹⁴², B.M. Cote ¹²²,
 J. Couthures ⁴, G. Cowan ⁹⁷, K. Cranmer ¹⁷³, L. Cremer ⁵⁰, D. Cremonini ^{24b,24a},
 S. Crépe-Renaudin ⁶¹, F. Crescioli ¹³⁰, M. Cristinziani ¹⁴⁴, M. Cristoforetti ^{79a,79b}, V. Croft ¹¹⁷,
 J.E. Crosby ¹²⁴, G. Crosetti ^{44b,44a}, A. Cueto ¹⁰¹, H. Cui ⁹⁸, Z. Cui ⁷, W.R. Cunningham ⁶⁰,
 F. Curcio ¹⁶⁶, J.R. Curran ⁵³, P. Czodrowski ³⁷, M.J. Da Cunha Sargedas De Sousa ^{58b,58a},
 J.V. Da Fonseca Pinto ^{84b}, C. Da Via ¹⁰³, W. Dabrowski ^{87a}, T. Dado ³⁷, S. Dahbi ¹⁵¹,
 T. Dai ¹⁰⁸, D. Dal Santo ²⁰, C. Dallapiccola ¹⁰⁵, M. Dam ⁴³, G. D'amen ³⁰, V. D'Amico ¹¹¹,
 J. Damp ¹⁰², J.R. Dandoy ³⁵, D. Dannheim ³⁷, M. Danninger ¹⁴⁵, V. Dao ¹⁴⁸, G. Darbo ^{58b},
 S.J. Das ^{30,ae}, F. Dattola ⁴⁹, S. D'Auria ^{72a,72b}, A. D'Avanzo ^{73a,73b}, C. David ^{34a}, T. Davidek ¹³⁶,
 I. Dawson ⁹⁶, H.A. Day-hall ¹³⁵, K. De ⁸, R. De Asmundis ^{73a}, N. De Biase ⁴⁹,
 S. De Castro ^{24b,24a}, N. De Groot ¹¹⁶, P. de Jong ¹¹⁷, H. De la Torre ¹¹⁸, A. De Maria ^{114a},
 A. De Salvo ^{76a}, U. De Sanctis ^{77a,77b}, F. De Santis ^{71a,71b}, A. De Santo ¹⁴⁹,
 J.B. De Vivie De Regie ⁶¹, J. Debec ⁹⁵, D.V. Dedovich ³⁹, J. Degens ⁹⁴, A.M. Deiana ⁴⁵,
 F. Del Corso ^{24b,24a}, J. Del Peso ¹⁰¹, L. Delagrangé ¹³⁰, F. Deliot ¹³⁸, C.M. Delitzsch ⁵⁰,
 M. Della Pietra ^{73a,73b}, D. Della Volpe ⁵⁷, A. Dell'Acqua ³⁷, L. Dell'Asta ^{72a,72b}, M. Delmastro ⁴,
 P.A. Delsart ⁶¹, S. Demers ¹⁷⁵, M. Demichev ³⁹, S.P. Denisov ³⁸, L. D'Eramo ⁴¹,
 D. Derendarz ⁸⁸, F. Derue ¹³⁰, P. Dervan ⁹⁴, K. Desch ²⁵, C. Deutsch ²⁵, F.A. Di Bello ^{58b,58a},
 A. Di Ciaccio ^{77a,77b}, L. Di Ciaccio ⁴, A. Di Domenico ^{76a,76b}, C. Di Donato ^{73a,73b},
 A. Di Girolamo ³⁷, G. Di Gregorio ³⁷, A. Di Luca ^{79a,79b}, B. Di Micco ^{78a,78b}, R. Di Nardo ^{78a,78b},
 K.F. Di Petrillo ⁴⁰, M. Diamantopoulou ³⁵, F.A. Dias ¹¹⁷, T. Dias Do Vale ¹⁴⁵,
 M.A. Diaz ^{140a,140b}, F.G. Diaz Capriles ²⁵, A.R. Didenko ³⁹, M. Didenko ¹⁶⁶, E.B. Diehl ¹⁰⁸,
 S. Díez Cornell ⁴⁹, C. Diez Pardos ¹⁴⁴, C. Dimitriadi ¹⁶⁴, A. Dimitrievska ²¹, J. Dingfelder ²⁵,
 T. Dingley ¹²⁹, I-M. Dinu ^{28b}, S.J. Dittmeier ^{64b}, F. Dittus ³⁷, M. Divisek ¹³⁶, B. Dixit ⁹⁴,
 F. Djama ¹⁰⁴, T. Djobava ^{152b}, C. Doglioni ^{103,100}, A. Dohnalova ^{29a}, J. Dolejsi ¹³⁶,
 Z. Dolezal ¹³⁶, K. Domijan ^{87a}, K.M. Dona ⁴⁰, M. Donadelli ^{84d}, B. Dong ¹⁰⁹, J. Donini ⁴¹,
 A. D'Onofrio ^{73a,73b}, M. D'Onofrio ⁹⁴, J. Dopke ¹³⁷, A. Doria ^{73a}, N. Dos Santos Fernandes ^{133a},
 P. Dougan ¹⁰³, M.T. Dova ⁹², A.T. Doyle ⁶⁰, M.A. Draguet ¹²⁹, M.P. Drescher ⁵⁶, E. Dreyer ¹⁷²,
 I. Drivas-koulouris ¹⁰, M. Drnevich ¹²⁰, M. Drozdova ⁵⁷, D. Du ^{63a}, T.A. du Pree ¹¹⁷,
 F. Dubinin ³⁸, M. Dubovsky ^{29a}, E. Duchovni ¹⁷², G. Duckeck ¹¹¹, O.A. Ducu ^{28b}, D. Duda ⁵³,
 A. Dudarev ³⁷, E.R. Duden ²⁷, M. D'uffizi ¹⁰³, L. Duflot ⁶⁷, M. Dührssen ³⁷, I. Duminica ^{28g},
 A.E. Dumitriu ^{28b}, M. Dunford ^{64a}, S. Dungs ⁵⁰, K. Dunne ^{48a,48b}, A. Duperrin ¹⁰⁴,
 H. Duran Yildiz ^{3a}, M. Düren ⁵⁹, A. Durglishvili ^{152b}, B.L. Dwyer ¹¹⁸, G.I. Dyckes ^{18a},
 M. Dyndal ^{87a}, B.S. Dziedzic ³⁷, Z.O. Earnshaw ¹⁴⁹, G.H. Eberwein ¹²⁹, B. Eckerova ^{29a},
 S. Eggebrecht ⁵⁶, E. Egidio Purcino De Souza ^{84e}, L.F. Ehrke ⁵⁷, G. Eigen ¹⁷, K. Einsweiler ^{18a},
 T. Ekelof ¹⁶⁴, P.A. Ekman ¹⁰⁰, S. El Farkh ^{36b}, Y. El Ghazali ^{63a}, H. El Jarrari ³⁷,
 A. El Moussaouy ^{36a}, V. Ellajosyula ¹⁶⁴, M. Ellert ¹⁶⁴, F. Ellinghaus ¹⁷⁴, N. Ellis ³⁷,
 J. Elmsheuser ³⁰, M. Elsayy ^{119a}, M. Elsing ³⁷, D. Emelianov ¹³⁷, Y. Enari ⁸⁵, I. Ene ^{18a},
 S. Epari ¹³, P.A. Erland ⁸⁸, D. Ernani Martins Neto ⁸⁸, M. Errenst ¹⁷⁴, M. Escalier ⁶⁷,

C. Escobar [ID166](#), E. Etzion [ID154](#), G. Evans [ID133a](#), H. Evans [ID69](#), L.S. Evans [ID97](#), A. Ezhilov [ID38](#),
 S. Ezzarqtouni [ID36a](#), F. Fabbri [ID24b,24a](#), L. Fabbri [ID24b,24a](#), G. Facini [ID98](#), V. Fadeyev [ID139](#),
 R.M. Fakhrutdinov [ID38](#), D. Fakoudis [ID102](#), S. Falciano [ID76a](#), L.F. Falda Ulhoa Coelho [ID37](#),
 F. Fallavollita [ID112](#), G. Falsetti [ID44b,44a](#), J. Faltova [ID136](#), C. Fan [ID165](#), K.Y. Fan [ID65b](#), Y. Fan [ID14](#),
 Y. Fang [ID14,114c](#), M. Fanti [ID72a,72b](#), M. Faraj [ID70a,70b](#), Z. Farazpay [ID99](#), A. Farbin [ID8](#), A. Farilla [ID78a](#),
 T. Farooque [ID109](#), S.M. Farrington [ID53](#), F. Fassi [ID36e](#), D. Fassouliotis [ID9](#), M. Faucci Giannelli [ID77a,77b](#),
 W.J. Fawcett [ID33](#), L. Fayard [ID67](#), P. Federic [ID136](#), P. Federicova [ID134](#), O.L. Fedin [ID38,a](#), M. Feickert [ID173](#),
 L. Feligioni [ID104](#), D.E. Fellers [ID126](#), C. Feng [ID63b](#), Z. Feng [ID117](#), M.J. Fenton [ID162](#), L. Ferencz [ID49](#),
 R.A.M. Ferguson [ID93](#), S.I. Fernandez Luengo [ID140f](#), P. Fernandez Martinez [ID13](#), M.J.V. Fernoux [ID104](#),
 J. Ferrando [ID93](#), A. Ferrari [ID164](#), P. Ferrari [ID117,116](#), R. Ferrari [ID74a](#), D. Ferrere [ID57](#), C. Ferretti [ID108](#),
 D. Fiacco [ID76a,76b](#), F. Fiedler [ID102](#), P. Fiedler [ID135](#), S. Filimonov [ID38](#), A. Filipčič [ID95](#), E.K. Filmer [ID159a](#),
 F. Filthaut [ID116](#), M.C.N. Fiolhais [ID133a,133c,c](#), L. Fiorini [ID166](#), W.C. Fisher [ID109](#), T. Fitschen [ID103](#),
 P.M. Fitzhugh [ID138](#), I. Fleck [ID144](#), P. Fleischmann [ID108](#), T. Flick [ID174](#), M. Flores [ID34d,z](#),
 L.R. Flores Castillo [ID65a](#), L. Flores Sanz De Acedo [ID37](#), F.M. Follega [ID79a,79b](#), N. Fomin [ID33](#),
 J.H. Foo [ID158](#), A. Formica [ID138](#), A.C. Forti [ID103](#), E. Fortin [ID37](#), A.W. Fortman [ID18a](#), M.G. Foti [ID18a](#),
 L. Fountas [ID9,i](#), D. Fournier [ID67](#), H. Fox [ID93](#), P. Francavilla [ID75a,75b](#), S. Francescato [ID62](#),
 S. Franchellucci [ID57](#), M. Franchini [ID24b,24a](#), S. Franchino [ID64a](#), D. Francis [ID37](#), L. Franco [ID116](#),
 V. Franco Lima [ID37](#), L. Franconi [ID49](#), M. Franklin [ID62](#), G. Frattari [ID27](#), Y.Y. Frid [ID154](#), J. Friend [ID60](#),
 N. Fritzsche [ID37](#), A. Froch [ID55](#), D. Froidevaux [ID37](#), J.A. Frost [ID129](#), Y. Fu [ID63a](#),
 S. Fuenzalida Garrido [ID140f](#), M. Fujimoto [ID104](#), K.Y. Fung [ID65a](#), E. Furtado De Simas Filho [ID84e](#),
 M. Furukawa [ID156](#), J. Fuster [ID166](#), A. Gaa [ID56](#), A. Gabrielli [ID24b,24a](#), A. Gabrielli [ID158](#), P. Gadow [ID37](#),
 G. Gagliardi [ID58b,58a](#), L.G. Gagnon [ID18a](#), S. Gaid [ID163](#), S. Galantzan [ID154](#), J. Gallagher [ID1](#),
 E.J. Gallas [ID129](#), B.J. Gallop [ID137](#), K.K. Gan [ID122](#), S. Ganguly [ID156](#), Y. Gao [ID53](#),
 F.M. Garay Walls [ID140a,140b](#), B. Garcia [ID30](#), C. García [ID166](#), A. Garcia Alonso [ID117](#),
 A.G. Garcia Caffaro [ID175](#), J.E. García Navarro [ID166](#), M. Garcia-Sciveres [ID18a](#), G.L. Gardner [ID131](#),
 R.W. Gardner [ID40](#), N. Garelli [ID161](#), D. Garg [ID81](#), R.B. Garg [ID146](#), J.M. Gargan [ID53](#), C.A. Garner [ID158](#),
 C.M. Garvey [ID34a](#), V.K. Gassmann [ID161](#), G. Gaudio [ID74a](#), V. Gautam [ID13](#), P. Gauzzi [ID76a,76b](#),
 J. Gavranovic [ID95](#), I.L. Gavrilenko [ID38](#), A. Gavriluk [ID38](#), C. Gay [ID167](#), G. Gaycken [ID126](#),
 E.N. Gazis [ID10](#), A.A. Geanta [ID28b](#), C.M. Gee [ID139](#), A. Gekow [ID122](#), C. Gemme [ID58b](#), M.H. Genest [ID61](#),
 A.D. Gentry [ID115](#), S. George [ID97](#), W.F. George [ID21](#), T. Geralis [ID47](#), P. Gessinger-Befurt [ID37](#),
 M.E. Geyik [ID174](#), M. Ghani [ID170](#), K. Ghorbanian [ID96](#), A. Ghosal [ID144](#), A. Ghosh [ID162](#), A. Ghosh [ID7](#),
 B. Giacobbe [ID24b](#), S. Giagu [ID76a,76b](#), T. Giani [ID117](#), A. Giannini [ID63a](#), S.M. Gibson [ID97](#), M. Gignac [ID139](#),
 D.T. Gil [ID87b](#), A.K. Gilbert [ID87a](#), B.J. Gilbert [ID42](#), D. Gillberg [ID35](#), G. Gilles [ID117](#), L. Ginabat [ID130](#),
 D.M. Gingrich [ID2,ac](#), M.P. Giordani [ID70a,70c](#), P.F. Giraud [ID138](#), G. Giugliarelli [ID70a,70c](#), D. Giugni [ID72a](#),
 F. Giuli [ID77a,77b](#), I. Gkialas [ID9,i](#), L.K. Gladilin [ID38](#), C. Glasman [ID101](#), G.R. Gledhill [ID126](#), G. Glemža [ID49](#),
 M. Glisic [ID126](#), I. Gnesi [ID44b](#), Y. Go [ID30](#), M. Goblirsch-Kolb [ID37](#), B. Gocke [ID50](#), D. Godin [ID110](#),
 B. Gokturk [ID22a](#), S. Goldfarb [ID107](#), T. Golling [ID57](#), M.G.D. Gololo [ID34g](#), D. Golubkov [ID38](#),
 J.P. Gombas [ID109](#), A. Gomes [ID133a,133b](#), G. Gomes Da Silva [ID144](#), A.J. Gomez Delegido [ID166](#),
 R. Gonçalves [ID133a](#), L. Gonella [ID21](#), A. Gongadze [ID152c](#), F. Gonnella [ID21](#), J.L. Gonski [ID146](#),
 R.Y. González Andana [ID53](#), S. González de la Hoz [ID166](#), R. Gonzalez Lopez [ID94](#),
 C. Gonzalez Renteria [ID18a](#), M.V. Gonzalez Rodrigues [ID49](#), R. Gonzalez Suarez [ID164](#),
 S. Gonzalez-Sevilla [ID57](#), L. Goossens [ID37](#), B. Gorini [ID37](#), E. Gorini [ID71a,71b](#), A. Gorišek [ID95](#),
 T.C. Gosart [ID131](#), A.T. Goshaw [ID52](#), M.I. Gostkin [ID39](#), S. Goswami [ID124](#), C.A. Gottardo [ID37](#),
 S.A. Gotz [ID111](#), M. Gouighri [ID36b](#), V. Goumarre [ID49](#), A.G. Goussiou [ID141](#), N. Govender [ID34c](#),
 R.P. Grabarczyk [ID129](#), I. Grabowska-Bold [ID87a](#), K. Graham [ID35](#), E. Gramstad [ID128](#),
 S. Grancagnolo [ID71a,71b](#), C.M. Grant [ID1,138](#), P.M. Gravila [ID28f](#), F.G. Gravili [ID71a,71b](#), H.M. Gray [ID18a](#),
 M. Greco [ID71a,71b](#), M.J. Green [ID1](#), C. Grefe [ID25](#), A.S. Grefsrud [ID17](#), I.M. Gregor [ID49](#), K.T. Greif [ID162](#),

P. Grenier ¹⁴⁶, S.G. Grewe ¹¹², A.A. Grillo ¹³⁹, K. Grimm ³², S. Grinstein ^{13,s}, J.-F. Grivaz ⁶⁷,
 E. Gross ¹⁷², J. Grosse-Knetter ⁵⁶, L. Guan ¹⁰⁸, J.G.R. Guerrero Rojas ¹⁶⁶, G. Guerrieri ³⁷,
 R. Gugel ¹⁰², J.A.M. Guhit ¹⁰⁸, A. Guida ¹⁹, E. Guilloton ¹⁷⁰, S. Guindon ³⁷, F. Guo ^{14,114c},
 J. Guo ^{63c}, L. Guo ⁴⁹, L. Guo ¹⁴, Y. Guo ¹⁰⁸, A. Gupta ⁵⁰, R. Gupta ¹³², S. Gurbuz ²⁵,
 S.S. Gurdasani ⁵⁵, G. Gustavino ^{76a,76b}, P. Gutierrez ¹²³, L.F. Gutierrez Zagazeta ¹³¹,
 M. Gutsche ⁵¹, C. Gutschow ⁹⁸, C. Gwenlan ¹²⁹, C.B. Gwilliam ⁹⁴, E.S. Haaland ¹²⁸,
 A. Haas ¹²⁰, M. Habedank ⁶⁰, C. Haber ^{18a}, H.K. Hadavand ⁸, A. Hadeef ⁵¹, S. Hadzic ¹¹²,
 A.I. Hagan ⁹³, J.J. Hahn ¹⁴⁴, E.H. Haines ⁹⁸, M. Haleem ¹⁶⁹, J. Haley ¹²⁴, G.D. Hallewell ¹⁰⁴,
 L. Halser ²⁰, K. Hamano ¹⁶⁸, M. Hamer ²⁵, E.J. Hampshire ⁹⁷, J. Han ^{63b}, L. Han ^{114a},
 L. Han ^{63a}, S. Han ^{18a}, Y.F. Han ¹⁵⁸, K. Hanagaki ⁸⁵, M. Hance ¹³⁹, D.A. Hangal ⁴²,
 H. Hanif ¹⁴⁵, M.D. Hank ¹³¹, J.B. Hansen ⁴³, P.H. Hansen ⁴³, D. Harada ⁵⁷, T. Harenberg ¹⁷⁴,
 S. Harkusha ¹⁷⁶, M.L. Harris ¹⁰⁵, Y.T. Harris ²⁵, J. Harrison ¹³, N.M. Harrison ¹²²,
 P.F. Harrison ¹⁷⁰, N.M. Hartman ¹¹², N.M. Hartmann ¹¹¹, R.Z. Hasan ^{97,137}, Y. Hasegawa ¹⁴³,
 F. Haslbeck ¹²⁹, S. Hassan ¹⁷, R. Hauser ¹⁰⁹, C.M. Hawkes ²¹, R.J. Hawkings ³⁷,
 Y. Hayashi ¹⁵⁶, D. Hayden ¹⁰⁹, C. Hayes ¹⁰⁸, R.L. Hayes ¹¹⁷, C.P. Hays ¹²⁹, J.M. Hays ⁹⁶,
 H.S. Hayward ⁹⁴, F. He ^{63a}, M. He ^{14,114c}, Y. He ⁴⁹, Y. He ⁹⁸, N.B. Heatley ⁹⁶, V. Hedberg ¹⁰⁰,
 A.L. Heggelund ¹²⁸, N.D. Hehir ^{96,*}, C. Heidegger ⁵⁵, K.K. Heidegger ⁵⁵, J. Heilman ³⁵,
 S. Heim ⁴⁹, T. Heim ^{18a}, J.G. Heinlein ¹³¹, J.J. Heinrich ¹²⁶, L. Heinrich ^{112,aa}, J. Hejbal ¹³⁴,
 A. Held ¹⁷³, S. Hellesund ¹⁷, C.M. Helling ¹⁶⁷, S. Hellman ^{48a,48b}, R.C.W. Henderson ⁹³,
 L. Henkelmann ³³, A.M. Henriques Correia ³⁷, H. Herde ¹⁰⁰, Y. Hernández Jiménez ¹⁴⁸,
 L.M. Herrmann ²⁵, T. Herrmann ⁵¹, G. Herten ⁵⁵, R. Hertenberg ¹¹¹, L. Hervas ³⁷,
 M.E. Hesping ¹⁰², N.P. Hessey ^{159a}, J. Hessler ¹¹², M. Hidaoui ^{36b}, N. Hidic ¹³⁶, E. Hill ¹⁵⁸,
 S.J. Hillier ²¹, J.R. Hinds ¹⁰⁹, F. Hinterkeuser ²⁵, M. Hirose ¹²⁷, S. Hirose ¹⁶⁰,
 D. Hirschbuehl ¹⁷⁴, T.G. Hitchings ¹⁰³, B. Hiti ⁹⁵, J. Hobbs ¹⁴⁸, R. Hobincu ^{28e}, N. Hod ¹⁷²,
 M.C. Hodgkinson ¹⁴², B.H. Hodgkinson ¹²⁹, A. Hoecker ³⁷, D.D. Hofer ¹⁰⁸, J. Hofer ¹⁶⁶,
 T. Holm ²⁵, M. Holzbock ³⁷, L.B.A.H. Hommels ³³, B.P. Honan ¹⁰³, J.J. Hong ⁶⁹, J. Hong ^{63c},
 T.M. Hong ¹³², B.H. Hooberman ¹⁶⁵, W.H. Hopkins ⁶, M.C. Hoppesch ¹⁶⁵, Y. Horii ¹¹³,
 M.E. Horstmann ¹¹², S. Hou ¹⁵¹, A.S. Howard ⁹⁵, J. Howarth ⁶⁰, J. Hoya ⁶, M. Hrabovsky ¹²⁵,
 A. Hrynevich ⁴⁹, T. Hryn'ova ⁴, P.J. Hsu ⁶⁶, S.-C. Hsu ¹⁴¹, T. Hsu ⁶⁷, M. Hu ^{18a}, Q. Hu ^{63a},
 S. Huang ³³, X. Huang ^{14,114c}, Y. Huang ¹⁴², Y. Huang ¹⁰², Y. Huang ¹⁴, Z. Huang ¹⁰³,
 Z. Hubacek ¹³⁵, M. Huebner ²⁵, F. Huegging ²⁵, T.B. Huffman ¹²⁹, C.A. Hugli ⁴⁹,
 M. Huhtinen ³⁷, S.K. Huiberts ¹⁷, R. Hulsken ¹⁰⁶, N. Huseynov ^{12,f}, J. Huston ¹⁰⁹, J. Huth ⁶²,
 R. Hyneman ¹⁴⁶, G. Iacobucci ⁵⁷, G. Iakovidis ³⁰, L. Iconomidou-Fayard ⁶⁷, J.P. Iddon ³⁷,
 P. Iengo ^{73a,73b}, R. Iguchi ¹⁵⁶, Y. Iiyama ¹⁵⁶, T. Iizawa ¹²⁹, Y. Ikegami ⁸⁵, N. Ilic ¹⁵⁸,
 H. Imam ^{84c}, G. Inacio Goncalves ^{84d}, T. Ingebretsen Carlson ^{48a,48b}, J.M. Inglis ⁹⁶,
 G. Introzzi ^{74a,74b}, M. Iodice ^{78a}, V. Ippolito ^{76a,76b}, R.K. Irwin ⁹⁴, M. Ishino ¹⁵⁶, W. Islam ¹⁷³,
 C. Issever ¹⁹, S. Istin ^{22a,ag}, H. Ito ¹⁷¹, R. Iuppa ^{79a,79b}, A. Ivina ¹⁷², J.M. Izen ⁴⁶, V. Izzo ^{73a},
 P. Jacka ¹³⁴, P. Jackson ¹, C.S. Jagfeld ¹¹¹, G. Jain ^{159a}, P. Jain ⁴⁹, K. Jakobs ⁵⁵,
 T. Jakoubek ¹⁷², J. Jamieson ⁶⁰, W. Jang ¹⁵⁶, M. Javurkova ¹⁰⁵, P. Jawahar ¹⁰³, L. Jeanty ¹²⁶,
 J. Jejelava ^{152a,y}, P. Jenni ^{55,e}, C.E. Jessiman ³⁵, C. Jia ^{63b}, H. Jia ¹⁶⁷, J. Jia ¹⁴⁸, X. Jia ^{14,114c},
 Z. Jia ^{114a}, C. Jiang ⁵³, S. Jiggins ⁴⁹, J. Jimenez Pena ¹³, S. Jin ^{114a}, A. Jinaru ^{28b},
 O. Jinnouchi ¹⁵⁷, P. Johansson ¹⁴², K.A. Johns ⁷, J.W. Johnson ¹³⁹, F.A. Jolly ⁴⁹,
 D.M. Jones ¹⁴⁹, E. Jones ⁴⁹, K.S. Jones ⁸, P. Jones ³³, R.W.L. Jones ⁹³, T.J. Jones ⁹⁴,
 H.L. Joos ^{56,37}, R. Joshi ¹²², J. Jovicevic ¹⁶, X. Ju ^{18a}, J.J. Junggeburth ¹⁰⁵, T. Junkermann ^{64a},
 A. Juste Rozas ^{13,s}, M.K. Juzek ⁸⁸, S. Kabana ^{140e}, A. Kaczmarska ⁸⁸, M. Kado ¹¹²,
 H. Kagan ¹²², M. Kagan ¹⁴⁶, A. Kahn ¹³¹, C. Kahra ¹⁰², T. Kaji ¹⁵⁶, E. Kajomovitz ¹⁵³,
 N. Kakati ¹⁷², I. Kalaitzidou ⁵⁵, C.W. Kalderon ³⁰, N.J. Kang ¹³⁹, D. Kar ^{34g}, K. Karava ¹²⁹,

M.J. Kareem [ID159b](#), E. Karentzos [ID55](#), O. Karkout [ID117](#), S.N. Karpov [ID39](#), Z.M. Karpova [ID39](#),
V. Kartvelishvili [ID93](#), A.N. Karyukhin [ID38](#), E. Kasimi [ID155](#), J. Katzy [ID49](#), S. Kaur [ID35](#), K. Kawade [ID143](#),
M.P. Kawale [ID123](#), C. Kawamoto [ID89](#), T. Kawamoto [ID63a](#), E.F. Kay [ID37](#), F.I. Kaya [ID161](#), S. Kazakos [ID109](#),
V.F. Kazanin [ID38](#), Y. Ke [ID148](#), J.M. Keaveney [ID34a](#), R. Keeler [ID168](#), G.V. Kehris [ID62](#), J.S. Keller [ID35](#),
J.J. Kempster [ID149](#), O. Kepka [ID134](#), B.P. Kerridge [ID137](#), S. Kersten [ID174](#), B.P. Kerševan [ID95](#),
L. Keszeghova [ID29a](#), S. Ketabchi Haghighat [ID158](#), R.A. Khan [ID132](#), A. Khanov [ID124](#), A.G. Kharlamov [ID38](#),
T. Kharlamova [ID38](#), E.E. Khoda [ID141](#), M. Kholodenko [ID133a](#), T.J. Khoo [ID19](#), G. Khorauli [ID169](#),
J. Khubua [ID152b,*](#), Y.A.R. Khwaira [ID130](#), B. Kibirige [ID34g](#), D. Kim [ID6](#), D.W. Kim [ID48a,48b](#), Y.K. Kim [ID40](#),
N. Kimura [ID98](#), M.K. Kingston [ID56](#), A. Kirchhoff [ID56](#), C. Kirfel [ID25](#), F. Kirfel [ID25](#), J. Kirk [ID137](#),
A.E. Kiryunin [ID112](#), S. Kita [ID160](#), C. Kitsaki [ID10](#), O. Kivernyk [ID25](#), M. Klassen [ID161](#), C. Klein [ID35](#),
L. Klein [ID169](#), M.H. Klein [ID45](#), S.B. Klein [ID57](#), U. Klein [ID94](#), A. Klimentov [ID30](#), T. Klioutchnikova [ID37](#),
P. Kluit [ID117](#), S. Kluth [ID112](#), E. Kneringer [ID80](#), T.M. Knight [ID158](#), A. Knue [ID50](#), D. Kobylanski [ID172](#),
S.F. Koch [ID129](#), M. Kocian [ID146](#), P. Kodyš [ID136](#), D.M. Koeck [ID126](#), P.T. Koenig [ID25](#), T. Koffas [ID35](#),
O. Kolay [ID51](#), I. Koletsou [ID4](#), T. Komarek [ID88](#), K. Köneke [ID55](#), A.X.Y. Kong [ID1](#), T. Kono [ID121](#),
N. Konstantinidis [ID98](#), P. Kontaxakis [ID57](#), B. Konya [ID100](#), R. Kopeliansky [ID42](#), S. Koperny [ID87a](#),
K. Korcyl [ID88](#), K. Kordas [ID155,d](#), A. Korn [ID98](#), S. Korn [ID56](#), I. Korolkov [ID13](#), N. Korotkova [ID38](#),
B. Kortman [ID117](#), O. Kortner [ID112](#), S. Kortner [ID112](#), W.H. Kostecka [ID118](#), V.V. Kostyukhin [ID144](#),
A. Kotskechagia [ID37](#), A. Kotwal [ID52](#), A. Koulouris [ID37](#), A. Kourkoumeli-Charalampidi [ID74a,74b](#),
C. Kourkoumelis [ID9](#), E. Kourlitis [ID112,aa](#), O. Kovanda [ID126](#), R. Kowalewski [ID168](#), W. Kozanecki [ID126](#),
A.S. Kozhin [ID38](#), V.A. Kramarenko [ID38](#), G. Kramberger [ID95](#), P. Kramer [ID102](#), M.W. Krasny [ID130](#),
A. Krasznahorkay [ID37](#), A.C. Kraus [ID118](#), J.W. Kraus [ID174](#), J.A. Kremer [ID49](#), T. Kresse [ID51](#),
L. Kretschmann [ID174](#), J. Kretschmar [ID94](#), K. Kreul [ID19](#), P. Krieger [ID158](#), M. Krivos [ID136](#), K. Krizka [ID21](#),
K. Kroeninger [ID50](#), H. Kroha [ID112](#), J. Kroll [ID134](#), J. Kroll [ID131](#), K.S. Krowpman [ID109](#), U. Kruchonak [ID39](#),
H. Krüger [ID25](#), N. Krumnack [ID82](#), M.C. Kruse [ID52](#), O. Kuchinskaia [ID38](#), S. Kuday [ID3a](#), S. Kuehn [ID37](#),
R. Kuesters [ID55](#), T. Kuhl [ID49](#), V. Kukhtin [ID39](#), Y. Kulchitsky [ID38,a](#), S. Kuleshov [ID140d,140b](#),
M. Kumar [ID34g](#), N. Kumari [ID49](#), P. Kumari [ID159b](#), A. Kupco [ID134](#), T. Kupfer [ID50](#), A. Kupich [ID38](#),
O. Kuprash [ID55](#), H. Kurashige [ID86](#), L.L. Kurchaninov [ID159a](#), O. Kurdysh [ID67](#), Y.A. Kurochkin [ID38](#),
A. Kurova [ID38](#), M. Kuze [ID157](#), A.K. Kvam [ID105](#), J. Kvita [ID125](#), T. Kwan [ID106](#), N.G. Kyriacou [ID108](#),
L.A.O. Laatu [ID104](#), C. Lacasta [ID166](#), F. Lacava [ID76a,76b](#), H. Lacker [ID19](#), D. Lacour [ID130](#), N.N. Lad [ID98](#),
E. Ladygin [ID39](#), A. Lafarge [ID41](#), B. Laforge [ID130](#), T. Lagouri [ID175](#), F.Z. Lahbabi [ID36a](#), S. Lai [ID56](#),
J.E. Lambert [ID168](#), S. Lammers [ID69](#), W. Lampl [ID7](#), C. Lampoudis [ID155,d](#), G. Lamprinoudis [ID102](#),
A.N. Lancaster [ID118](#), E. Lançon [ID30](#), U. Landgraf [ID55](#), M.P.J. Landon [ID96](#), V.S. Lang [ID55](#),
O.K.B. Langrekken [ID128](#), A.J. Lankford [ID162](#), F. Lanni [ID37](#), K. Lantzsck [ID25](#), A. Lanza [ID74a](#),
M. Lanzac Berrocal [ID166](#), J.F. Laporte [ID138](#), T. Lari [ID72a](#), F. Lasagni Manghi [ID24b](#), M. Lassnig [ID37](#),
V. Latonova [ID134](#), A. Laurier [ID153](#), S.D. Lawlor [ID142](#), Z. Lawrence [ID103](#), R. Lazaridou [ID170](#),
M. Lazzaroni [ID72a,72b](#), B. Le [ID103](#), H.D.M. Le [ID109](#), E.M. Le Boulicaut [ID175](#), L.T. Le Pottier [ID18a](#),
B. Leban [ID24b,24a](#), A. Lebedev [ID82](#), M. LeBlanc [ID103](#), F. Ledroit-Guillon [ID61](#), S.C. Lee [ID151](#),
S. Lee [ID48a,48b](#), T.F. Lee [ID94](#), L.L. Leeuw [ID34c](#), H.P. Lefebvre [ID97](#), M. Lefebvre [ID168](#), C. Leggett [ID18a](#),
G. Lehmann Miotto [ID37](#), M. Leigh [ID57](#), W.A. Leight [ID105](#), W. Leinonen [ID116](#), A. Leisos [ID155,q](#),
M.A.L. Leite [ID84c](#), C.E. Leitgeb [ID19](#), R. Leitner [ID136](#), K.J.C. Leney [ID45](#), T. Lenz [ID25](#), S. Leone [ID75a](#),
C. Leonidopoulos [ID53](#), A. Leopold [ID147](#), R. Les [ID109](#), C.G. Lester [ID33](#), M. Levchenko [ID38](#), J. Levêque [ID4](#),
L.J. Levinson [ID172](#), G. Levrini [ID24b,24a](#), M.P. Lewicki [ID88](#), C. Lewis [ID141](#), D.J. Lewis [ID4](#), L. Lewitt [ID142](#),
A. Li [ID30](#), B. Li [ID63b](#), C. Li [ID63a](#), C-Q. Li [ID112](#), H. Li [ID63a](#), H. Li [ID63b](#), H. Li [ID114a](#), H. Li [ID15](#), H. Li [ID63b](#),
J. Li [ID63c](#), K. Li [ID14](#), L. Li [ID63c](#), M. Li [ID14,114c](#), S. Li [ID14,114c](#), S. Li [ID63d,63c](#), T. Li [ID5](#), X. Li [ID106](#),
Z. Li [ID156](#), Z. Li [ID14,114c](#), Z. Li [ID63a](#), S. Liang [ID14,114c](#), Z. Liang [ID14](#), M. Liberatore [ID138](#), B. Liberti [ID77a](#),
K. Lie [ID65c](#), J. Lieber Marin [ID84e](#), H. Lien [ID69](#), H. Lin [ID108](#), K. Lin [ID109](#), R.E. Lindley [ID7](#),
J.H. Lindon [ID2](#), J. Ling [ID62](#), E. Lipeles [ID131](#), A. Lipniacka [ID17](#), A. Lister [ID167](#), J.D. Little [ID69](#),

B. Liu ¹⁴, B.X. Liu ^{114b}, D. Liu ^{63d,63c}, E.H.L. Liu ²¹, J.B. Liu ^{63a}, J.K.K. Liu ³³, K. Liu ^{63d},
 K. Liu ^{63d,63c}, M. Liu ^{63a}, M.Y. Liu ^{63a}, P. Liu ¹⁴, Q. Liu ^{63d,141,63c}, X. Liu ^{63a}, X. Liu ^{63b},
 Y. Liu ^{114b,114c}, Y.L. Liu ^{63b}, Y.W. Liu ^{63a}, S.L. Lloyd ⁹⁶, E.M. Lobodzinska ⁴⁹, P. Loch ⁷,
 E. Lodhi ¹⁵⁸, T. Lohse ¹⁹, K. Lohwasser ¹⁴², E. Loiacono ⁴⁹, J.D. Lomas ²¹, J.D. Long ⁴²,
 I. Longarini ¹⁶², R. Longo ¹⁶⁵, I. Lopez Paz ⁶⁸, A. Lopez Solis ⁴⁹, N.A. Lopez-canelas ⁷,
 N. Lorenzo Martinez ⁴, A.M. Lory ¹¹¹, M. Losada ^{119a}, G. Löschcke Centeno ¹⁴⁹, O. Loseva ³⁸,
 X. Lou ^{48a,48b}, X. Lou ^{14,114c}, A. Lounis ⁶⁷, P.A. Love ⁹³, G. Lu ^{14,114c}, M. Lu ⁶⁷, S. Lu ¹³¹,
 Y.J. Lu ⁶⁶, H.J. Lubatti ¹⁴¹, C. Luci ^{76a,76b}, F.L. Lucio Alves ^{114a}, F. Luehring ⁶⁹,
 O. Lukianchuk ⁶⁷, B.S. Lunday ¹³¹, O. Lundberg ¹⁴⁷, B. Lund-Jensen ^{147,*}, N.A. Luongo ⁶,
 M.S. Lutz ³⁷, A.B. Lux ²⁶, D. Lynn ³⁰, R. Lysak ¹³⁴, E. Lytken ¹⁰⁰, V. Lyubushkin ³⁹,
 T. Lyubushkina ³⁹, M.M. Lyukova ¹⁴⁸, M.Firdaus M. Soberi ⁵³, H. Ma ³⁰, K. Ma ^{63a},
 L.L. Ma ^{63b}, W. Ma ^{63a}, Y. Ma ¹²⁴, J.C. MacDonald ¹⁰², P.C. Machado De Abreu Farias ^{84e},
 R. Madar ⁴¹, T. Madula ⁹⁸, J. Maeda ⁸⁶, T. Maeno ³⁰, H. Maguire ¹⁴², V. Maiboroda ¹³⁸,
 A. Maio ^{133a,133b,133d}, K. Maj ^{87a}, O. Majersky ⁴⁹, S. Majewski ¹²⁶, N. Makovec ⁶⁷,
 V. Maksimovic ¹⁶, B. Malaescu ¹³⁰, Pa. Malecki ⁸⁸, V.P. Maleev ³⁸, F. Malek ^{61,m}, M. Mali ⁹⁵,
 D. Malito ⁹⁷, U. Mallik ⁸¹, S. Maltezos ¹⁰, S. Malyukov ³⁹, J. Mamuzic ¹³, G. Mancini ⁵⁴,
 M.N. Mancini ²⁷, G. Manco ^{74a,74b}, J.P. Mandalia ⁹⁶, S.S. Mandarry ¹⁴⁹, I. Mandić ⁹⁵,
 L. Manhaes de Andrade Filho ^{84a}, I.M. Maniatis ¹⁷², J. Manjarres Ramos ⁹¹, D.C. Mankad ¹⁷²,
 A. Mann ¹¹¹, S. Manzoni ³⁷, L. Mao ^{63c}, X. Mapekula ^{34c}, A. Marantis ^{155,q}, G. Marchiori ⁵,
 M. Marcisovsky ¹³⁴, C. Marcon ^{72a}, M. Marinescu ²¹, S. Marium ⁴⁹, M. Marjanovic ¹²³,
 A. Markhoos ⁵⁵, M. Markovitch ⁶⁷, E.J. Marshall ⁹³, Z. Marshall ^{18a}, S. Marti-Garcia ¹⁶⁶,
 J. Martin ⁹⁸, T.A. Martin ¹³⁷, V.J. Martin ⁵³, B. Martin dit Latour ¹⁷, L. Martinelli ^{76a,76b},
 M. Martinez ^{13,s}, P. Martinez Agullo ¹⁶⁶, V.I. Martinez Outschoorn ¹⁰⁵, P. Martinez Suarez ¹³,
 S. Martin-Haugh ¹³⁷, G. Martinovicova ¹³⁶, V.S. Martoiu ^{28b}, A.C. Martyniuk ⁹⁸, A. Marzin ³⁷,
 D. Mascione ^{79a,79b}, L. Masetti ¹⁰², J. Masik ¹⁰³, A.L. Maslennikov ³⁸, P. Massarotti ^{73a,73b},
 P. Mastrandrea ^{75a,75b}, A. Mastroberardino ^{44b,44a}, T. Masubuchi ¹²⁷, T.T. Mathew ¹²⁶,
 T. Mathisen ¹⁶⁴, J. Matousek ¹³⁶, D.M. Mattern ⁵⁰, J. Maurer ^{28b}, T. Maurin ⁶⁰, A.J. Maury ⁶⁷,
 B. Maček ⁹⁵, D.A. Maximov ³⁸, A.E. May ¹⁰³, R. Mazini ¹⁵¹, I. Maznas ¹¹⁸, M. Mazza ¹⁰⁹,
 S.M. Mazza ¹³⁹, E. Mazzeo ^{72a,72b}, C. Mc Ginn ³⁰, J.P. Mc Gowan ¹⁶⁸, S.P. Mc Kee ¹⁰⁸,
 C.A. Mc Lean ⁶, C.C. McCracken ¹⁶⁷, E.F. McDonald ¹⁰⁷, A.E. McDougall ¹¹⁷,
 J.A. Mcfayden ¹⁴⁹, R.P. McGovern ¹³¹, R.P. McKenzie ^{34g}, T.C. McLachlan ⁴⁹, D.J. Mclaughlin ⁹⁸,
 S.J. McMahon ¹³⁷, C.M. Mcpartland ⁹⁴, R.A. McPherson ^{168,w}, S. Mehlhase ¹¹¹, A. Mehta ⁹⁴,
 D. Melini ¹⁶⁶, B.R. Mellado Garcia ^{34g}, A.H. Melo ⁵⁶, F. Meloni ⁴⁹,
 A.M. Mendes Jacques Da Costa ¹⁰³, H.Y. Meng ¹⁵⁸, L. Meng ⁹³, S. Menke ¹¹², M. Mentink ³⁷,
 E. Meoni ^{44b,44a}, G. Mercado ¹¹⁸, S. Merianos ¹⁵⁵, C. Merlassino ^{70a,70c}, L. Merola ^{73a,73b},
 C. Meroni ^{72a,72b}, J. Metcalfe ⁶, A.S. Mete ⁶, E. Meuser ¹⁰², C. Meyer ⁶⁹, J-P. Meyer ¹³⁸,
 R.P. Middleton ¹³⁷, L. Mijović ⁵³, G. Mikenberg ¹⁷², M. Mikestikova ¹³⁴, M. Mikuž ⁹⁵,
 H. Mildner ¹⁰², A. Milic ³⁷, D.W. Miller ⁴⁰, E.H. Miller ¹⁴⁶, L.S. Miller ³⁵, A. Milov ¹⁷²,
 D.A. Milstead ^{48a,48b}, T. Min ^{114a}, A.A. Minaenko ³⁸, I.A. Minashvili ^{152b}, L. Mince ⁶⁰,
 A.I. Mincer ¹²⁰, B. Mindur ^{87a}, M. Mineev ³⁹, Y. Mino ⁸⁹, L.M. Mir ¹³, M. Miralles Lopez ⁶⁰,
 M. Mironova ^{18a}, M.C. Missio ¹¹⁶, A. Mitra ¹⁷⁰, V.A. Mitsou ¹⁶⁶, Y. Mitsumori ¹¹³, O. Miu ¹⁵⁸,
 P.S. Miyagawa ⁹⁶, T. Mkrtchyan ^{64a}, M. Mlinarevic ⁹⁸, T. Mlinarevic ⁹⁸, M. Mlynarikova ³⁷,
 S. Mobius ²⁰, P. Mogg ¹¹¹, M.H. Mohamed Farook ¹¹⁵, A.F. Mohammed ^{14,114c}, S. Mohapatra ⁴²,
 G. Mokgatitwane ^{34g}, L. Moleri ¹⁷², B. Mondal ¹⁴⁴, S. Mondal ¹³⁵, K. Mönig ⁴⁹,
 E. Monnier ¹⁰⁴, L. Monsonis Romero ¹⁶⁶, J. Montejo Berlingen ¹³, A. Montella ^{48a,48b},
 M. Montella ¹²², F. Montekali ^{78a,78b}, F. Monticelli ⁹², S. Monzani ^{70a,70c}, A. Morancho Tarda ⁴³,
 N. Morange ⁶⁷, A.L. Moreira De Carvalho ⁴⁹, M. Moreno Llácer ¹⁶⁶, C. Moreno Martinez ⁵⁷,

J.M. Moreno Perez^{23b}, P. Morettini^{58b}, S. Morgenstern³⁷, M. Morii⁶², M. Morinaga¹⁵⁶, M. Moritsu⁹⁰, F. Morodei^{76a,76b}, P. Moschovakos³⁷, B. Moser¹²⁹, M. Mosidze^{152b}, T. Moskalets⁴⁵, P. Moskvitina¹¹⁶, J. Moss^{32j}, P. Moszkowicz^{87a}, A. Moussa^{36d}, E.J.W. Moyse¹⁰⁵, O. Mtintsilana^{34g}, S. Muanza¹⁰⁴, J. Mueller¹³², D. Muenstermann⁹³, R. Müller³⁷, G.A. Mullier¹⁶⁴, A.J. Mullin³³, J.J. Mullin¹³¹, A.E. Mulski⁶², D.P. Mungo¹⁵⁸, D. Munoz Perez¹⁶⁶, F.J. Munoz Sanchez¹⁰³, M. Murin¹⁰³, W.J. Murray^{170,137}, M. Muškinja⁹⁵, C. Mwewa³⁰, A.G. Myagkov^{38,a}, A.J. Myers⁸, G. Myers¹⁰⁸, M. Myska¹³⁵, B.P. Nachman^{18a}, O. Nackenhorst⁵⁰, K. Nagai¹²⁹, K. Nagano⁸⁵, J.L. Nagle^{30,ae}, E. Nagy¹⁰⁴, A.M. Nairz³⁷, Y. Nakahama⁸⁵, K. Nakamura⁸⁵, K. Nakkalil⁵, H. Nanjo¹²⁷, E.A. Narayanan¹¹⁵, I. Naryshkin³⁸, L. Nasella^{72a,72b}, M. Naseri³⁵, S. Nasri^{119b}, C. Nass²⁵, G. Navarro^{23a}, J. Navarro-Gonzalez¹⁶⁶, R. Nayak¹⁵⁴, A. Nayaz¹⁹, P.Y. Nechaeva³⁸, S. Nechaeva^{24b,24a}, F. Nechansky¹³⁴, L. Nedic¹²⁹, T.J. Neep²¹, A. Negri^{74a,74b}, M. Negrini^{24b}, C. Nellist¹¹⁷, C. Nelson¹⁰⁶, K. Nelson¹⁰⁸, S. Nemecek¹³⁴, M. Nessi^{37,g}, M.S. Neubauer¹⁶⁵, F. Neuhaus¹⁰², J. Neundorff⁴⁹, J. Newell⁹⁴, P.R. Newman²¹, C.W. Ng¹³², Y.W.Y. Ng⁴⁹, B. Ngair^{119a}, H.D.N. Nguyen¹¹⁰, R.B. Nickerson¹²⁹, R. Nicolaidou¹³⁸, J. Nielsen¹³⁹, M. Niemeyer⁵⁶, J. Niermann⁵⁶, N. Nikiforou³⁷, V. Nikolaenko^{38,a}, I. Nikolic-Audit¹³⁰, K. Nikolopoulos²¹, P. Nilsson³⁰, I. Ninca⁴⁹, G. Ninio¹⁵⁴, A. Nisati^{76a}, N. Nishu², R. Nisius¹¹², N. Nitika^{70a,70c}, J-E. Nitschke⁵¹, E.K. Nkadimeng^{34g}, T. Nobe¹⁵⁶, T. Nommensen¹⁵⁰, M.B. Norfolk¹⁴², B.J. Norman³⁵, M. Noury^{36a}, J. Novak⁹⁵, T. Novak⁹⁵, L. Novotny¹³⁵, R. Novotny¹¹⁵, L. Nozka¹²⁵, K. Ntekas¹⁶², N.M.J. Nunes De Moura Junior^{84b}, J. Ocariz¹³⁰, A. Ochi⁸⁶, I. Ochoa^{133a}, S. Oerdek^{49,t}, J.T. Offermann⁴⁰, A. Ogrodnik¹³⁶, A. Oh¹⁰³, C.C. Ohm¹⁴⁷, H. Oide⁸⁵, R. Oishi¹⁵⁶, M.L. Ojeda³⁷, Y. Okumura¹⁵⁶, L.F. Oleiro Seabra^{133a}, I. Oleksiyuk⁵⁷, S.A. Olivares Pino^{140d}, G. Oliveira Correa¹³, D. Oliveira Damazio³⁰, J.L. Oliver¹⁶², Ö.O. Öncel⁵⁵, A.P. O'Neill²⁰, A. Onofre^{133a,133e}, P.U.E. Onyisi¹¹, M.J. Oreglia⁴⁰, G.E. Orellana⁹², D. Orestano^{78a,78b}, N. Orlando¹³, R.S. Orr¹⁵⁸, L.M. Osojnak¹³¹, R. Ospanov^{63a}, G. Otero y Garzon³¹, H. Otono⁹⁰, P.S. Ott^{64a}, G.J. Ottino^{18a}, M. Ouchrif^{36d}, F. Ould-Saada¹²⁸, T. Ovsiannikova¹⁴¹, M. Owen⁶⁰, R.E. Owen¹³⁷, V.E. Ozcan^{22a}, F. Ozturk⁸⁸, N. Ozturk⁸, S. Ozturk⁸³, H.A. Pacey¹²⁹, A. Pacheco Pages¹³, C. Padilla Aranda¹³, G. Padovano^{76a,76b}, S. Pagan Griso^{18a}, G. Palacino⁶⁹, A. Palazzo^{71a,71b}, J. Pampel²⁵, J. Pan¹⁷⁵, T. Pan^{65a}, D.K. Panchal¹¹, C.E. Pandini¹¹⁷, J.G. Panduro Vazquez¹³⁷, H.D. Pandya¹, H. Pang¹⁵, P. Pani⁴⁹, G. Panizzo^{70a,70c}, L. Panwar¹³⁰, L. Paolozzi⁵⁷, S. Parajuli¹⁶⁵, A. Paramonov⁶, C. Paraskevopoulos⁵⁴, D. Paredes Hernandez^{65b}, A. Pareti^{74a,74b}, K.R. Park⁴², T.H. Park¹⁵⁸, M.A. Parker³³, F. Parodi^{58b,58a}, E.W. Parrish¹¹⁸, V.A. Parrish⁵³, J.A. Parsons⁴², U. Parzefall⁵⁵, B. Pascual Dias¹¹⁰, L. Pascual Dominguez¹⁰¹, E. Pasqualucci^{76a}, S. Passaggio^{58b}, F. Pastore⁹⁷, P. Patel⁸⁸, U.M. Patel⁵², J.R. Pater¹⁰³, T. Pauly³⁷, F. Pauwels¹³⁶, C.I. Pazos¹⁶¹, M. Pedersen¹²⁸, R. Pedro^{133a}, S.V. Peleganchuk³⁸, O. Penc³⁷, E.A. Pender⁵³, S. Peng¹⁵, G.D. Penn¹⁷⁵, K.E. Penski¹¹¹, M. Penzin³⁸, B.S. Peralva^{84d}, A.P. Pereira Peixoto¹⁴¹, L. Pereira Sanchez¹⁴⁶, D.V. Perepelitsa^{30,ae}, G. Perera¹⁰⁵, E. Perez Codina^{159a}, M. Perganti¹⁰, H. Pernegger³⁷, S. Perrella^{76a,76b}, O. Perrin⁴¹, K. Peters⁴⁹, R.F.Y. Peters¹⁰³, B.A. Petersen³⁷, T.C. Petersen⁴³, E. Petit¹⁰⁴, V. Petousis¹³⁵, C. Petridou^{155,d}, T. Petru¹³⁶, A. Petrukhin¹⁴⁴, M. Pettee^{18a}, A. Petukhov³⁸, K. Petukhova³⁷, R. Pezoa^{140f}, L. Pezzotti³⁷, G. Pezzullo¹⁷⁵, A.J. Pflieger³⁷, T.M. Pham¹⁷³, T. Pham¹⁰⁷, P.W. Phillips¹³⁷, G. Piacquadio¹⁴⁸, E. Pianori^{18a}, F. Piazza¹²⁶, R. Piegai³¹, D. Pietreanu^{28b}, A.D. Pilkington¹⁰³, M. Pinamonti^{70a,70c}, J.L. Pinfeld², B.C. Pinheiro Pereira^{133a}, J. Pinol Bel¹³, A.E. Pinto Pinoargote^{138,138}, L. Pintucci^{70a,70c}, K.M. Piper¹⁴⁹, A. Pirttikoski⁵⁷, D.A. Pizzi³⁵, L. Pizzimento^{65b}, A. Pizzini¹¹⁷, M.-A. Pleier³⁰, V. Pleskot¹³⁶, E. Plotnikova³⁹,

G. Poddar ⁹⁶, R. Poettgen ¹⁰⁰, L. Poggioli ¹³⁰, I. Pokharel ⁵⁶, S. Polacek ¹³⁶, G. Polesello ^{74a}, A. Poley ^{145,159a}, A. Polini ^{24b}, C.S. Pollard ¹⁷⁰, Z.B. Pollock ¹²², E. Pompa Pacchi ^{76a,76b}, N.I. Pond ⁹⁸, D. Ponomarenko ⁶⁹, L. Pontecorvo ³⁷, S. Popa ^{28a}, G.A. Popeneciu ^{28d}, A. Poreba ³⁷, D.M. Portillo Quintero ^{159a}, S. Pospisil ¹³⁵, M.A. Postill ¹⁴², P. Postolache ^{28c}, K. Potamianos ¹⁷⁰, P.A. Potepa ^{87a}, I.N. Potrap ³⁹, C.J. Potter ³³, H. Potti ¹⁵⁰, J. Poveda ¹⁶⁶, M.E. Pozo Astigarraga ³⁷, A. Prades Ibanez ^{77a,77b}, J. Pretel ¹⁶⁸, D. Price ¹⁰³, M. Primavera ^{71a}, L. Primomo ^{70a,70c}, M.A. Principe Martin ¹⁰¹, R. Privara ¹²⁵, T. Procter ⁶⁰, M.L. Proffitt ¹⁴¹, N. Proklova ¹³¹, K. Prokofiev ^{65c}, G. Proto ¹¹², J. Proudfoot ⁶, M. Przybycien ^{87a}, W.W. Przygoda ^{87b}, A. Psallidas ⁴⁷, J.E. Puddefoot ¹⁴², D. Pudzha ⁵⁵, D. Pyatiizbyantseva ³⁸, J. Qian ¹⁰⁸, D. Qichen ¹⁰³, Y. Qin ¹³, T. Qiu ⁵³, A. Quadt ⁵⁶, M. Queitsch-Maitland ¹⁰³, G. Quetant ⁵⁷, R.P. Quinn ¹⁶⁷, G. Rabanal Bolanos ⁶², D. Rafanoharana ⁵⁵, F. Raffaelli ^{77a,77b}, F. Ragusa ^{72a,72b}, J.L. Rainbolt ⁴⁰, J.A. Raine ⁵⁷, S. Rajagopalan ³⁰, E. Ramakoti ³⁸, L. Rambelli ^{58b,58a}, I.A. Ramirez-Berend ³⁵, K. Ran ^{49,114c}, D.S. Rankin ¹³¹, N.P. Rapheeha ^{34g}, H. Rasheed ^{28b}, V. Raskina ¹³⁰, D.F. Rassloff ^{64a}, A. Rastogi ^{18a}, S. Rave ¹⁰², S. Ravera ^{58b,58a}, B. Ravina ⁵⁶, I. Ravinovich ¹⁷², M. Raymond ³⁷, A.L. Read ¹²⁸, N.P. Readioff ¹⁴², D.M. Rebuzzi ^{74a,74b}, G. Redlinger ³⁰, A.S. Reed ¹¹², K. Reeves ²⁷, J.A. Reidelsturz ¹⁷⁴, D. Reikher ¹²⁶, A. Rej ⁵⁰, C. Rembser ³⁷, M. Renda ^{28b}, F. Renner ⁴⁹, A.G. Rennie ¹⁶², A.L. Rescia ⁴⁹, S. Resconi ^{72a}, M. Ressegotti ^{58b,58a}, S. Rettie ³⁷, J.G. Reyes Rivera ¹⁰⁹, E. Reynolds ^{18a}, O.L. Rezanova ³⁸, P. Reznicek ¹³⁶, H. Riani ^{36d}, N. Ribaric ⁵², E. Ricci ^{79a,79b}, R. Richter ¹¹², S. Richter ^{48a,48b}, E. Richter-Was ^{87b}, M. Ridel ¹³⁰, S. Ridouani ^{36d}, P. Rieck ¹²⁰, P. Riedler ³⁷, E.M. Riefel ^{48a,48b}, J.O. Rieger ¹¹⁷, M. Rijssenbeek ¹⁴⁸, M. Rimoldi ³⁷, L. Rinaldi ^{24b,24a}, P. Rincke ^{56,164}, T.T. Rinn ³⁰, M.P. Rinnagel ¹¹¹, G. Ripellino ¹⁶⁴, I. Riu ¹³, J.C. Rivera Vergara ¹⁶⁸, F. Rizatdinova ¹²⁴, E. Rizvi ⁹⁶, B.R. Roberts ^{18a}, S.S. Roberts ¹³⁹, S.H. Robertson ^{106,w}, D. Robinson ³³, M. Robles Manzano ¹⁰², A. Robson ⁶⁰, A. Rocchi ^{77a,77b}, C. Roda ^{75a,75b}, S. Rodriguez Bosca ³⁷, Y. Rodriguez Garcia ^{23a}, A. Rodriguez Rodriguez ⁵⁵, A.M. Rodríguez Vera ¹¹⁸, S. Roe ³⁷, J.T. Roemer ³⁷, A.R. Roepe-Gier ¹³⁹, O. Røhne ¹²⁸, R.A. Rojas ¹⁰⁵, C.P.A. Roland ¹³⁰, J. Roloff ³⁰, A. Romaniouk ³⁸, E. Romano ^{74a,74b}, M. Romano ^{24b}, A.C. Romero Hernandez ¹⁶⁵, N. Rompotis ⁹⁴, L. Roos ¹³⁰, S. Rosati ^{76a}, B.J. Rosser ⁴⁰, E. Rossi ¹²⁹, E. Rossi ^{73a,73b}, L.P. Rossi ⁶², L. Rossini ⁵⁵, R. Rosten ¹²², M. Rotaru ^{28b}, B. Rottler ⁵⁵, C. Rougier ⁹¹, D. Rousseau ⁶⁷, D. Rousso ⁴⁹, A. Roy ¹⁶⁵, S. Roy-Garand ¹⁵⁸, A. Rozanov ¹⁰⁴, Z.M.A. Rozario ⁶⁰, Y. Rozen ¹⁵³, A. Rubio Jimenez ¹⁶⁶, A.J. Ruby ⁹⁴, V.H. Ruelas Rivera ¹⁹, T.A. Ruggeri ¹, A. Ruggiero ¹²⁹, A. Ruiz-Martinez ¹⁶⁶, A. Rummler ³⁷, Z. Rurikova ⁵⁵, N.A. Rusakovich ³⁹, H.L. Russell ¹⁶⁸, G. Russo ^{76a,76b}, J.P. Rutherford ⁷, S. Rutherford Colmenares ³³, M. Rybar ¹³⁶, E.B. Rye ¹²⁸, A. Ryzhov ⁴⁵, J.A. Sabater Iglesias ⁵⁷, H.F.W. Sadrozinski ¹³⁹, F. Safai Tehrani ^{76a}, B. Safarzadeh Samani ¹³⁷, S. Saha ¹, M. Sahinsoy ⁸³, A. Saibel ¹⁶⁶, M. Saimpert ¹³⁸, M. Saito ¹⁵⁶, T. Saito ¹⁵⁶, A. Sala ^{72a,72b}, D. Salamani ³⁷, A. Salnikov ¹⁴⁶, J. Salt ¹⁶⁶, A. Salvador Salas ¹⁵⁴, D. Salvatore ^{44b,44a}, F. Salvatore ¹⁴⁹, A. Salzburger ³⁷, D. Sammel ⁵⁵, E. Sampson ⁹³, D. Sampsonidis ^{155,d}, D. Sampsonidou ¹²⁶, J. Sánchez ¹⁶⁶, V. Sanchez Sebastian ¹⁶⁶, H. Sandaker ¹²⁸, C.O. Sander ⁴⁹, J.A. Sandesara ¹⁰⁵, M. Sandhoff ¹⁷⁴, C. Sandoval ^{23b}, L. Sanfilippo ^{64a}, D.P.C. Sankey ¹³⁷, T. Sano ⁸⁹, A. Sansoni ⁵⁴, L. Santi ^{37,76b}, C. Santoni ⁴¹, H. Santos ^{133a,133b}, A. Santra ¹⁷², E. Sanzani ^{24b,24a}, K.A. Saoucha ¹⁶³, J.G. Saraiva ^{133a,133d}, J. Sardain ⁷, O. Sasaki ⁸⁵, K. Sato ¹⁶⁰, C. Sauer ^{64b}, E. Sauvan ⁴, P. Savard ^{158,ac}, R. Sawada ¹⁵⁶, C. Sawyer ¹³⁷, L. Sawyer ⁹⁹, C. Sbarra ^{24b}, A. Sbrizzi ^{24b,24a}, T. Scanlon ⁹⁸, J. Schaarschmidt ¹⁴¹, U. Schäfer ¹⁰², A.C. Schaffer ^{67,45}, D. Schaile ¹¹¹, R.D. Schamberger ¹⁴⁸, C. Scharf ¹⁹, M.M. Schefer ²⁰, V.A. Schegelsky ³⁸, D. Scheirich ¹³⁶, M. Schernau ¹⁶², C. Scheulen ⁵⁶, C. Schiavi ^{58b,58a}, M. Schioppa ^{44b,44a}, B. Schlag ^{146,1}, S. Schlenker ³⁷,

J. Schmeing ¹⁷⁴, M.A. Schmidt ¹⁷⁴, K. Schmieden ¹⁰², C. Schmitt ¹⁰², N. Schmitt ¹⁰²,
 S. Schmitt ⁴⁹, L. Schoeffel ¹³⁸, A. Schoening ^{64b}, P.G. Scholer ³⁵, E. Schopf ¹²⁹, M. Schott ²⁵,
 J. Schovancova ³⁷, S. Schramm ⁵⁷, T. Schroer ⁵⁷, H-C. Schultz-Coulon ^{64a}, M. Schumacher ⁵⁵,
 B.A. Schumm ¹³⁹, Ph. Schune ¹³⁸, A.J. Schuy ¹⁴¹, H.R. Schwartz ¹³⁹, A. Schwartzman ¹⁴⁶,
 T.A. Schwarz ¹⁰⁸, Ph. Schwemling ¹³⁸, R. Schwienhorst ¹⁰⁹, F.G. Sciacca ²⁰, A. Sciandra ³⁰,
 G. Sciolla ²⁷, F. Scuri ^{75a}, C.D. Sebastiani ⁹⁴, K. Sedlaczek ¹¹⁸, S.C. Seidel ¹¹⁵, A. Seiden ¹³⁹,
 B.D. Seidlitz ⁴², C. Seitz ⁴⁹, J.M. Seixas ^{84b}, G. Sekhniaidze ^{73a}, L. Selem ⁶¹,
 N. Semprini-Cesari ^{24b,24a}, D. Sengupta ⁵⁷, V. Senthilkumar ¹⁶⁶, L. Serin ⁶⁷, M. Sessa ^{77a,77b},
 H. Severini ¹²³, F. Sforza ^{58b,58a}, A. Sfyrta ⁵⁷, Q. Sha ¹⁴, E. Shabalina ⁵⁶, A.H. Shah ³³,
 R. Shaheen ¹⁴⁷, J.D. Shahinian ¹³¹, D. Shaked Renous ¹⁷², L.Y. Shan ¹⁴, M. Shapiro ^{18a},
 A. Sharma ³⁷, A.S. Sharma ¹⁶⁷, P. Sharma ⁸¹, P.B. Shatalov ³⁸, K. Shaw ¹⁴⁹, S.M. Shaw ¹⁰³,
 Q. Shen ^{63c}, D.J. Sheppard ¹⁴⁵, P. Sherwood ⁹⁸, L. Shi ⁹⁸, X. Shi ¹⁴, S. Shimizu ⁸⁵,
 C.O. Shimmin ¹⁷⁵, J.D. Shinner ⁹⁷, I.P.J. Shipsey ¹²⁹, S. Shirabe ⁹⁰, M. Shiyakova ^{39,u},
 M.J. Shochet ⁴⁰, D.R. Shope ¹²⁸, B. Shrestha ¹²³, S. Shrestha ^{122,af}, I. Shreyber ³⁸,
 M.J. Shroff ¹⁶⁸, P. Sicho ¹³⁴, A.M. Sickles ¹⁶⁵, E. Sideras Haddad ^{34g}, A.C. Sidley ¹¹⁷,
 A. Sidoti ^{24b}, F. Siegert ⁵¹, Dj. Sijacki ¹⁶, F. Sili ⁹², J.M. Silva ⁵³, I. Silva Ferreira ^{84b},
 M.V. Silva Oliveira ³⁰, S.B. Silverstein ^{48a}, S. Simion ⁶⁷, R. Simoniello ³⁷, E.L. Simpson ¹⁰³,
 H. Simpson ¹⁴⁹, L.R. Simpson ¹⁰⁸, S. Simsek ⁸³, S. Sindhu ⁵⁶, P. Sinervo ¹⁵⁸, S. Singh ³⁰,
 S. Sinha ⁴⁹, S. Sinha ¹⁰³, M. Sioli ^{24b,24a}, I. Siral ³⁷, E. Sitnikova ⁴⁹, J. Sjölin ^{48a,48b},
 A. Skaf ⁵⁶, E. Skorda ²¹, P. Skubic ¹²³, M. Slawinska ⁸⁸, V. Smakhtin ¹⁷², B.H. Smart ¹³⁷,
 S.Yu. Smirnov ³⁸, Y. Smirnov ³⁸, L.N. Smirnova ^{38,a}, O. Smirnova ¹⁰⁰, A.C. Smith ⁴²,
 D.R. Smith ¹⁶², E.A. Smith ⁴⁰, J.L. Smith ¹⁰³, R. Smith ¹⁴⁶, M. Smizanska ⁹³, K. Smolek ¹³⁵,
 A.A. Snesarev ³⁸, H.L. Snoek ¹¹⁷, S. Snyder ³⁰, R. Sobie ^{168,w}, A. Soffer ¹⁵⁴,
 C.A. Solans Sanchez ³⁷, E.Yu. Soldatov ³⁸, U. Soldevila ¹⁶⁶, A.A. Solodkov ³⁸, S. Solomon ²⁷,
 A. Soloshenko ³⁹, K. Solovieva ⁵⁵, O.V. Solovyanov ⁴¹, P. Sommer ⁵¹, A. Sonay ¹³,
 W.Y. Song ^{159b}, A. Sopczak ¹³⁵, A.L. Soppio ⁵³, F. Sopkova ^{29b}, J.D. Sorenson ¹¹⁵,
 I.R. Sotarriva Alvarez ¹⁵⁷, V. Sothilingam ^{64a}, O.J. Soto Sandoval ^{140c,140b}, S. Sottocornola ⁶⁹,
 R. Soualah ¹⁶³, Z. Soumami ^{36e}, D. South ⁴⁹, N. Soybelman ¹⁷², S. Spagnolo ^{71a,71b},
 M. Spalla ¹¹², D. Sperlich ⁵⁵, G. Spigo ³⁷, B. Spisso ^{73a,73b}, D.P. Spiteri ⁶⁰, M. Spousta ¹³⁶,
 E.J. Staats ³⁵, R. Stamen ^{64a}, A. Stampekis ²¹, E. Stanecka ⁸⁸, W. Stanek-Maslouska ⁴⁹,
 M.V. Stange ⁵¹, B. Stanislaus ^{18a}, M.M. Stanitzki ⁴⁹, B. Stapf ⁴⁹, E.A. Starchenko ³⁸,
 G.H. Stark ¹³⁹, J. Stark ⁹¹, P. Staroba ¹³⁴, P. Starovoitov ^{64a}, S. Stärz ¹⁰⁶, R. Staszewski ⁸⁸,
 G. Stavropoulos ⁴⁷, P. Steinberg ³⁰, B. Stelzer ^{145,159a}, H.J. Stelzer ¹³², O. Stelzer-Chilton ^{159a},
 H. Stenzel ⁵⁹, T.J. Stevenson ¹⁴⁹, G.A. Stewart ³⁷, J.R. Stewart ¹²⁴, M.C. Stockton ³⁷,
 G. Stoicea ^{28b}, M. Stolarski ^{133a}, S. Stonjek ¹¹², A. Straessner ⁵¹, J. Strandberg ¹⁴⁷,
 S. Strandberg ^{48a,48b}, M. Stratmann ¹⁷⁴, M. Strauss ¹²³, T. Streblner ¹⁰⁴, P. Strizenc ^{29b},
 R. Ströhmer ¹⁶⁹, D.M. Strom ¹²⁶, R. Stroynowski ⁴⁵, A. Strubig ^{48a,48b}, S.A. Stucci ³⁰,
 B. Stugu ¹⁷, J. Stupak ¹²³, N.A. Styles ⁴⁹, D. Su ¹⁴⁶, S. Su ^{63a}, W. Su ^{63d}, X. Su ^{63a},
 D. Suchy ^{29a}, K. Sugizaki ¹⁵⁶, V.V. Sulin ³⁸, M.J. Sullivan ⁹⁴, D.M.S. Sultan ¹²⁹,
 L. Sultanaliyeva ³⁸, S. Sultansoy ^{3b}, T. Sumida ⁸⁹, S. Sun ¹⁷³, O. Sunneborn Gudnadottir ¹⁶⁴,
 N. Sur ¹⁰⁴, M.R. Sutton ¹⁴⁹, H. Suzuki ¹⁶⁰, M. Svatos ¹³⁴, M. Swiatlowski ^{159a}, T. Swirski ¹⁶⁹,
 I. Sykora ^{29a}, M. Sykora ¹³⁶, T. Sykora ¹³⁶, D. Ta ¹⁰², K. Tackmann ^{49,t}, A. Taffard ¹⁶²,
 R. Tafirout ^{159a}, J.S. Tafuya Vargas ⁶⁷, Y. Takubo ⁸⁵, M. Talby ¹⁰⁴, A.A. Talyshev ³⁸,
 K.C. Tam ^{65b}, N.M. Tamir ¹⁵⁴, A. Tanaka ¹⁵⁶, J. Tanaka ¹⁵⁶, R. Tanaka ⁶⁷, M. Tanasini ¹⁴⁸,
 Z. Tao ¹⁶⁷, S. Tapia Araya ^{140f}, S. Tapprogge ¹⁰², A. Tarek Abouelfadl Mohamed ¹⁰⁹,
 S. Tarem ¹⁵³, K. Tariq ¹⁴, G. Tarna ^{28b}, G.F. Tartarelli ^{72a}, M.J. Tartarin ⁹¹, P. Tas ¹³⁶,
 M. Tasevsky ¹³⁴, E. Tassi ^{44b,44a}, A.C. Tate ¹⁶⁵, G. Tateno ¹⁵⁶, Y. Tayalati ^{36e,v}, G.N. Taylor ¹⁰⁷,

W. Taylor [ID159b](#), R. Teixeira De Lima [ID146](#), P. Teixeira-Dias [ID97](#), J.J. Teoh [ID158](#), K. Terashi [ID156](#),
 J. Terron [ID101](#), S. Terzo [ID13](#), M. Testa [ID54](#), R.J. Teuscher [ID158.w](#), A. Thaler [ID80](#), O. Theiner [ID57](#),
 T. Thevenaux-Pelzer [ID104](#), O. Thielmann [ID174](#), D.W. Thomas [ID97](#), J.P. Thomas [ID21](#), E.A. Thompson [ID18a](#),
 P.D. Thompson [ID21](#), E. Thomson [ID131](#), R.E. Thornberry [ID45](#), C. Tian [ID63a](#), Y. Tian [ID57](#),
 V. Tikhomirov [ID38.a](#), Yu.A. Tikhonov [ID38](#), S. Timoshenko [ID38](#), D. Timoshyn [ID136](#), E.X.L. Ting [ID1](#),
 P. Tipton [ID175](#), A. Tishelman-Charny [ID30](#), S.H. Tlou [ID34g](#), K. Todome [ID157](#), S. Todorova-Nova [ID136](#),
 S. Todt [ID51](#), L. Toffolin [ID70a,70c](#), M. Togawa [ID85](#), J. Tojo [ID90](#), S. Tokár [ID29a](#), K. Tokushuku [ID85](#),
 O. Toldaiev [ID69](#), M. Tomoto [ID85,113](#), L. Tompkins [ID146,1](#), K.W. Topolnicki [ID87b](#), E. Torrence [ID126](#),
 H. Torres [ID91](#), E. Torró Pastor [ID166](#), M. Toscani [ID31](#), C. Tosciri [ID40](#), M. Tost [ID11](#), D.R. Tovey [ID142](#),
 I.S. Trandafir [ID28b](#), T. Trefzger [ID169](#), A. Tricoli [ID30](#), I.M. Trigger [ID159a](#), S. Trincaz-Duvoid [ID130](#),
 D.A. Trischuk [ID27](#), B. Trocmé [ID61](#), A. Tropina [ID39](#), L. Truong [ID34c](#), M. Trzebinski [ID88](#), A. Trzupek [ID88](#),
 F. Tsai [ID148](#), M. Tsai [ID108](#), A. Tsiamis [ID155](#), P.V. Tsiarehshka [ID38](#), S. Tsigaridas [ID159a](#), A. Tsigiridis [ID155.q](#),
 V. Tsiskaridze [ID158](#), E.G. Tskhadadze [ID152a](#), M. Tsopoulou [ID155](#), Y. Tsujikawa [ID89](#), I.I. Tsukerman [ID38](#),
 V. Tsulaia [ID18a](#), S. Tsuno [ID85](#), K. Tsuru [ID121](#), D. Tsybychev [ID148](#), Y. Tu [ID65b](#), A. Tudorache [ID28b](#),
 V. Tudorache [ID28b](#), A.N. Tuna [ID62](#), S. Turchikhin [ID58b,58a](#), I. Turk Cakir [ID3a](#), R. Turra [ID72a](#),
 T. Turtuvshin [ID39](#), P.M. Tuts [ID42](#), S. Tzamarias [ID155,d](#), E. Tzovara [ID102](#), F. Ukegawa [ID160](#),
 P.A. Ulloa Poblete [ID140c,140b](#), E.N. Umaka [ID30](#), G. Unal [ID37](#), A. Undrus [ID30](#), G. Unel [ID162](#), J. Urban [ID29b](#),
 P. Urrejola [ID140a](#), G. Usai [ID8](#), R. Ushioda [ID157](#), M. Usman [ID110](#), F. Ustuner [ID53](#), Z. Uysal [ID83](#),
 V. Vacek [ID135](#), B. Vachon [ID106](#), T. Vafeiadis [ID37](#), A. Vaitkus [ID98](#), C. Valderanis [ID111](#),
 E. Valdes Santurio [ID48a,48b](#), M. Valente [ID159a](#), S. Valentinetti [ID24b,24a](#), A. Valero [ID166](#),
 E. Valiente Moreno [ID166](#), A. Vallier [ID91](#), J.A. Valls Ferrer [ID166](#), D.R. Van Arneman [ID117](#),
 T.R. Van Daalen [ID141](#), A. Van Der Graaf [ID50](#), P. Van Gemmeren [ID6](#), M. Van Rijnbach [ID37](#),
 S. Van Stroud [ID98](#), I. Van Vulpen [ID117](#), P. Vana [ID136](#), M. Vanadia [ID77a,77b](#), U.M. Vande Voorde [ID147](#),
 W. Vandelli [ID37](#), E.R. Vandewall [ID124](#), D. Vannicola [ID154](#), L. Vannoli [ID54](#), R. Vari [ID76a](#), E.W. Varnes [ID7](#),
 C. Varni [ID18b](#), T. Varol [ID151](#), D. Varouchas [ID67](#), L. Varriale [ID166](#), K.E. Varvell [ID150](#), M.E. Vasile [ID28b](#),
 L. Vaslin [ID85](#), G.A. Vasquez [ID168](#), A. Vasyukov [ID39](#), L.M. Vaughan [ID124](#), R. Vavricka [ID102](#),
 T. Vazquez Schroeder [ID37](#), J. Veatch [ID32](#), V. Vecchio [ID103](#), M.J. Veen [ID105](#), I. Veliscek [ID30](#),
 L.M. Veloce [ID158](#), F. Veloso [ID133a,133c](#), S. Veneziano [ID76a](#), A. Ventura [ID71a,71b](#), S. Ventura Gonzalez [ID138](#),
 A. Verbytskyi [ID112](#), M. Verducci [ID75a,75b](#), C. Vergis [ID96](#), M. Verissimo De Araujo [ID84b](#),
 W. Verkerke [ID117](#), J.C. Vermeulen [ID117](#), C. Vernieri [ID146](#), M. Vessella [ID105](#), M.C. Vetterli [ID145.ac](#),
 A. Vgenopoulos [ID102](#), N. Viaux Maira [ID140f](#), T. Vickey [ID142](#), O.E. Vickey Boeriu [ID142](#),
 G.H.A. Viehhauser [ID129](#), L. Vigani [ID64b](#), M. Vigl [ID112](#), M. Villa [ID24b,24a](#), M. Villaplana Perez [ID166](#),
 E.M. Villhauer [ID53](#), E. Vilucchi [ID54](#), M.G. Vincter [ID35](#), A. Visibile [ID117](#), C. Vittori [ID37](#), I. Vivarelli [ID24b,24a](#),
 E. Voevodina [ID112](#), F. Vogel [ID111](#), J.C. Voigt [ID51](#), P. Vokac [ID135](#), Yu. Volkotrub [ID87b](#), E. Von Toerne [ID25](#),
 B. Vormwald [ID37](#), V. Vorobel [ID136](#), K. Vorobev [ID38](#), M. Vos [ID166](#), K. Voss [ID144](#), M. Vozak [ID117](#),
 L. Vozdecky [ID123](#), N. Vranjes [ID16](#), M. Vranjes Milosavljevic [ID16](#), M. Vreeswijk [ID117](#), N.K. Vu [ID63d,63c](#),
 R. Vuillermet [ID37](#), O. Vujinovic [ID102](#), I. Vukotic [ID40](#), I.K. Vyas [ID35](#), S. Wada [ID160](#), C. Wagner [ID146](#),
 J.M. Wagner [ID18a](#), W. Wagner [ID174](#), S. Wahdan [ID174](#), H. Wahlberg [ID92](#), C.H. Waits [ID123](#), J. Walder [ID137](#),
 R. Walker [ID111](#), W. Walkowiak [ID144](#), A. Wall [ID131](#), E.J. Wallin [ID100](#), T. Wamorkar [ID6](#), A.Z. Wang [ID139](#),
 C. Wang [ID102](#), C. Wang [ID11](#), H. Wang [ID18a](#), J. Wang [ID65c](#), P. Wang [ID98](#), R. Wang [ID62](#), R. Wang [ID6](#),
 S.M. Wang [ID151](#), S. Wang [ID63b](#), S. Wang [ID14](#), T. Wang [ID63a](#), W.T. Wang [ID81](#), W. Wang [ID14](#),
 X. Wang [ID114a](#), X. Wang [ID165](#), X. Wang [ID63c](#), Y. Wang [ID63d](#), Y. Wang [ID114a](#), Y. Wang [ID63a](#),
 Z. Wang [ID108](#), Z. Wang [ID63d,52,63c](#), Z. Wang [ID108](#), A. Warburton [ID106](#), R.J. Ward [ID21](#), N. Warrack [ID60](#),
 S. Waterhouse [ID97](#), A.T. Watson [ID21](#), H. Watson [ID53](#), M.F. Watson [ID21](#), E. Watton [ID60,137](#), G. Watts [ID141](#),
 B.M. Waugh [ID98](#), J.M. Webb [ID55](#), C. Weber [ID30](#), H.A. Weber [ID19](#), M.S. Weber [ID20](#), S.M. Weber [ID64a](#),
 C. Wei [ID63a](#), Y. Wei [ID55](#), A.R. Weidberg [ID129](#), E.J. Weik [ID120](#), J. Weingarten [ID50](#), C. Weiser [ID55](#),
 C.J. Wells [ID49](#), T. Wenaus [ID30](#), B. Wendland [ID50](#), T. Wengler [ID37](#), N.S. Wenke [ID112](#), N. Wermes [ID25](#),

M. Wessels ¹, A.M. Wharton ⁹³, A.S. White ⁶², A. White ⁸, M.J. White ¹, D. Whiteson ¹⁶², L. Wickremasinghe ¹²⁷, W. Wiedenmann ¹⁷³, M. Wielers ¹³⁷, C. Wiglesworth ⁴³, D.J. Wilbern ¹²³, H.G. Wilkens ³⁷, J.J.H. Wilkinson ³³, D.M. Williams ⁴², H.H. Williams ¹³¹, S. Williams ³³, S. Willocq ¹⁰⁵, B.J. Wilson ¹⁰³, P.J. Windischhofer ⁴⁰, F.I. Winkel ³¹, F. Winklmeier ¹²⁶, B.T. Winter ⁵⁵, J.K. Winter ¹⁰³, M. Wittgen ¹⁴⁶, M. Wobisch ⁹⁹, T. Wojtkowski ⁶¹, Z. Wolffs ¹¹⁷, J. Wollrath ¹⁶², M.W. Wolter ⁸⁸, H. Wolters ^{133a,133c}, M.C. Wong ¹³⁹, E.L. Woodward ⁴², S.D. Worm ⁴⁹, B.K. Wosiek ⁸⁸, K.W. Woźniak ⁸⁸, S. Wozniowski ⁵⁶, K. Wraight ⁶⁰, C. Wu ²¹, M. Wu ^{114b}, M. Wu ¹¹⁶, S.L. Wu ¹⁷³, X. Wu ⁵⁷, Y. Wu ^{63a}, Z. Wu ⁴, J. Wuerzinger ^{112,aa}, T.R. Wyatt ¹⁰³, B.M. Wynne ⁵³, S. Xella ⁴³, L. Xia ^{114a}, M. Xia ¹⁵, M. Xie ^{63a}, S. Xin ^{14,114c}, A. Xiong ¹²⁶, J. Xiong ^{18a}, D. Xu ¹⁴, H. Xu ^{63a}, L. Xu ^{63a}, R. Xu ¹³¹, T. Xu ¹⁰⁸, Y. Xu ¹⁵, Z. Xu ⁵³, Z. Xu ^{114a}, B. Yabsley ¹⁵⁰, S. Yacoub ^{34a}, Y. Yamaguchi ⁸⁵, E. Yamashita ¹⁵⁶, H. Yamauchi ¹⁶⁰, T. Yamazaki ^{18a}, Y. Yamazaki ⁸⁶, S. Yan ⁶⁰, Z. Yan ¹⁰⁵, H.J. Yang ^{63c,63d}, H.T. Yang ^{63a}, S. Yang ^{63a}, T. Yang ^{65c}, X. Yang ³⁷, X. Yang ¹⁴, Y. Yang ⁴⁵, Y. Yang ^{63a}, Z. Yang ^{63a}, W.-M. Yao ^{18a}, H. Ye ^{114a}, H. Ye ⁵⁶, J. Ye ¹⁴, S. Ye ³⁰, X. Ye ^{63a}, Y. Yeh ⁹⁸, I. Yeletsikh ³⁹, B.K. Yeo ^{18b}, M.R. Yexley ⁹⁸, T.P. Yildirim ¹²⁹, P. Yin ⁴², K. Yorita ¹⁷¹, S. Younas ^{28b}, C.J.S. Young ³⁷, C. Young ¹⁴⁶, C. Yu ^{14,114c}, Y. Yu ^{63a}, J. Yuan ^{14,114c}, M. Yuan ¹⁰⁸, R. Yuan ^{63d,63c}, L. Yue ⁹⁸, M. Zaazoua ^{63a}, B. Zabinski ⁸⁸, E. Zaid ⁵³, Z.K. Zak ⁸⁸, T. Zakareishvili ¹⁶⁶, S. Zambito ⁵⁷, J.A. Zamora Saa ^{140d,140b}, J. Zang ¹⁵⁶, D. Zanzi ⁵⁵, O. Zaplatilek ¹³⁵, C. Zeitnitz ¹⁷⁴, H. Zeng ¹⁴, J.C. Zeng ¹⁶⁵, D.T. Zenger Jr ²⁷, O. Zenin ³⁸, T. Ženiš ^{29a}, S. Zenz ⁹⁶, S. Zerradi ^{36a}, D. Zerwas ⁶⁷, M. Zhai ^{14,114c}, D.F. Zhang ¹⁴², J. Zhang ^{63b}, J. Zhang ⁶, K. Zhang ^{14,114c}, L. Zhang ^{63a}, L. Zhang ^{114a}, P. Zhang ^{14,114c}, R. Zhang ¹⁷³, S. Zhang ¹⁰⁸, S. Zhang ⁹¹, T. Zhang ¹⁵⁶, X. Zhang ^{63c}, X. Zhang ^{63b}, Y. Zhang ¹⁴¹, Y. Zhang ⁹⁸, Y. Zhang ^{114a}, Z. Zhang ^{18a}, Z. Zhang ^{63b}, Z. Zhang ⁶⁷, H. Zhao ¹⁴¹, T. Zhao ^{63b}, Y. Zhao ¹³⁹, Z. Zhao ^{63a}, Z. Zhao ^{63a}, A. Zhemchugov ³⁹, J. Zheng ^{114a}, K. Zheng ¹⁶⁵, X. Zheng ^{63a}, Z. Zheng ¹⁴⁶, D. Zhong ¹⁶⁵, B. Zhou ¹⁰⁸, H. Zhou ⁷, N. Zhou ^{63c}, Y. Zhou ¹⁵, Y. Zhou ^{114a}, Y. Zhou ⁷, C.G. Zhu ^{63b}, J. Zhu ¹⁰⁸, X. Zhu ^{63d}, Y. Zhu ^{63c}, Y. Zhu ^{63a}, X. Zhuang ¹⁴, K. Zhukov ⁶⁹, N.I. Zimine ³⁹, J. Zinsser ^{64b}, M. Ziolkowski ¹⁴⁴, L. Živković ¹⁶, A. Zoccoli ^{24b,24a}, K. Zoch ⁶², T.G. Zorbas ¹⁴², O. Zormpa ⁴⁷, W. Zou ⁴², L. Zwalinski ³⁷.

¹Department of Physics, University of Adelaide, Adelaide; Australia.

²Department of Physics, University of Alberta, Edmonton AB; Canada.

³(^a)Department of Physics, Ankara University, Ankara; (^b)Division of Physics, TOBB University of Economics and Technology, Ankara; Türkiye.

⁴LAPP, Université Savoie Mont Blanc, CNRS/IN2P3, Annecy; France.

⁵APC, Université Paris Cité, CNRS/IN2P3, Paris; France.

⁶High Energy Physics Division, Argonne National Laboratory, Argonne IL; United States of America.

⁷Department of Physics, University of Arizona, Tucson AZ; United States of America.

⁸Department of Physics, University of Texas at Arlington, Arlington TX; United States of America.

⁹Physics Department, National and Kapodistrian University of Athens, Athens; Greece.

¹⁰Physics Department, National Technical University of Athens, Zografou; Greece.

¹¹Department of Physics, University of Texas at Austin, Austin TX; United States of America.

¹²Institute of Physics, Azerbaijan Academy of Sciences, Baku; Azerbaijan.

¹³Institut de Física d'Altes Energies (IFAE), Barcelona Institute of Science and Technology, Barcelona; Spain.

¹⁴Institute of High Energy Physics, Chinese Academy of Sciences, Beijing; China.

¹⁵Physics Department, Tsinghua University, Beijing; China.

- ¹⁶Institute of Physics, University of Belgrade, Belgrade; Serbia.
- ¹⁷Department for Physics and Technology, University of Bergen, Bergen; Norway.
- ¹⁸(^a)Physics Division, Lawrence Berkeley National Laboratory, Berkeley CA;(^b)University of California, Berkeley CA; United States of America.
- ¹⁹Institut für Physik, Humboldt Universität zu Berlin, Berlin; Germany.
- ²⁰Albert Einstein Center for Fundamental Physics and Laboratory for High Energy Physics, University of Bern, Bern; Switzerland.
- ²¹School of Physics and Astronomy, University of Birmingham, Birmingham; United Kingdom.
- ²²(^a)Department of Physics, Bogazici University, Istanbul;(^b)Department of Physics Engineering, Gaziantep University, Gaziantep;(^c)Department of Physics, Istanbul University, Istanbul; Türkiye.
- ²³(^a)Facultad de Ciencias y Centro de Investigaciones, Universidad Antonio Nariño, Bogotá;(^b)Departamento de Física, Universidad Nacional de Colombia, Bogotá; Colombia.
- ²⁴(^a)Dipartimento di Fisica e Astronomia A. Righi, Università di Bologna, Bologna;(^b)INFN Sezione di Bologna; Italy.
- ²⁵Physikalisches Institut, Universität Bonn, Bonn; Germany.
- ²⁶Department of Physics, Boston University, Boston MA; United States of America.
- ²⁷Department of Physics, Brandeis University, Waltham MA; United States of America.
- ²⁸(^a)Transilvania University of Brasov, Brasov;(^b)Horia Hulubei National Institute of Physics and Nuclear Engineering, Bucharest;(^c)Department of Physics, Alexandru Ioan Cuza University of Iasi, Iasi;(^d)National Institute for Research and Development of Isotopic and Molecular Technologies, Physics Department, Cluj-Napoca;(^e)National University of Science and Technology Politehnica, Bucharest;(^f)West University in Timisoara, Timisoara;(^g)Faculty of Physics, University of Bucharest, Bucharest; Romania.
- ²⁹(^a)Faculty of Mathematics, Physics and Informatics, Comenius University, Bratislava;(^b)Department of Subnuclear Physics, Institute of Experimental Physics of the Slovak Academy of Sciences, Kosice; Slovak Republic.
- ³⁰Physics Department, Brookhaven National Laboratory, Upton NY; United States of America.
- ³¹Universidad de Buenos Aires, Facultad de Ciencias Exactas y Naturales, Departamento de Física, y CONICET, Instituto de Física de Buenos Aires (IFIBA), Buenos Aires; Argentina.
- ³²California State University, CA; United States of America.
- ³³Cavendish Laboratory, University of Cambridge, Cambridge; United Kingdom.
- ³⁴(^a)Department of Physics, University of Cape Town, Cape Town;(^b)iThemba Labs, Western Cape;(^c)Department of Mechanical Engineering Science, University of Johannesburg, Johannesburg;(^d)National Institute of Physics, University of the Philippines Diliman (Philippines);(^e)University of South Africa, Department of Physics, Pretoria;(^f)University of Zululand, KwaDlangezwa;(^g)School of Physics, University of the Witwatersrand, Johannesburg; South Africa.
- ³⁵Department of Physics, Carleton University, Ottawa ON; Canada.
- ³⁶(^a)Faculté des Sciences Ain Chock, Réseau Universitaire de Physique des Hautes Energies - Université Hassan II, Casablanca;(^b)Faculté des Sciences, Université Ibn-Tofail, Kénitra;(^c)Faculté des Sciences Semlalia, Université Cadi Ayyad, LPHEA-Marrakech;(^d)LPMR, Faculté des Sciences, Université Mohamed Premier, Oujda;(^e)Faculté des sciences, Université Mohammed V, Rabat;(^f)Institute of Applied Physics, Mohammed VI Polytechnic University, Ben Guerir; Morocco.
- ³⁷CERN, Geneva; Switzerland.
- ³⁸Affiliated with an institute covered by a cooperation agreement with CERN.
- ³⁹Affiliated with an international laboratory covered by a cooperation agreement with CERN.
- ⁴⁰Enrico Fermi Institute, University of Chicago, Chicago IL; United States of America.
- ⁴¹LPC, Université Clermont Auvergne, CNRS/IN2P3, Clermont-Ferrand; France.
- ⁴²Nevis Laboratory, Columbia University, Irvington NY; United States of America.

- ⁴³Niels Bohr Institute, University of Copenhagen, Copenhagen; Denmark.
- ⁴⁴(^a)Dipartimento di Fisica, Università della Calabria, Rende; (^b)INFN Gruppo Collegato di Cosenza, Laboratori Nazionali di Frascati; Italy.
- ⁴⁵Physics Department, Southern Methodist University, Dallas TX; United States of America.
- ⁴⁶Physics Department, University of Texas at Dallas, Richardson TX; United States of America.
- ⁴⁷National Centre for Scientific Research "Demokritos", Agia Paraskevi; Greece.
- ⁴⁸(^a)Department of Physics, Stockholm University; (^b)Oskar Klein Centre, Stockholm; Sweden.
- ⁴⁹Deutsches Elektronen-Synchrotron DESY, Hamburg and Zeuthen; Germany.
- ⁵⁰Fakultät Physik, Technische Universität Dortmund, Dortmund; Germany.
- ⁵¹Institut für Kern- und Teilchenphysik, Technische Universität Dresden, Dresden; Germany.
- ⁵²Department of Physics, Duke University, Durham NC; United States of America.
- ⁵³SUPA - School of Physics and Astronomy, University of Edinburgh, Edinburgh; United Kingdom.
- ⁵⁴INFN e Laboratori Nazionali di Frascati, Frascati; Italy.
- ⁵⁵Physikalisches Institut, Albert-Ludwigs-Universität Freiburg, Freiburg; Germany.
- ⁵⁶II. Physikalisches Institut, Georg-August-Universität Göttingen, Göttingen; Germany.
- ⁵⁷Département de Physique Nucléaire et Corpusculaire, Université de Genève, Genève; Switzerland.
- ⁵⁸(^a)Dipartimento di Fisica, Università di Genova, Genova; (^b)INFN Sezione di Genova; Italy.
- ⁵⁹II. Physikalisches Institut, Justus-Liebig-Universität Giessen, Giessen; Germany.
- ⁶⁰SUPA - School of Physics and Astronomy, University of Glasgow, Glasgow; United Kingdom.
- ⁶¹LPSC, Université Grenoble Alpes, CNRS/IN2P3, Grenoble INP, Grenoble; France.
- ⁶²Laboratory for Particle Physics and Cosmology, Harvard University, Cambridge MA; United States of America.
- ⁶³(^a)Department of Modern Physics and State Key Laboratory of Particle Detection and Electronics, University of Science and Technology of China, Hefei; (^b)Institute of Frontier and Interdisciplinary Science and Key Laboratory of Particle Physics and Particle Irradiation (MOE), Shandong University, Qingdao; (^c)School of Physics and Astronomy, Shanghai Jiao Tong University, Key Laboratory for Particle Astrophysics and Cosmology (MOE), SKLPPC, Shanghai; (^d)Tsung-Dao Lee Institute, Shanghai; (^e)School of Physics and Microelectronics, Zhengzhou University; China.
- ⁶⁴(^a)Kirchhoff-Institut für Physik, Ruprecht-Karls-Universität Heidelberg, Heidelberg; (^b)Physikalisches Institut, Ruprecht-Karls-Universität Heidelberg, Heidelberg; Germany.
- ⁶⁵(^a)Department of Physics, Chinese University of Hong Kong, Shatin, N.T., Hong Kong; (^b)Department of Physics, University of Hong Kong, Hong Kong; (^c)Department of Physics and Institute for Advanced Study, Hong Kong University of Science and Technology, Clear Water Bay, Kowloon, Hong Kong; China.
- ⁶⁶Department of Physics, National Tsing Hua University, Hsinchu; Taiwan.
- ⁶⁷IJCLab, Université Paris-Saclay, CNRS/IN2P3, 91405, Orsay; France.
- ⁶⁸Centro Nacional de Microelectrónica (IMB-CNM-CSIC), Barcelona; Spain.
- ⁶⁹Department of Physics, Indiana University, Bloomington IN; United States of America.
- ⁷⁰(^a)INFN Gruppo Collegato di Udine, Sezione di Trieste, Udine; (^b)ICTP, Trieste; (^c)Dipartimento Politecnico di Ingegneria e Architettura, Università di Udine, Udine; Italy.
- ⁷¹(^a)INFN Sezione di Lecce; (^b)Dipartimento di Matematica e Fisica, Università del Salento, Lecce; Italy.
- ⁷²(^a)INFN Sezione di Milano; (^b)Dipartimento di Fisica, Università di Milano, Milano; Italy.
- ⁷³(^a)INFN Sezione di Napoli; (^b)Dipartimento di Fisica, Università di Napoli, Napoli; Italy.
- ⁷⁴(^a)INFN Sezione di Pavia; (^b)Dipartimento di Fisica, Università di Pavia, Pavia; Italy.
- ⁷⁵(^a)INFN Sezione di Pisa; (^b)Dipartimento di Fisica E. Fermi, Università di Pisa, Pisa; Italy.
- ⁷⁶(^a)INFN Sezione di Roma; (^b)Dipartimento di Fisica, Sapienza Università di Roma, Roma; Italy.
- ⁷⁷(^a)INFN Sezione di Roma Tor Vergata; (^b)Dipartimento di Fisica, Università di Roma Tor Vergata, Roma; Italy.

- ^{78(a)}INFN Sezione di Roma Tre; ^(b)Dipartimento di Matematica e Fisica, Università Roma Tre, Roma; Italy.
- ^{79(a)}INFN-TIFPA; ^(b)Università degli Studi di Trento, Trento; Italy.
- ⁸⁰Universität Innsbruck, Department of Astro and Particle Physics, Innsbruck; Austria.
- ⁸¹University of Iowa, Iowa City IA; United States of America.
- ⁸²Department of Physics and Astronomy, Iowa State University, Ames IA; United States of America.
- ⁸³Istinye University, Sariyer, Istanbul; Türkiye.
- ^{84(a)}Departamento de Engenharia Elétrica, Universidade Federal de Juiz de Fora (UFJF), Juiz de Fora; ^(b)Universidade Federal do Rio De Janeiro COPPE/EE/IF, Rio de Janeiro; ^(c)Instituto de Física, Universidade de São Paulo, São Paulo; ^(d)Rio de Janeiro State University, Rio de Janeiro; ^(e)Federal University of Bahia, Bahia; Brazil.
- ⁸⁵KEK, High Energy Accelerator Research Organization, Tsukuba; Japan.
- ⁸⁶Graduate School of Science, Kobe University, Kobe; Japan.
- ^{87(a)}AGH University of Krakow, Faculty of Physics and Applied Computer Science, Krakow; ^(b)Marian Smoluchowski Institute of Physics, Jagiellonian University, Krakow; Poland.
- ⁸⁸Institute of Nuclear Physics Polish Academy of Sciences, Krakow; Poland.
- ⁸⁹Faculty of Science, Kyoto University, Kyoto; Japan.
- ⁹⁰Research Center for Advanced Particle Physics and Department of Physics, Kyushu University, Fukuoka ; Japan.
- ⁹¹L2IT, Université de Toulouse, CNRS/IN2P3, UPS, Toulouse; France.
- ⁹²Instituto de Física La Plata, Universidad Nacional de La Plata and CONICET, La Plata; Argentina.
- ⁹³Physics Department, Lancaster University, Lancaster; United Kingdom.
- ⁹⁴Oliver Lodge Laboratory, University of Liverpool, Liverpool; United Kingdom.
- ⁹⁵Department of Experimental Particle Physics, Jožef Stefan Institute and Department of Physics, University of Ljubljana, Ljubljana; Slovenia.
- ⁹⁶School of Physics and Astronomy, Queen Mary University of London, London; United Kingdom.
- ⁹⁷Department of Physics, Royal Holloway University of London, Egham; United Kingdom.
- ⁹⁸Department of Physics and Astronomy, University College London, London; United Kingdom.
- ⁹⁹Louisiana Tech University, Ruston LA; United States of America.
- ¹⁰⁰Fysiska institutionen, Lunds universitet, Lund; Sweden.
- ¹⁰¹Departamento de Física Teórica C-15 and CIAFF, Universidad Autónoma de Madrid, Madrid; Spain.
- ¹⁰²Institut für Physik, Universität Mainz, Mainz; Germany.
- ¹⁰³School of Physics and Astronomy, University of Manchester, Manchester; United Kingdom.
- ¹⁰⁴CPPM, Aix-Marseille Université, CNRS/IN2P3, Marseille; France.
- ¹⁰⁵Department of Physics, University of Massachusetts, Amherst MA; United States of America.
- ¹⁰⁶Department of Physics, McGill University, Montreal QC; Canada.
- ¹⁰⁷School of Physics, University of Melbourne, Victoria; Australia.
- ¹⁰⁸Department of Physics, University of Michigan, Ann Arbor MI; United States of America.
- ¹⁰⁹Department of Physics and Astronomy, Michigan State University, East Lansing MI; United States of America.
- ¹¹⁰Group of Particle Physics, University of Montreal, Montreal QC; Canada.
- ¹¹¹Fakultät für Physik, Ludwig-Maximilians-Universität München, München; Germany.
- ¹¹²Max-Planck-Institut für Physik (Werner-Heisenberg-Institut), München; Germany.
- ¹¹³Graduate School of Science and Kobayashi-Maskawa Institute, Nagoya University, Nagoya; Japan.
- ^{114(a)}Department of Physics, Nanjing University, Nanjing; ^(b)School of Science, Shenzhen Campus of Sun Yat-sen University; ^(c)University of Chinese Academy of Science (UCAS), Beijing; China.
- ¹¹⁵Department of Physics and Astronomy, University of New Mexico, Albuquerque NM; United States of

America.

¹¹⁶Institute for Mathematics, Astrophysics and Particle Physics, Radboud University/Nikhef, Nijmegen; Netherlands.

¹¹⁷Nikhef National Institute for Subatomic Physics and University of Amsterdam, Amsterdam; Netherlands.

¹¹⁸Department of Physics, Northern Illinois University, DeKalb IL; United States of America.

¹¹⁹(^a)New York University Abu Dhabi, Abu Dhabi;(^b)United Arab Emirates University, Al Ain; United Arab Emirates.

¹²⁰Department of Physics, New York University, New York NY; United States of America.

¹²¹Ochanomizu University, Otsuka, Bunkyo-ku, Tokyo; Japan.

¹²²Ohio State University, Columbus OH; United States of America.

¹²³Homer L. Dodge Department of Physics and Astronomy, University of Oklahoma, Norman OK; United States of America.

¹²⁴Department of Physics, Oklahoma State University, Stillwater OK; United States of America.

¹²⁵Palacký University, Joint Laboratory of Optics, Olomouc; Czech Republic.

¹²⁶Institute for Fundamental Science, University of Oregon, Eugene, OR; United States of America.

¹²⁷Graduate School of Science, Osaka University, Osaka; Japan.

¹²⁸Department of Physics, University of Oslo, Oslo; Norway.

¹²⁹Department of Physics, Oxford University, Oxford; United Kingdom.

¹³⁰LPNHE, Sorbonne Université, Université Paris Cité, CNRS/IN2P3, Paris; France.

¹³¹Department of Physics, University of Pennsylvania, Philadelphia PA; United States of America.

¹³²Department of Physics and Astronomy, University of Pittsburgh, Pittsburgh PA; United States of America.

¹³³(^a)Laboratório de Instrumentação e Física Experimental de Partículas - LIP, Lisboa;(^b)Departamento de Física, Faculdade de Ciências, Universidade de Lisboa, Lisboa;(^c)Departamento de Física, Universidade de Coimbra, Coimbra;(^d)Centro de Física Nuclear da Universidade de Lisboa, Lisboa;(^e)Departamento de Física, Universidade do Minho, Braga;(^f)Departamento de Física Teórica y del Cosmos, Universidad de Granada, Granada (Spain);(^g)Departamento de Física, Instituto Superior Técnico, Universidade de Lisboa, Lisboa; Portugal.

¹³⁴Institute of Physics of the Czech Academy of Sciences, Prague; Czech Republic.

¹³⁵Czech Technical University in Prague, Prague; Czech Republic.

¹³⁶Charles University, Faculty of Mathematics and Physics, Prague; Czech Republic.

¹³⁷Particle Physics Department, Rutherford Appleton Laboratory, Didcot; United Kingdom.

¹³⁸IRFU, CEA, Université Paris-Saclay, Gif-sur-Yvette; France.

¹³⁹Santa Cruz Institute for Particle Physics, University of California Santa Cruz, Santa Cruz CA; United States of America.

¹⁴⁰(^a)Departamento de Física, Pontificia Universidad Católica de Chile, Santiago;(^b)Millennium Institute for Subatomic physics at high energy frontier (SAPHIR), Santiago;(^c)Instituto de Investigación Multidisciplinario en Ciencia y Tecnología, y Departamento de Física, Universidad de La Serena;(^d)Universidad Andres Bello, Department of Physics, Santiago;(^e)Instituto de Alta Investigación, Universidad de Tarapacá, Arica;(^f)Departamento de Física, Universidad Técnica Federico Santa María, Valparaíso; Chile.

¹⁴¹Department of Physics, University of Washington, Seattle WA; United States of America.

¹⁴²Department of Physics and Astronomy, University of Sheffield, Sheffield; United Kingdom.

¹⁴³Department of Physics, Shinshu University, Nagano; Japan.

¹⁴⁴Department Physik, Universität Siegen, Siegen; Germany.

¹⁴⁵Department of Physics, Simon Fraser University, Burnaby BC; Canada.

- ¹⁴⁶SLAC National Accelerator Laboratory, Stanford CA; United States of America.
- ¹⁴⁷Department of Physics, Royal Institute of Technology, Stockholm; Sweden.
- ¹⁴⁸Departments of Physics and Astronomy, Stony Brook University, Stony Brook NY; United States of America.
- ¹⁴⁹Department of Physics and Astronomy, University of Sussex, Brighton; United Kingdom.
- ¹⁵⁰School of Physics, University of Sydney, Sydney; Australia.
- ¹⁵¹Institute of Physics, Academia Sinica, Taipei; Taiwan.
- ¹⁵²(^a) E. Andronikashvili Institute of Physics, Iv. Javakhishvili Tbilisi State University, Tbilisi; (^b) High Energy Physics Institute, Tbilisi State University, Tbilisi; (^c) University of Georgia, Tbilisi; Georgia.
- ¹⁵³Department of Physics, Technion, Israel Institute of Technology, Haifa; Israel.
- ¹⁵⁴Raymond and Beverly Sackler School of Physics and Astronomy, Tel Aviv University, Tel Aviv; Israel.
- ¹⁵⁵Department of Physics, Aristotle University of Thessaloniki, Thessaloniki; Greece.
- ¹⁵⁶International Center for Elementary Particle Physics and Department of Physics, University of Tokyo, Tokyo; Japan.
- ¹⁵⁷Department of Physics, Tokyo Institute of Technology, Tokyo; Japan.
- ¹⁵⁸Department of Physics, University of Toronto, Toronto ON; Canada.
- ¹⁵⁹(^a) TRIUMF, Vancouver BC; (^b) Department of Physics and Astronomy, York University, Toronto ON; Canada.
- ¹⁶⁰Division of Physics and Tomonaga Center for the History of the Universe, Faculty of Pure and Applied Sciences, University of Tsukuba, Tsukuba; Japan.
- ¹⁶¹Department of Physics and Astronomy, Tufts University, Medford MA; United States of America.
- ¹⁶²Department of Physics and Astronomy, University of California Irvine, Irvine CA; United States of America.
- ¹⁶³University of Sharjah, Sharjah; United Arab Emirates.
- ¹⁶⁴Department of Physics and Astronomy, University of Uppsala, Uppsala; Sweden.
- ¹⁶⁵Department of Physics, University of Illinois, Urbana IL; United States of America.
- ¹⁶⁶Instituto de Física Corpuscular (IFIC), Centro Mixto Universidad de Valencia - CSIC, Valencia; Spain.
- ¹⁶⁷Department of Physics, University of British Columbia, Vancouver BC; Canada.
- ¹⁶⁸Department of Physics and Astronomy, University of Victoria, Victoria BC; Canada.
- ¹⁶⁹Fakultät für Physik und Astronomie, Julius-Maximilians-Universität Würzburg, Würzburg; Germany.
- ¹⁷⁰Department of Physics, University of Warwick, Coventry; United Kingdom.
- ¹⁷¹Waseda University, Tokyo; Japan.
- ¹⁷²Department of Particle Physics and Astrophysics, Weizmann Institute of Science, Rehovot; Israel.
- ¹⁷³Department of Physics, University of Wisconsin, Madison WI; United States of America.
- ¹⁷⁴Fakultät für Mathematik und Naturwissenschaften, Fachgruppe Physik, Bergische Universität Wuppertal, Wuppertal; Germany.
- ¹⁷⁵Department of Physics, Yale University, New Haven CT; United States of America.
- ¹⁷⁶Yerevan Physics Institute, Yerevan; Armenia.
- ^a Also Affiliated with an institute covered by a cooperation agreement with CERN.
- ^b Also at An-Najah National University, Nablus; Palestine.
- ^c Also at Borough of Manhattan Community College, City University of New York, New York NY; United States of America.
- ^d Also at Center for Interdisciplinary Research and Innovation (CIRI-AUTH), Thessaloniki; Greece.
- ^e Also at CERN, Geneva; Switzerland.
- ^f Also at CMD-AC UNEC Research Center, Azerbaijan State University of Economics (UNEC); Azerbaijan.
- ^g Also at Département de Physique Nucléaire et Corpusculaire, Université de Genève, Genève;

Switzerland.

^h Also at Departament de Física de la Universitat Autònoma de Barcelona, Barcelona; Spain.

ⁱ Also at Department of Financial and Management Engineering, University of the Aegean, Chios; Greece.

^j Also at Department of Physics, California State University, Sacramento; United States of America.

^k Also at Department of Physics, King's College London, London; United Kingdom.

^l Also at Department of Physics, Stanford University, Stanford CA; United States of America.

^m Also at Department of Physics, Stellenbosch University; South Africa.

ⁿ Also at Department of Physics, University of Fribourg, Fribourg; Switzerland.

^o Also at Department of Physics, University of Thessaly; Greece.

^p Also at Department of Physics, Westmont College, Santa Barbara; United States of America.

^q Also at Hellenic Open University, Patras; Greece.

^r Also at Imam Mohammad Ibn Saud Islamic University; Saudi Arabia.

^s Also at Institutio Catalana de Recerca i Estudis Avancats, ICREA, Barcelona; Spain.

^t Also at Institut für Experimentalphysik, Universität Hamburg, Hamburg; Germany.

^u Also at Institute for Nuclear Research and Nuclear Energy (INRNE) of the Bulgarian Academy of Sciences, Sofia; Bulgaria.

^v Also at Institute of Applied Physics, Mohammed VI Polytechnic University, Ben Guerir; Morocco.

^w Also at Institute of Particle Physics (IPP); Canada.

^x Also at Institute of Physics, Azerbaijan Academy of Sciences, Baku; Azerbaijan.

^y Also at Institute of Theoretical Physics, Ilia State University, Tbilisi; Georgia.

^z Also at National Institute of Physics, University of the Philippines Diliman (Philippines); Philippines.

^{aa} Also at Technical University of Munich, Munich; Germany.

^{ab} Also at The Collaborative Innovation Center of Quantum Matter (CICQM), Beijing; China.

^{ac} Also at TRIUMF, Vancouver BC; Canada.

^{ad} Also at Università di Napoli Parthenope, Napoli; Italy.

^{ae} Also at University of Colorado Boulder, Department of Physics, Colorado; United States of America.

^{af} Also at Washington College, Chestertown, MD; United States of America.

^{ag} Also at Yeditepe University, Physics Department, Istanbul; Türkiye.

* Deceased